공학박사학위논문

Investigation of the Grain Boundary Effect on the Electrical Property of Graphene

그래핀의 결정립이

전기적 특성에 미치는 영향 고찰

2021년 2월

서울대학교 대학원

재료공학부

김 기 주

Investigation of the Grain Boundary Effect on the Electrical Property of Graphene

지도 교수 김 기 범

이 논문을 공학박사 학위논문으로 제출함

2021 년 1 월
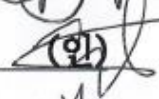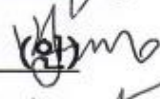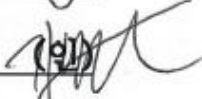
서울대학교 대학원

재료공학부

김 기 주

김기주의 공학박사 학위논문을 인준함

2021 년 1 월

위 원 장	남 기 태	(인)
부위원장	김 기 범	(인)
위 원	장 호 원	(인)
위 원	박 진 성	(인)
위 원	김 형 근	(인)

Investigation of the Grain Boundary Effect on the Electrical Property of Graphene

그래핀의 결정립이

전기적 특성에 미치는 영향 고찰

A DISSERTATION SUBMITTED TO

DEPARTMENT OF MATERIALS SCIENCE AND ENGINEERING

SEOUL NATIONAL UNIVERSITY

FOR THE DEGREE OF

DOCTOR OF PHILOSOPHY

Ki-Ju Kim

February 2021

Abstract

Investigation of the Grain Boundary Effect on the Electrical Property of Graphene

Ki-Ju Kim

Department of Materials Science and Engineering

The Graduate School

Seoul National University

Graphene is two-dimensional (2D) material showing outstanding electrical, mechanical, optical property, which opens the 2D material research field. However, most promising properties is from the single crystal graphene which only can collect dozens of um size. To synthesize wafer scale graphene chemical exfoliation, selective sublimation of Si from SiC, and CVD process were proposed, CVD is the one of the most promising method because of its unlimited scalability and high quality. The CVD grown graphene, however, does not showing remarkable property as single crystal graphene for several reason. Therefore, massive efforts and studies were conducted to increase electrical property of graphene.

Chapters 1 and 2 are the introductory sections. In Chapter 1, basic property and synthesis method for graphene is placed. In chapter 2, the electrical limiting factors will be described, the bulk resistivity of graphene, substrate scattering, grain boundary scattering and other scattering factors. Then, the current approaches to overcome the limits and to enhancing electrical property of graphene will be summarized. Among them, doping and enlarging grain size emphasized as a major electrical property enhancing methods.

Chapter 3 is the preparation part of chapter 4, synthesizing various size of graphene to study grain boundary effect. The basis theory for CVD growth is studied and reducing carbon source supply enlarging grain size of graphene was achieved. During optimizing experimental condition, the electropolishing process and two-step growth process were proposed, to prevent heterogeneous nucleation and unfilled gap problem because of low

carbon source supply.

In chapter 4, one of the two main part on this study, grain size dependence on electrical property of undoped/doped graphene is evaluated. The sheet resistance is reduced as the grain size increased since the carrier mobility enhanced, regardless of undoping/doping. Further analysis conducted by ohmic scaling model, it shows that 17 um size of graphene has 20 % of grain boundary sheet resistance. Another model, Mayadas-Shatzkes model, also applied on graphene, the resultant shows 0.97 of reflection coefficient, much large than other metals. In both model studies, grain boundary is considerably act as strong scattering center and controlling grain size turned out to be very important. The doping process also applied on various size of graphene and the similar result was observed form both models, considering grain boundary, the noticeable presumptive fact revealed that the doping efficiency is higher on the grain boundary of graphene. The conjugated experiment of doping and enlarging grain size shows that at small grain size *i.g.*, 1 um, grain size effect is too strong, even doping process applied about 1000 ohm/sq can be achieved, however, more than 10 um of grain size, doping process becomes more effect than enlarging grain size. Therefore, it was confirmed that the most efficient way for enhancing electrical property of graphene is growing over 10 um size of graphene and conducting doping process.

In Chapter 5 grain boundary effect on doping is further studied by employing Ru ALD on graphene. By the selective Ru deposition on grain boundary of graphene 180 ohm/sq at 20 cycle, 125 ohm/sq at 50 cycle is achieved. The control experiment, Ru evaporation is conducted to compare the doping effect with Ru ALD. The result shows that doping is occurred more efficiently on grain boundary of graphene.

To conclude, the characteristic of graphene grain boundary on electrical property massively performed in this study. The grain boundary is revealed to the high impact on electrical property of graphene. Interestingly, the grain boundary acts as scattering center for carrier transport, however, it also acts as aa efficient doping site for doping process. In this study, the basics of the grain boundary property on undoped/doped graphene is established and expected to the fundamentals for the grain boundary involving electrical property researches.

Key words: graphene, CVD, grain boundary, doping, atomic layer deposition, sheet resistance, enhancing electrical property.

Student number: 2011-20622

Table of contents

List of tables

Chapter 1

Table 1-1. Chemical approaches to make chemically modified graphene sheets

Table 1-2. Comparison of graphene synthesis method.

Chapter 2

Table 2-1. The summary of graphene doping articles using various dopant and doping method. R2R is roll to roll transfer process.

Table 2-2. The summary of electrical property of mm size of graphene. The electrical property was made on single grain of graphene.

Chapter 3

Table 3-1. The parameters of shape factor n and its significance.

Table 3-2. The growth parameters of CVD graphene to synthesize different grain size.

Chapter 4

List of figures

Chapter 1

Chapter 2

position and orientation. (c) Fully covered graphene growth, with grain boundary formation.

Figure 2-8. Stone-Wales graphene grain boundary observed in high resolution transmission electron microscopy (HR-TEM) image. Grains are mis-aligned with 27 degrees, and grain boundaries consist of penta- and heptagon.

Figure 2-9. Various form of graphene grain boundary in polycrystalline CVD graphene.

Figure 2-10. Resistance measurement inside of grains, and in between graphene grains.

Figure 2-11. (a) The current measurement and (b) the histogram of sheet resistance of graphene with two different grain size. Small domains have 50 um, and large domains has 2 mm size of graphene.

Figure 2-12. Sheet resistance and carrier mobility of graphene with different grain size. In the x-axis, grain size is 0.1, 1.2, 1.2, 4.5 um in sequence.

Figure 2-13. (a) optical microscopy image of CVD graphene after transfer process. Cracks are additionally generated and observed after transfer. (b) TEM image of CVD graphene after transfer process, and PMMA residue exist on graphene layer.

Figure 2-14. $1/\mu$ vs time graph of K atom deposition in UHV system. As the time goes by,

K atoms deposited on graphene layer and the carrier mobility decreased with 5×10^{15}/Vs of C.

Figure 2-15. HR-TEM image of single void on graphene layer (upper image) and SEM image of wrinkle in graphene layer. (downer image) Hexagonal dark image is additional double layer of graphene in SEM.

Figure 2-16. The yearly reported CVD graphene grain size.

Chapter 3

Figure 3-1. Energy profile of dehydrogenation process of CH_4 on (111), (100) Cu surfaces.

Figure 3-2. (a) density of nuclei vs growth temperature in CVD growth graphene, inset is the illustration of carbon monomer consuming process, nucleation, captured by nuclei, desorption. (b) is the SEM image of CVD graphene on Cu as increasing growth temperature 940, 980, 1000, 1030 ℃. The higher growth temperature shows decreased nucleation density.

Figure 3-3. The overall illustration of the nucleation growth mechanism of graphene on Cu.

Figure 3-4. The geometric structures of Cu (111) surface in dehydrogenation process of

CH$_4$ gas. I.S. is the initial state, T.S. is the transitional state and F.S. is the final state.

that of electropolished Cu foil (right image).

Figure 3-12. The JMAK fitting of synthesized graphene with growth condition in **Table 3-2**, 10 sccm (black, square), 5 sccm (red, circle), 0.5 sccm (blue, upper triangle), 0.1 sccm (green, downer triangle).

Figure 3-13. The optical microscopy image of grown graphene with the condition **Table 3-2**.

Chapter 4

Figure 4-1. The schematic illustration of experimental scheme to evaluate the graphene grain boundary and doping effect on electrical property of graphene.

Figure 4-2. The electrical property of undoped graphene with various grain size measured by Hall measurement system. The sheet resistance (left graph), carrier concentration (right graph, left side of vertical axis with black square) and carrier mobility (right graph, right side of vertical axis with upper triangle).

Figure 4-3. The electrical property of undoped/dope graphene with various grain size. (a) the sheet resistance of undoped (square) and doped (upper triangle) graphene with average grain size. (b) the carrier concentration of undoped/doped graphene. (c) the carrier mobility of doped graphene.

background scattering on grain.

at 17 um graphene grain.

Chapter 5

peaks for each graphene grain are indicate by circles.

Figure 5-6. Magnified bright-field TEM image of **Figure 5-4(a)**.

Figure 5-7. Electrical and optical properties of graphene. (a) Sheet resistance of graphene after Ru ALD (gray square) and Ru ALD without graphene (red circle), (b) density and mobility of charge carriers, (c) sheet resistance as a function of time, (d) optical transmittance at 550 nm as a function of the number of ALD cycles.

Figure 5-8. Work functions of graphene as a function of the number of ALD cycles.

Figure 5-9. UPS spectra of graphene.

Figure 5-10. Electrical and optical properties of Ru deposited on graphene by evaporation as a function of deposition thickness. (a) Sheet resistance, (b) density and mobility of charge carrier, (c) transmittance at 550 nm, and (d) density of charge carrier as a function of transmittance (numbers represent evaporated layer thickness and number of ALD cycles).

CHAPTER 1.

Introduction

1.1. The fundamentals of graphene

Graphene has been known after since the invention of X-ray crystallography and the thin graphite samples with a few graphene layers were observed by Transmission Electron Microscopy (TEM) in 1948[1], but the term 'graphene' first appeared in 1987 in order to describe a monolayer graphite [2]. The theoretical studies of graphene initiated from 1947 as a starting point of exploration for 3D graphite electrical property [3]. From 1990 to 2004, hundreds of researchers tried to produce a single layer graphene by mechanical and chemical exfoliation, however, normally 50~100 layers of graphene were produced [4] [5]. In 2004, A. Geim and K. Novoselov successfully extract a single layer graphene from the highly oriented pyrolytic graphite (HOPG) and characterize ballistic transport in graphene system using mechanical cleavage, so-called Scotch tape technique, winning the Nobel Prize in Physics in 2010 as a "For groundbreaking experiments regarding the two-dimensional material graphene". Since 2004, in many different subfields, numerous researches were performed to reveal exceptional properties of graphene [6].

Graphene is a representative 2-dimensional material with a honeycomb structure, which have a hexagonal Bravias lattice in 2D space containing two carbon atoms in unit cell as shown in **Figure 1-1**. (with the unit cell vector $a_1 = (\frac{\sqrt{3}}{2}a, \frac{1}{2}a)$, $a_2 = (\frac{\sqrt{3}}{2}a, -\frac{1}{2}a)$) Here, bonding length between carbon atoms are 0.142 nm. This short bonding length is originated from strong *sp2* hybridized covalent bonding nature of graphene. Carbon has 4 out-shell electrons, and electrons in three out-shell which parallel to basal plane of graphene involve in *sp2* bonding, *2s*, *2p_x* and *2p_y* orbital form *sp2* hybridized orbital

bonding with three nearby carbon atoms.[7] The remained electron occupies $2p_z$ orbital which perpendicular to basal plane of graphene. And these orbitals hybridize and from two half-filled bands of free electrons, π and π^*, which is the origin of the unique electrical properties of graphene.[7]
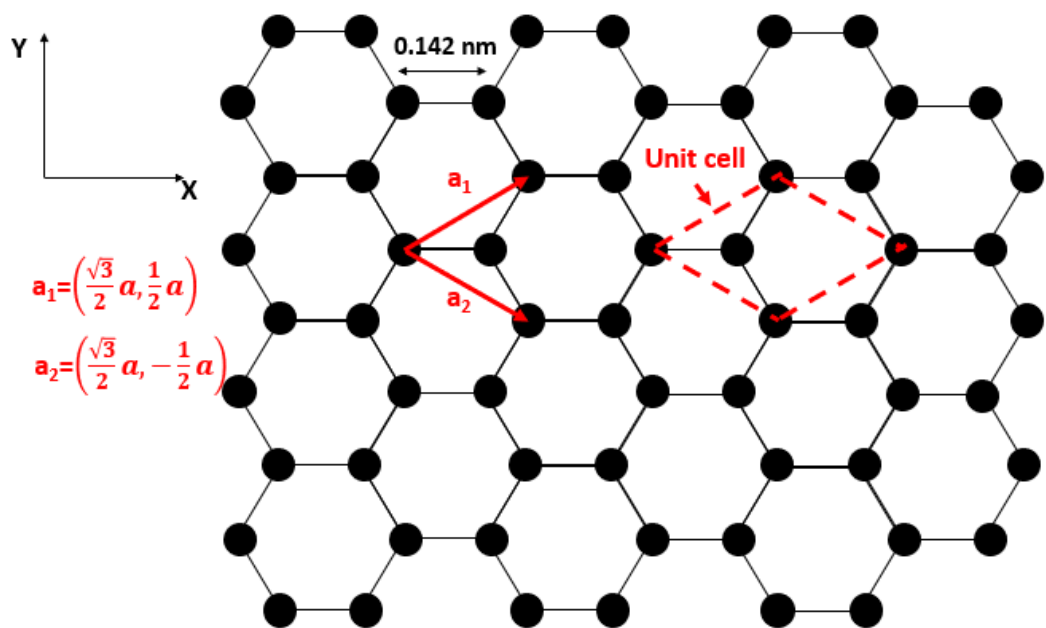
Figure 1-1. The unit cell of graphene and unit vector.

1.2. Electrical property of graphene

From the unique π and π^* originated by *2p_z*, various electrical property is shown in graphene. The conventional tight-binding model the dispersion relationship in graphene can be expressed as follows, [8-10]

$$E(k_x, k_y) = \pm\gamma_0 \sqrt{1 + 4\cos^2\frac{1}{2}ak_x + 4cos\frac{1}{2}ak_x \cdot cos\frac{\sqrt{3}}{2}ak_y}$$

k is the wave vector and a is the lattice constant about 2.46 Å. And following band structure is in the **Figure 1-2**.[8] As it can be seen in **Figure 1-2**, π and π^* band are not interacting with each other, two bands touches six points, Dirac point. The symmetry from the Dirac point enable zero-gap semiconductor property, in pure, free-standing graphene, electrons and holes have same property theoretically. The experimental result of single crystal graphene is first made on 2004,[6] shows massless electron property of graphene, the highest mobility measurement is reported on 2008,[11] 230,000 cm^2/Vs with ~2×10^{11} /cm^2 of carrier concentration with ~135 ohm/sq of sheet resistance. In this experiment, to remove all possible mobility scattering factors, graphene was synthesized on mechanical cleavage method on suspended form as **Figure 1-3**, the current annealing procedure was conducted before mobility measurement to remove possible contamination on single crystal graphene.[11] The electrical property of ideal graphene will be further discussed in chapter 2.
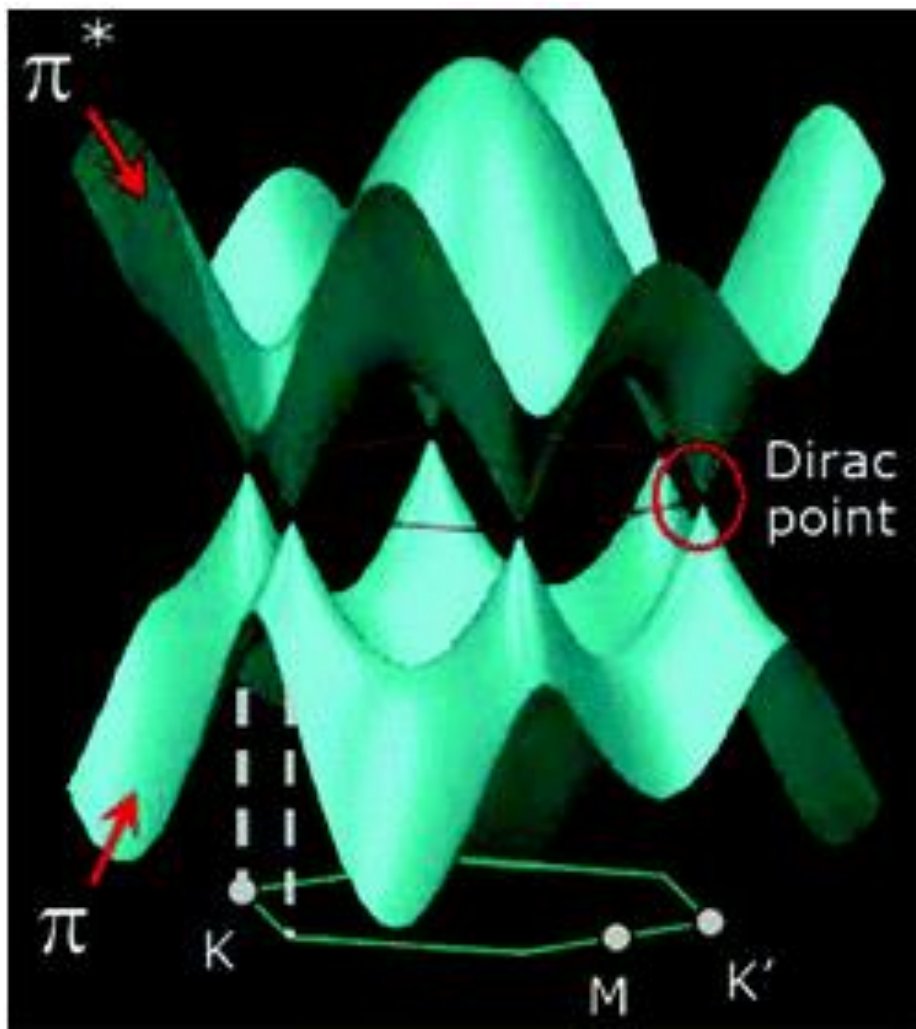
Figure 1-2. The 3D band diagram of structure of graphene.
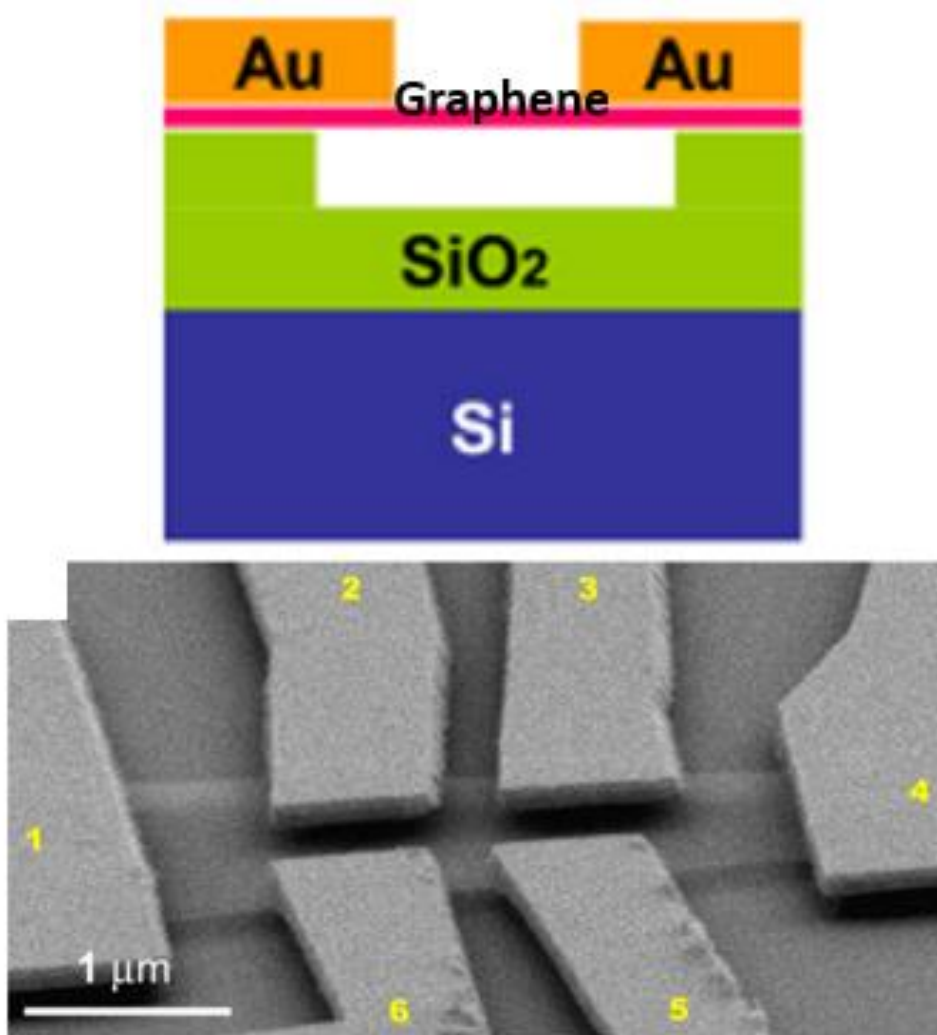
Figure 1-3. The structure of suspended graphene on SiO₂ substrate and SEM image.

1.3. Synthesis method of graphene for wafer scale

  Lots of outstanding and unique properties of graphene are, however, mainly observed in single crystal graphene which collected from mechanical cleavage method. The basic concept of mechanical cleavage method is extracting graphene from graphite, which also called as Scotch tape method. The process is very simple. Firstly, tape Highly ordered pyrolytic graphite (HOPG) and stick it to arbitrary substrate such as SiO_2/Si and just peel it. Then this process breaks Van der Waals forces separating graphene layers approximately half of its layer. And by continuing this process, single-layered graphene is collected on substrate. With this method, a lot of remarkable properties of graphene were measured and reported, however, this mechanical exfoliation method has neither high throughput nor high yield, only few um scales of single crystal graphene is collected. To apply graphene into industrial purpose, the needs of wafer scale graphene synthesis method arise, and 3 synthesis methods are dominantly researched.

  The one is liquid-phase exfoliation of graphite. Liquid-phase exfoliation is a widely used method to make colloidal dispersions of graphene in a variety of solvents. The utilization of surface-active organic liquids is the key of this process. And it should be noted that this approach has manifested itself quite well in the resolution of the issue related to the separation of carbon nanotubes[12], which are usually produced in the form of closely packed bundles requiring further separation. Simply, typical procedure of the method involves exposure of graphite or graphite oxide powders to particular solvents, and then exposing the solutions to sonication[13]. First, Graphite or Graphite Oxide power is exposed to solvent. As a layered structure of graphite permits atoms or molecules of various kinds to penetrate

into the interlayer space of crystalline graphite, there is an enhancement of the interlayer

distance and correspondingly lowering the energy of interaction between the interlayers[12].

Then, the separation of graphite layers becomes possible by prolonged sonication or/and

centrifugation. As a result, the formation of a suspension containing suspended single-

layer graphene sheets and few-layer graphene samples can be obtained and this process is

well illustrated in **Figure 1-4**. Normally, reduction of these sheets is required to remove

remained functional groups on the sheets in order to prevent this functionalization to

disrupting the electronic structure of graphene[14]. This method has a great advantage of high

production. However, the main drawback is the probable existence of defects, coming from

incomplete graphite oxide reduction or shortened flakes when using sonication[15].

Therefore, most of studies relating this method are basically focusing on finding better

stating graphite sources and dispersible solvents which is shown in **Table 1-1**.

Another way to manufacture graphene is by using Silicon Carbide. The general idea is by

heating silicon carbide (SiC) at high enough temperature (>1000℃) and selectively

sublimated silicon atoms to reduce graphene as in **Figure 1-5**. The growth of graphene on

SiC surface is highly dependent on which SiC face is used. SiC grows in cubic and number

of hexagonal polytypes but graphene growth is only available in hexagonal 6H and 4H

surfaces. Both SiC and graphene have similar lattice structure where this led to nearly

commensurate structure with the SiC (0001) and (000-1) surfaces. The formation of

structure is strongly depended on the specific SiC polar face chosen for growth along with

other experimental conditions. Hence, two polar faces of SiC (0001), Si-face with one

dangling Si-bond/Si atom, and SiC (000-1), C-face with one dangling bond per C atom,

which are the surface for graphene growth to occur. However, Si-face (0001) is much

slower than C-face[16] due to the bonding between Si and C atoms with graphene bonding are hybridized into a sp^2 configuration[17]. Hence, both of faces can achieve graphene growth but the structures of graphene on these two polar faces will be different. Additionally, Si-face graphene is epitaxial with an orientational phase rotated 30° relative to the SiC while C-face films can have multiple orientational phases. Because of the orientational disorder in C-face grown graphene, most structural, growth and electronic studies of epitaxial graphene focused on Si-face graphene and Si-face graphene growth is concentrated[17]. Prior to graphene growth to occur, pre-treatment is required in order to form desire surface area for graphene to growth *i.e.*, (0001) and (000-1). SiC is usually etched with hydrogen in a furnace in order to remove any scratches from polishing as well as re-ordering its structure for desired surface. When H_2 etching is finished, there might be some oxides formed in the surface. Hence, the sample is re-heated in the presence of a Si flux to remove any oxides that have formed while preserving the surface chemical stoichiometry[18-20]. This is not graphene yet but it is SiC buffer layer which is the precursor structure before the formation of graphene. Reducing SiC buffer layer by heating to higher temperature (1250-1350℃) in ultra-high vacuum (UHV) will produce graphene[21]. The graphene formed on Si-face grows epitaxially, rotated at about 30° from SiC substrate. The advantage of this technique is that the epitaxial graphene growth is robust and large grain size can be achieved due to single crystal of SiC for any laboratorial researches but cannot be batch produced as well as the cost of process is very high due to its usage of ultra-high vacuum and temperature. Hence, this method is good for laboratorial research works but poor to commercialize.

  Graphene can be grown on metal catalysts by CVD (Chemical Vapor Deposition) process. Growing process itself is very similar but distinctive compared with typical CVD process

in the sense of segregation. The Typical growing process of CVD growth of graphene is illustrated in **Figure 1-6**. When methane gas flowed on Ni surface, it will be decomposed to active carbon, C or CH_x at about 1000°C. (High temperature is required for decomposition of methane gas, relatively stable molecule) Then carbon will diffuse into Ni because of its carbon solubility. At high temperature, active carbons will migrate and form graphene nuclei on Ni surface with carbon solved inside of Ni. While cooling, solubility of Ni is decreased, therefore carbon diffuse out to Ni-Ni interstitials which have crystalline geometry, hexagonal in the case of FCC (111) face [22]. But graphene is not only growing on the metal surface which has 'hexagonal surface orientation'. Rather, graphene grows at the surface which has 'crystalline orientation'. In short, graphene is formed on the surface and segregated from dissolved carbon in metal at the same time. So, depending on solubility of metal, layer thickness of graphene is determined [23-25]. However, graphene growth process on Cu metal has very low carbon solubility. From low carbon solubility, carbon atoms won't diffuse into cu metal, therefore, in this case, carbon source decomposed into active carbon atom such as carbon monomer and nucleation and growth process proceed by surface diffusion of active carbon atoms. (as shown in **Figure 1-7**) In result, single layer of graphene grows dominantly unlike Ni[26].

  These CVD grown graphene is one of promising candidate of industrial application. Process is very simple and controlling layer thickness or large area production are possible. In 2010, 30-inch size of graphene is fabricated by CVD process using Cu foil, and has succeeded in making display panel [27]. Sometimes, transfer technique is needed after CVD growth method because graphene grew on metal surface. Typically, wet-transfer process is employed in most of laboratory. Wet-transfer process consists of few steps. Firstly,

adhesive polymer material, such as PMMA, is coated on graphene. Secondly, Cu foil is etched away by etchant. Then polymer coated graphene will float on etchant surface. Finally, after being scooped out, remaining polymer materials were removed[5]. (See **Figure 1-8**) This wet-transfer process is very handy and also generate additional defect such as cleavage or residue of polymer which degrade graphene quality [28, 29].

The basic properties of various graphene synthesis method were summarized in **Table 1-2**. All of the graphene synthesis method has its own advantage, for instance, liquid-phase exfoliation method is most proper for mass production, and graphene synthesis using SiC produce most high-quality graphene. However, among these various graphene synthesis methods, CVD growth has almost unlimited scalability, (scale of produced graphene is limited by metal catalyst size) and produce high quality of graphene and therefore, intensively researched as one of the best graphene synthesis methods.

Exposure to solvent

Graphite or Graphite Oxide powder

Bigger – distance of the interlayer
Lower - binding force of the interlayer

Sonication

Graphene sheet

Reduction

High-yield production of graphene
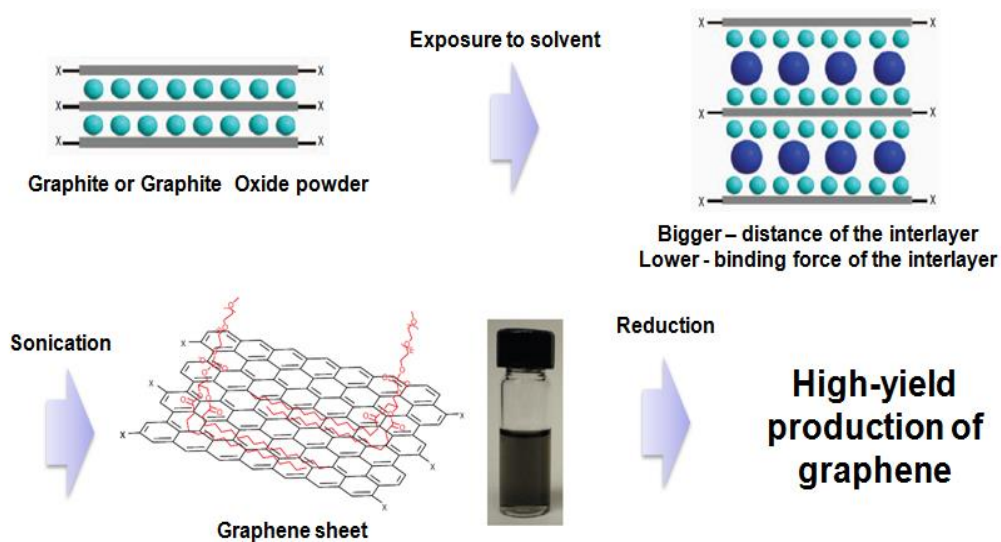
Figure 1-4. General process of obtain graphene by liquid phase exfoliation of graphite [13].

#	Starting materials	Dispersible solvents	Concentration (mg/ml)	Lateral size	Thickness (nm)
1	GO/MH	Water	1	-	-7
2	GO/MH	DMF, NMP, DMSO, HMPA	1	~ 560 nm	1
3	GO/O	DMF, THF, CCl$_4$, DCE	0.5	-	0.5~2.5
4	GIC	NMP	0.15	Hundreds nm	0.35
5	EG	Water, DMF, DMSO	0.015~0.020	Hundreds nm	2~3 layer

Table 1-1. Chemical approaches to make chemically modified graphene sheets [30].

Note. GO (graphite oxide), MH (modified Hummers method), O(their own method), GIC (graphite intercalation compound), EG (expandable graphite), DMF (dimethylformamide), NMP (N-methylpyrrolidone), DMSO (dimethylsulphoxide), HMPA (hexamethylphosphoramide), THF (tetrahydrofuran), DCE (1,2-dicholoroethane)

Surface reconstruction

Graphene
D_G — "layer-2"
D_G — "layer-1"
D_1
D_0 — Interface "layer-0"

σ_G

H_2 etching

SiC

$T\sim1500^\circ C$

Bulk SiC

Heat ($\sim$1250-1350℃)

Graphene

SiC   Graphene layers
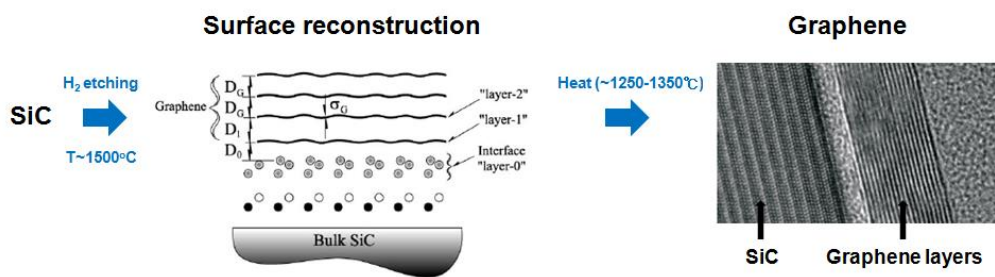
Figure 1-5. Epitaxial growth of graphene form SiC[17].
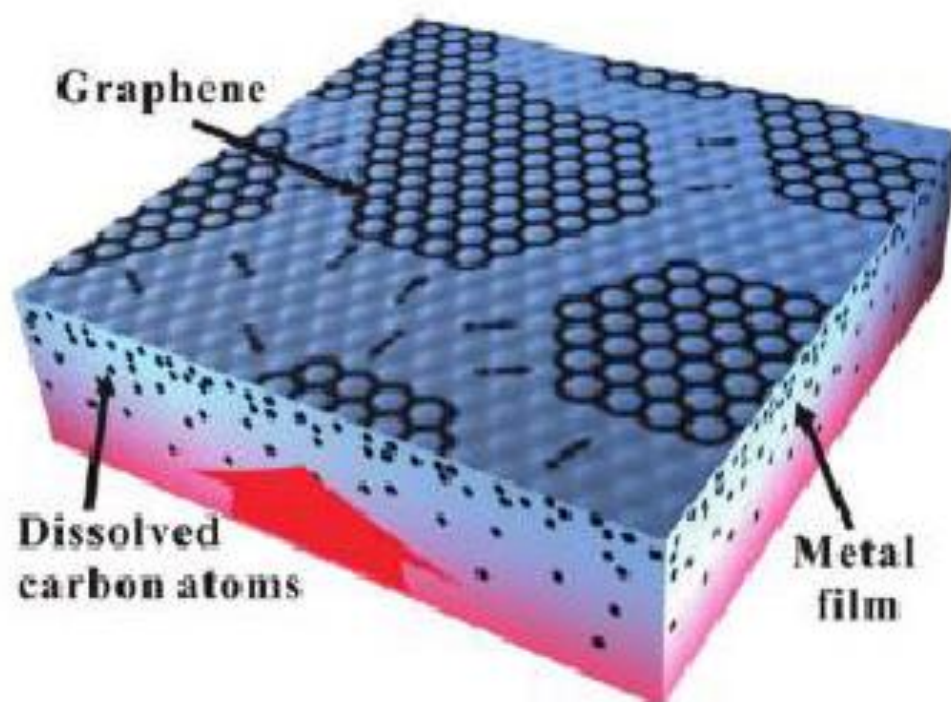
Figure 1-6. Graphene growth on Ni [22].
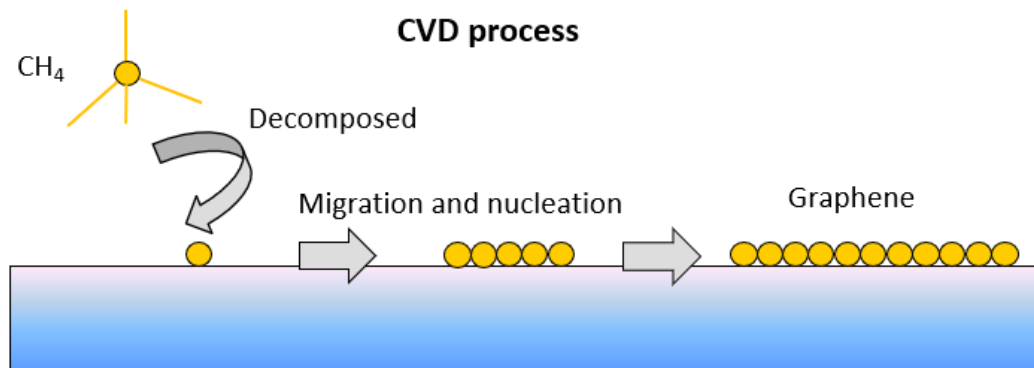
Figure 1-7. Graphene growth on Cu.
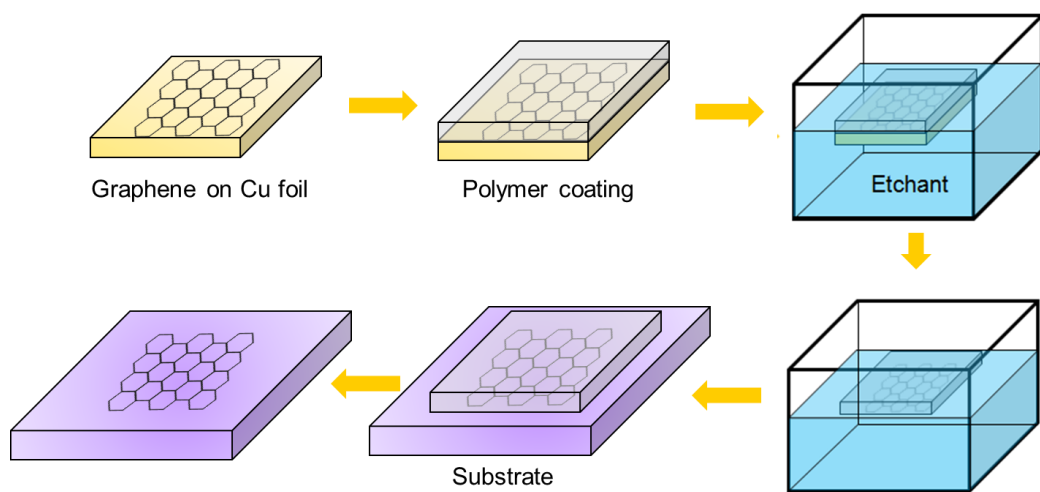
Figure 1-8. Wet-transfer process.

Properties	Mechanical cleavage	Liquid-phase exfoliation	Selective Si sublimation of SiC	CVD
Scalability	Few um	Unlimited	SiC wafer scale	Metal catalyst scale
Graphene size	Single crystal	Very small (~nm)	Large	~ sub cm
Quality	Highest	Low	High	High
Cost	-	Cheap	Expensive	Cheap
Transfer simplicity (industrial point of view)	-	Easy	Hard	Easy

Table 1-2. Comparison of graphene synthesis method.

References

1.   Ruess, G.; Vogt, F., Höchstlamellarer Kohlenstoff aus Graphitoxyhydroxyd. *Monatshefte für Chemie und verwandte Teile anderer Wissenschaften* **1948,** *78* (3), 222-242.

2.   Hamwi, A.; Mouras, S.; Djurado, D.; Cousseins, J. C., New synthesis of first stage graphite intercalation compounds with fluorides. *Journal of Fluorine Chemistry* **1987,** *35* (1), 151.

3.   DiVincenzo, D. P.; Mele, E. J., Self-consistent effective-mass theory for intralayer screening in graphite intercalation compounds. *Phys Rev B* **1984,** *29* (4), 1685-1694.

4.   Geim, A. K.; Novoselov, K. S., The rise of graphene. *Nat Mater* **2007,** *6* (3), 183-191.

5.   Kim, K. S.; Zhao, Y.; Jang, H.; Lee, S. Y.; Kim, J. M.; Kim, K. S.; Ahn, J.-H.; Kim, P.; Choi, J.-Y.; Hong, B. H., Large-scale pattern growth of graphene films for stretchable transparent electrodes. *Nature* **2009,** *457* (7230), 706-710.

6.   Novoselov, K. S.; Geim, A. K.; Morozov, S. V.; Jiang, D.; Zhang, Y.; Dubonos, S. V.; Grigorieva, I. V.; Firsov, A. A., Electric field effect in atomically thin carbon films. *Science* **2004,** *306* (5696), 666-669.

7.   Cooper, D. R.; D'Anjou, B.; Ghattamaneni, N.; Harack, B.; Hilke, M.; Horth, A.; Majlis, N.; Massicotte, M.; Vandsburger, L.; Whiteway, E.; Yu, V., Experimental Review of Graphene. *ISRN Condensed Matter Physics* **2012,** *2012*, 501686.

8.   Avouris, P., Graphene: Electronic and Photonic Properties and Devices. *Nano Lett* **2010,** *10* (11), 4285-4294.

9.   Wallace, P. R., The Band Theory of Graphite. *Phys Rev* **1947,** *71* (9), 622-634.

10.   Semenoff, G. W., Condensed-Matter Simulation of a Three-Dimensional Anomaly. *Phys Rev Lett* **1984,** *53* (26), 2449-2452.

11.   Bolotin, K. I.;   Sikes, K. J.;   Jiang, Z.;   Klima, M.;   Fudenberg, G.;   Hone, J.;   Kim, P.; Stormer, H. L., Ultrahigh electron mobility in suspended graphene. *Solid State Commun* **2008,** *146* (9-10), 351-355.

12.   Eletskii, A. V.;   Iskandarova, I. M.;   Knizhnik, A. A.; Krasikov, D. N., Graphene: fabrication methods and thermophysical properties. *Phys-Usp+* **2011,** *54* (3), 227-258.

13.   Li, X.;   Zhang, G.;   Bai, X.;   Sun, X.;   Wang, X.;   Wang, E.; Dai, H., Highly conducting graphene sheets and Langmuir–Blodgett films. *Nat Nanotechnol* **2008,** *3* (9), 538-542.

14.   Hernandez, Y.;   Nicolosi, V.;   Lotya, M.;   Blighe, F. M.;   Sun, Z.;   De, S.;   McGovern, I. T.;   Holland, B.;   Byrne, M.;   Gun'Ko, Y. K.;   Boland, J. J.;   Niraj, P.;   Duesberg, G.;   Krishnamurthy, S.;   Goodhue, R.;   Hutchison, J.;   Scardaci, V.;   Ferrari, A. C.; Coleman, J. N., High-yield production of graphene by liquid-phase exfoliation of graphite. *Nat Nanotechnol* **2008,** *3* (9), 563-568.

15.   Vallés, C.;   Drummond, C.;   Saadaoui, H.;   Furtado, C. A.;   He, M.;   Roubeau, O.;   Ortolani, L.;   Monthioux, M.; Pénicaud, A., Solutions of Negatively Charged Graphene Sheets and Ribbons. *Journal of the American Chemical Society* **2008,** *130* (47), 15802-15804.

16.   Muehlhoff, L.;   Choyke, W. J.;   Bozack, M. J.;   Jr., J. T. Y., Comparative electron spectroscopic studies of surface segregation on SiC(0001) and SiC(000Ī). *J Appl Phys* **1986,** *60* (8), 2842-2853.

17.   Hass, J.;   de Heer, W. A.; Conrad, E. H., The growth and morphology of epitaxial multilayer graphene. *Journal of Physics: Condensed Matter* **2008,** *20* (32), 323202.

18.   Li, L.; Tsong, I. S. T., Atomic structures of 6H   SiC (0001) and (0001̄) surfaces. *Surf Sci* **1996,** *351* (1), 141-148.

19.   Forbeaux, I.;   Themlin, J. M.;   Charrier, A.;   Thibaudau, F.; Debever, J. M., Solid-state graphitization mechanisms of silicon carbide 6H–SiC polar faces. *Appl Surf Sci* **2000,** *162-163*, 406-412.

20.   Kaplan, R., Surface structure and composition of β- and 6H-SiC. *Surf Sci* **1989,** *215* (1), 111-134.

21.   Johansson, L. I.;   Owman, F.; Mårtensson, P., High-resolution core-level study of 6H-SiC(0001). *Phys Rev B* **1996,** *53* (20), 13793-13802.

22.   Liu, N.;   Fu, L.;   Dai, B.;   Yan, K.;   Liu, X.;   Zhao, R.;   Zhang, Y.; Liu, Z., Universal Segregation Growth Approach to Wafer-Size Graphene from Non-Noble Metals. *Nano Lett* **2011,** *11* (1), 297-303.

23.   Losurdo, M.;   Giangregorio, M. M.;   Capezzuto, P.; Bruno, G., Graphene CVD growth on copper and nickel: role of hydrogen in kinetics and structure. *Phys Chem Chem Phys* **2011,** *13* (46), 20836-20843.

24.   Park, H. J.;   Meyer, J.;   Roth, S.; Skakalova, V., Growth and properties of few-layer graphene prepared by chemical vapor deposition. *Carbon* **2010,** *48* (4), 1088-1094.

25.   Reina, A.;   Jia, X.;   Ho, J.;   Nezich, D.;   Son, H.;   Bulovic, V.;   Dresselhaus, M. S.; Kong, J., Large Area, Few-Layer Graphene Films on Arbitrary Substrates by Chemical Vapor Deposition. *Nano Lett* **2008,** *9* (1), 30-35.

26.   Li, X. S.;   Cai, W. W.;   An, J. H.;   Kim, S.;   Nah, J.;   Yang, D. X.;   Piner,

R.; Velamakanni, A.; Jung, I.; Tutuc, E.; Banerjee, S. K.; Colombo, L.; Ruoff, R. S., Large-Area Synthesis of High-Quality and Uniform Graphene Films on Copper Foils. *Science* **2009,** *324* (5932), 1312-1314.

27. Bae, S.; Kim, H.; Lee, Y.; Xu, X.; Park, J.-S.; Zheng, Y.; Balakrishnan, J.; Lei, T.; Ri Kim, H.; Song, Y. I.; Kim, Y.-J.; Kim, K. S.; Ozyilmaz, B.; Ahn, J.-H.; Hong, B. H.; Iijima, S., Roll-to-roll production of 30-inch graphene films for transparent electrodes. *Nat Nano* **2010,** *5* (8), 574-578.

28. Li, X.; Zhu, Y.; Cai, W.; Borysiak, M.; Han, B.; Chen, D.; Piner, R. D.; Colombo, L.; Ruoff, R. S., Transfer of Large-Area Graphene Films for High-Performance Transparent Conductive Electrodes. *Nano Lett* **2009,** *9* (12), 4359-4363.

29. Lin, Y.-C.; Lu, C.-C.; Yeh, C.-H.; Jin, C.; Suenaga, K.; Chiu, P.-W., Graphene Annealing: How Clean Can It Be? *Nano Lett* **2011,** *12* (1), 414-419.

30. Park, S.; Ruoff, R. S., Chemical methods for the production of graphenes. *Nat Nanotechnol* **2009,** *4* (4), 217-224.

CHAPTER 2.

Limiting factors in CVD graphene growth

2.1. Electrical property of CVD graphene

As reviewed in chapter 1, electrical property of CVD graphene show better quality comparing with other graphene synthesis methods, however, still it is hard to meet the electrical property from single crystal graphene which collected from mechanical cleavage method. To identify electrical property of CVD graphene, about 150 graphene sample were prepared by Low Pressure CVD (LPCVD) process having ~50 um of grain size. After LPCVD growth, samples were transferred to 285 nm SiO_2/Si substrate with 1 square centimeter size and Au/Ti contact pad was deposited on each corner to make Van der Pauw structure. Hall measurement were conducted to estimated electrical property of LPCVD graphene. The histogram for electrical property of CVD graphene is shown in **Figure 2-1**. The average R_s of CVD graphene show 509±133 ohm/sq, and carrier concentration and carrier mobility show $1.70 \times 10^{13} \pm 0.62 \times 10^{13}$ /cm², 862±354 cm²/Vs, respectively. Considering single crystal graphene show 200,000 cm²/Vs of mobility and ~2×10¹¹ /cm² of carrier concentration, with the ~150 ohm/sq of R_s[1], CVD graphene has degraded electrical property compare to single crystal graphene. even though carrier concentration increased from 2 orders higher, the drastic mobility decrease give rise the R_s of CVD graphene. Besides CVD graphene from our lab, the 16 reported electrical property of CVD graphene were summarized in **Figure 2-2**.[2-17] In measurement of electrical property of graphene, the sample size could be key issue in showing its electrical property, *i.e.*, measuring R_s of few um of graphene are not large enough to estimate CVD graphene which has few ~ dozens of grain size, and the grain boundary effect on R_s possibly does not show in result because of the its measurement scale. Therefore, for reliability of electrical

property of CVD graphene, relatively large sample measured articles are selected for representative CVD graphene. As it can be shown in **Figure 2-2**, the average R_s of CVD graphene show 536 ± 334 ohm/sq which is similar to our average R_s value.
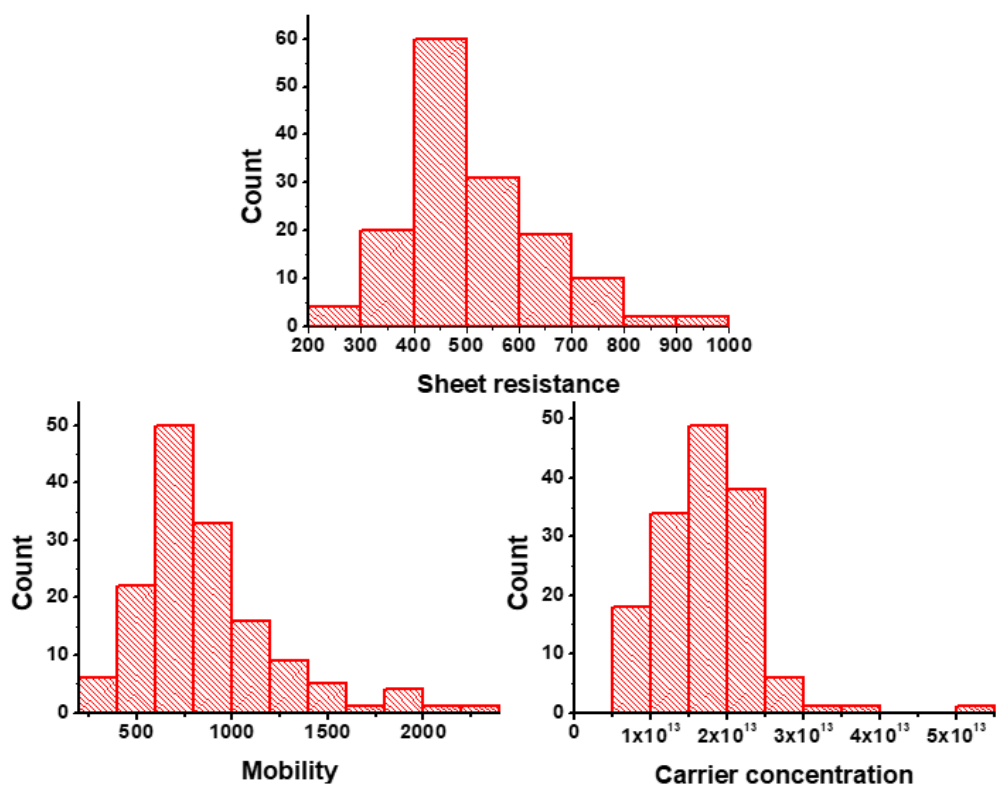
Figure 2-1. Electrical property of CVD graphene grown in Nano Fabrication laboratory.

(NFL)
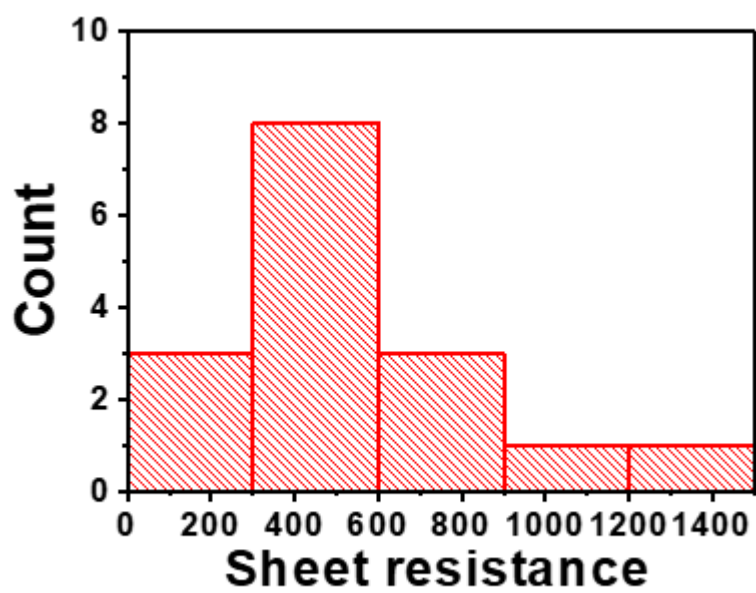
Figure 2-2. Electrical property of reported CVD graphene.

2.2. Limiting factors in CVD growth graphene

So far, the origin for degradation of electrical property in CVD graphene is not systematically established by numerical formula, some factors such as substrate, grain boundary and defects, are intensively studied and confirmed as scattering factor in CVD graphene. Therefore, according to so far reported degradation factors on CVD graphene, electrical property of graphene can be divided into 4 terms as follows

$$R_S = R_S^{bulk} + R_S^{sub} + R_S^{GB} + R_S^{etc.}$$

Here, R_S is total sheet resistance of graphene, R_S^{bulk} is bulk sheet resistance of graphene which from the lattice phonon scattering of graphene lattice, R_S^{sub} is the sheet resistance from substrate scattering, R_S^{GB} is sheet resistance from graphene grain boundary, and other factors which raise sheet resistance of graphene express as $R_S^{etc.}$.

2.2.1. Lattice phonon scattering

Lots of electrical property of behavior of graphene is similar to that of metal electrical property, therefore, understanding electrical property of metal is beneficial to understanding electrical behavior of graphene. For instance, the temperature dependence of the bulk resistivity of metal are originated by electron and lattice phonon scattering mechanism, and known to follow Bloch-Grüneisen model[18].

$$\rho(T) = A\left(\frac{T}{\theta_R}\right)^n \int_o^{\theta_R/T} \frac{t^n}{(e^t - 1)(1 - e^t)} dt$$

Here, ρ is resistivity of metal, T is temperature, θ_R is Bloch-Grüneisen temperature which is very closely matches the value of Debye temperature. According to Bloch-

Grüneisen model, resistivity of metal has different temperature dependence on the basis of electron and phonon momentum. At low-enough temperature, T < θ_R, where the electron momentum which lies on Fermi surface with the value of $\hbar k_F$, higher than lattice thermal phonon, $k_B T / v_s$, then, the electron only scatters in small angle and resistance of metal (R) proportional to T^5, R$\propto$ T^5. (v_s is sound velocity) On the other hand, if temperature is high-enough and lattice thermal phonon interact with electron strongly, and the electron experience large angle scattering events and resistance of metal proportional to temperature, R R$\propto$T. At certain temperature, the momentum of electron and lattice phonon are coherent and this temperature is called Bloch-Grüneisen temperature as illustrated in **Figure 2-3** and **Figure 2-4**. Graphene is also known to follows Bloch-Grüneisen model[19-21] like normal metal, and the Bloch-Grüneisen temperature of graphene is calculated as 8 K and above ~20 K, resistivity of graphene shows linear temperature dependency according to the numerical calculation.[21] Above 20 K, the resistivity of graphene is determined by longitudinal acoustic (LA) phonon scattering,[21-23] and independent of carrier density as follows,[20]

$$\rho(V_g, T) = \rho_0(V_g) + \rho_A(T)$$

$$\rho_A(T) = \left(\frac{h}{e^2}\right) \frac{\pi^2 D_A^2 k_B T}{2 h^2 \rho_s v_s^2 v_F^2}$$

where, ρ_0 is residual resistivity of graphene, ρ_A is the resisvity due to the LA phonon scattering, V_g is gate voltage, k_B is Boltzman constant, ρ_s is 2-D mass density of graphene, 7.6×10^{-7} kg/m^2, v_F is the Fermi velocity and D_A is the acoustic deformation potential. Except the V_g and T, other parameters are constant, resistivity of graphene shows linear temperature dependency. The experimental value for resistivity of graphene is in

Figure 2-5 by fabricating field effect (FE) device on the single crystal graphene transferred on SiO2 substrate. To collect temperature dependence of graphene resistivity in the point of phonon scattering, measurement was performed in ultrahigh vacuum (UHV) to minimize molecular adsorption and desorption. other scattering factors should be removed.[20] In **Figure 2-5**, until 100 ~ 150 K, experimental data and the equation of LA phonon scattering of graphene is well matched, however, above certain temperature (*i.g.*, >150 K), resistivity of graphene is higher than numerical calculation because of the substrate scattering. In FE device, graphene has different electrical property from each applied gate voltage, since carrier concentration of graphene is proportional to applied gate, $n_S = c_g V_g / e$, n_S is sheet carrier density of graphene, and c_g is gate capacitance with 1.15×10^{-8} F/cm^2. Therefore, to compare electrical property of graphene, normally, n_S is set to ~ 10^{12} /cm^2. At $V_g = 14$ V, n_S is about 10^{12} /cm^2, then expected carrier mobility of graphene can be calculated from LA phonon scattering equation, then, the mobility μ at room temperature (RT) is 200,000 cm^2/Vs. Therefore, considering LA phonon scattering only, the sheet resistance of graphene at RT condition can be calculated as

$$R_S^{bulk} = \frac{1}{n_S q u} = \frac{1}{[10^{12} \ /cm^2] q [200000 \ cm^2/Vs]} = 31 \ ohm/sq$$
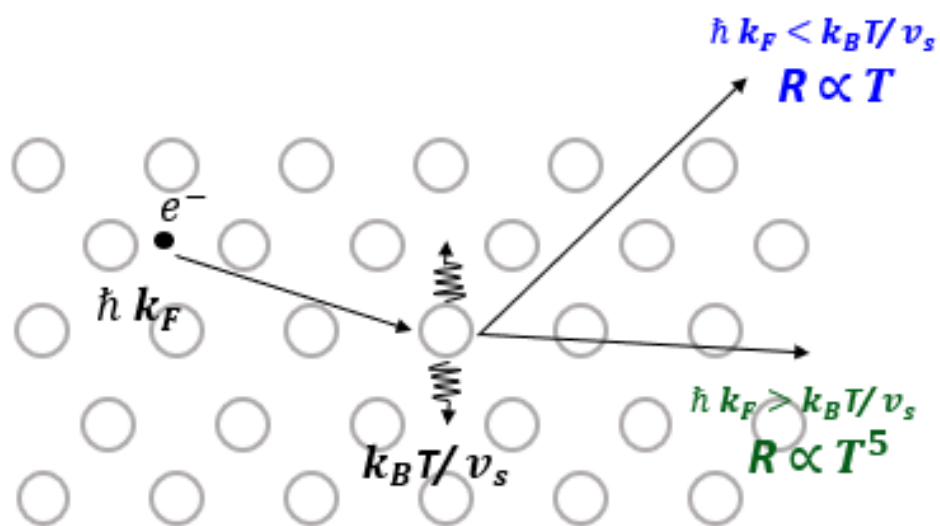
Figure 2-3. Illustration of electron and phonon scattering with small angle ($\hbar k_F > k_B T/v_s$) and large angle ($\hbar k_F < k_B T/v_s$).
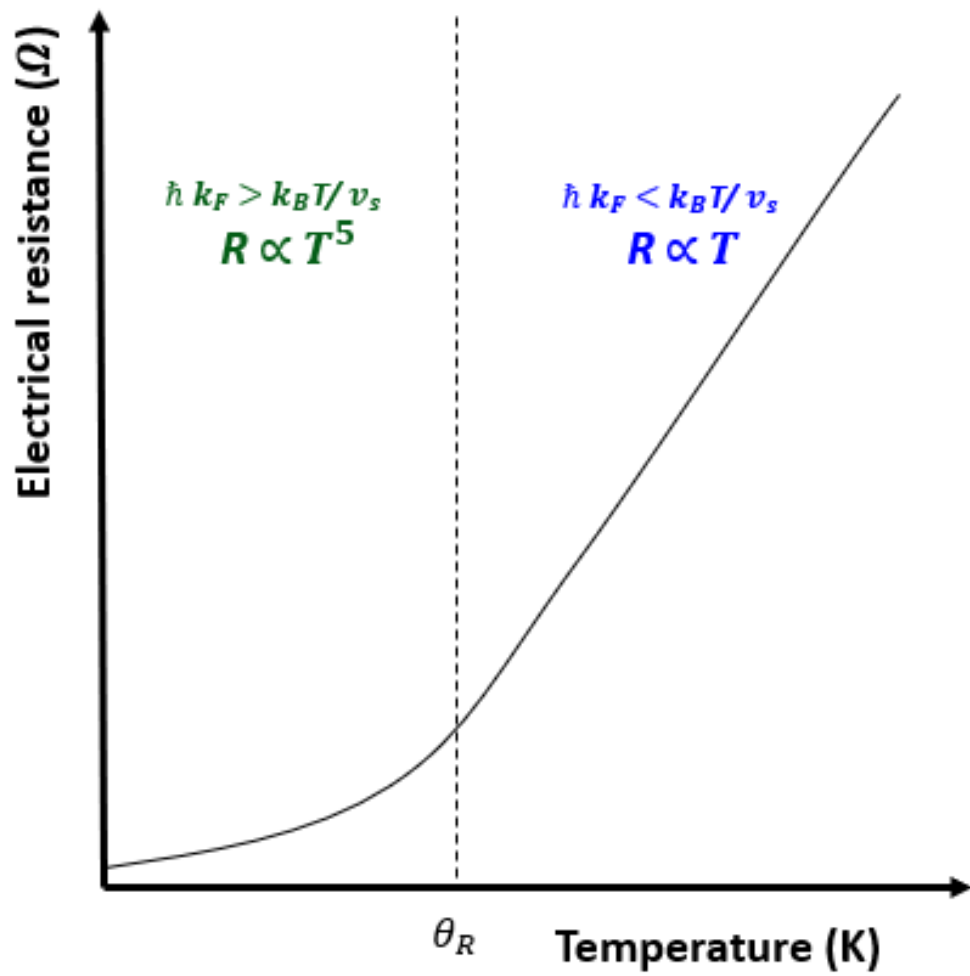
Figure 2-4. Temperature dependence of metal electrical resistivity.
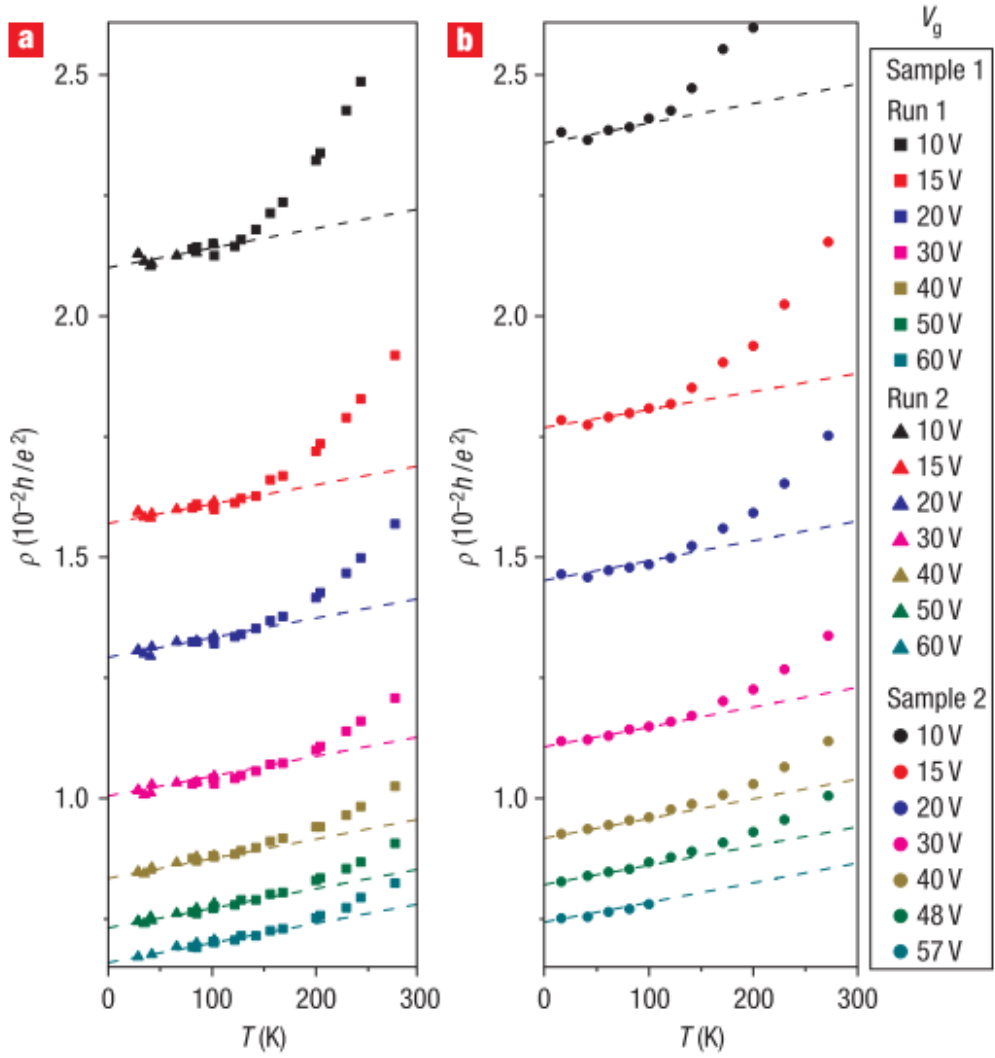
Figure 2-5. Temperature-dependent of graphene on SiO_2. (a) and (b) show the resistivity of the sample 1, and sample 2, respectively. The Dash lines are fit to equation of acoustic phonon scattering. [20]

2.2.2. Substrate scattering

In the graphene, above temperature 100~150 K, the temperature is high enough and the carrier in graphene possibly interact with substrate surface. Within the few nm ranges, it is known that the SiO_2 surface polar phonon can interact with surface material remotely[24], the carriers in graphene inelastically interact to two strongest surface optical phonon modes in SiO_2[25]. $(\hbar\omega_1 \approx 59 \text{ meV}, \hbar\omega_2 \approx 155 \text{ meV})$[25, 26] Since, the scattering occurs not in the graphene itself but in between graphene and SiO_2 substrate remotely, it is called remote interfacial phonon (RIP) scattering. Considering LA phonon scattering and RIP scattering, the temperature dependence of graphene resistivity is as follows, [20]

$$\rho\left(V_g, T\right) = \rho_0\left(V_g\right) + \rho_A(T) + \rho_B\left(V_g, T\right)$$

$$\rho_{B1}\left(V_g, T\right) = B_1 V_g^{-\alpha 1}\left(\frac{s_1}{e^{\hbar\omega_1/k_B T} - 1} - \frac{s_2}{e^{\hbar\omega_2/k_B T} - 1}\right)$$

Or

$$\rho_{B2}\left(V_g, T\right) = B_2 V_g^{-\alpha 2}\left(\frac{1}{e^{E_0/k_B T} - 1}\right)$$

$\rho_B\left(V_g, T\right)$ is the resistivity of graphene expressing RIP considering two strongest SiO_2 optical polar phonon as Bose-Einstein distribution (ρ_{B1}), or a single Bose-Einstein distribution. (ρ_{B2}) B and α are global parameters having B_1=0.607(h/e^2) $V^{\alpha 1}$, $\alpha 1 = 1.04$, B2=0.607(h/e2) $V^{\alpha 2}$, $\alpha 2$=1.04, and s is scattering ratio in two strongest SiO_2 optical polar phonon with 1:6.5, E_0 is fitted to 104 meV. The same experimental result in **Figure 2-5** were fitted to LA phonon scattering and RIP scattering in **Figure 2-6**, here, even above 100~150 K of temperature, experimental resistivity of graphene is well fitted to numerical calculation considering LA phonon and RIP scattering. At RT condition, the carrier mobility shows 40,000 cm^2/Vs, therefore, R_s^{sub} can be calculated as,

$$R_S^{bulk} + R_S^{sub} = 156 \ ohm/sq$$

$$R_S^{sub} = 125 \ ohm/sq$$
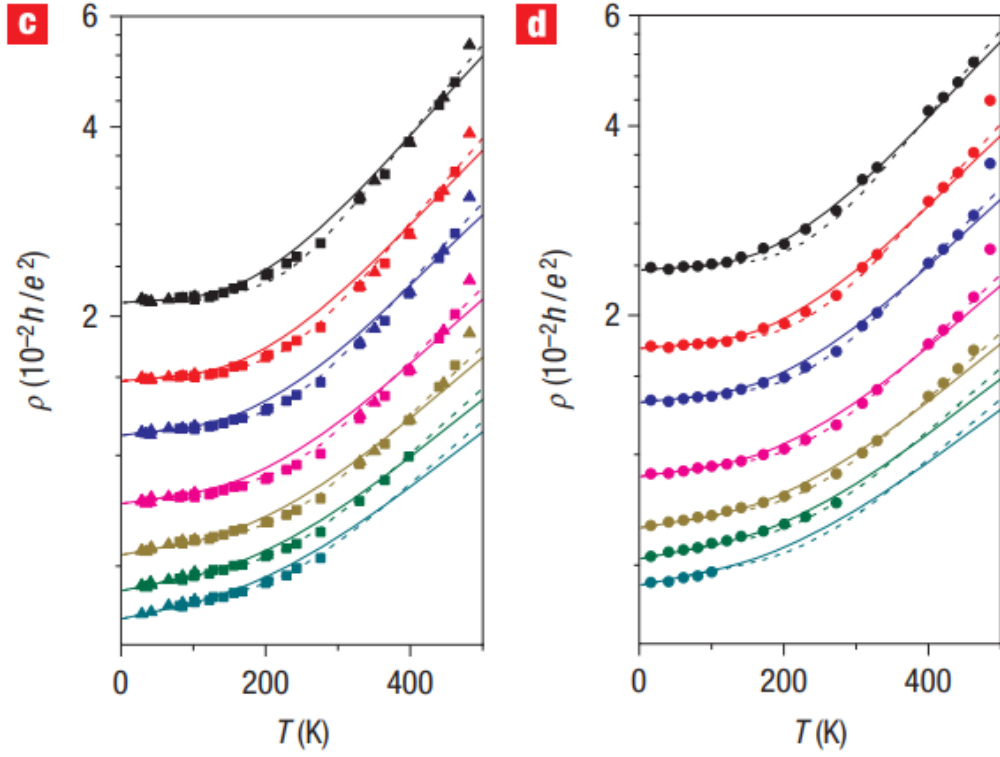
Figure 2-6. Temperature-dependent of graphene on SiO_2. (a) and (b) show the resistivity of the sample 1, and sample 2, respectively. The dash lines are fit to $\rho_0(V_g) + \rho_A(T) + \rho_{B1}(V_g, T)$ and solid lines are fit to $\rho_0(V_g) + \rho_A(T) + \rho_{B2}(V_g, T)$.[20]

2.2.3. Grain boundary scattering

When graphene nuclei formed during CVD growth, each nucleus has random orientation. After full growth of graphene, because grains have its own orientation, grain boundary is formed between grains as illustrated in **Figure 2-7**.[27] When the grain boundaries are formed, because each nucleus has different orientation, grain boundaries cannot be in the form of hexagonal ring, rather in the form of hepta-, penta-, and other polygon shape. Graphene is bonded with *sp2* covalent bonding, therefore when the grain boundaries are formed, hexagonal form tend to form relatively stable hepta-, penta-bonding, having Stone-Wales grain boundary. (See **Figure 2-8**)[28] However, also voids, cracks and other polygon shape also exist on graphene grain boundaries as it can be seen in **Figure 2-9**.[29] Those graphene grain boundaries are considered to strong scattering center and one of the main degradation factors of electrical property of graphene, intensive studies were conducted by numerous researchers.[30-34] For instance, in **Figure 2-10**, two hexagonal grains formed single grain boundary and electrical measurement were conducted to evaluated graphene grain boundary. According to this article, each grain has 550 (left grain) and 550 Ω (right grain) of resistance while 3000 Ω was measured from inter-grain resistance measurement.[31] In another reports, graphene with larger grain size shows more reduced sheet resistance as shown in **Figure 2-11**,[32] since larger grain sized graphene has less grain boundary scattering centers and accordingly larger grain sized graphene has enhance carrier mobility as shown in **Figure 2-12**.[33] As described above, numerous studies for CVD graphene grain boundary proved that grain boundary acts as a scattering center in electrical property of graphene, degrading its sheet resistance and carrier mobility.
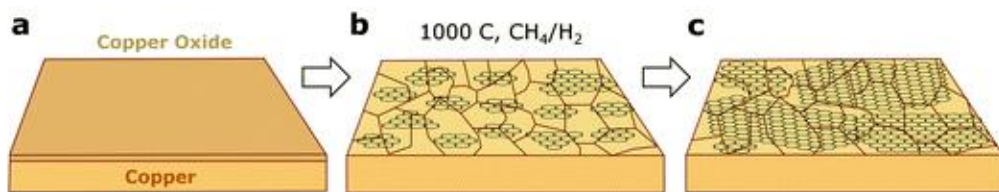
Figure 2-7. Schematic illustration of graphene growth on Cu by CVD. (a) Cu foil with native copper oxide. (b) Initial stage of graphene growth, nucleus formed with random position and orientation. (c) Fully covered graphene growth, with grain boundary formation.
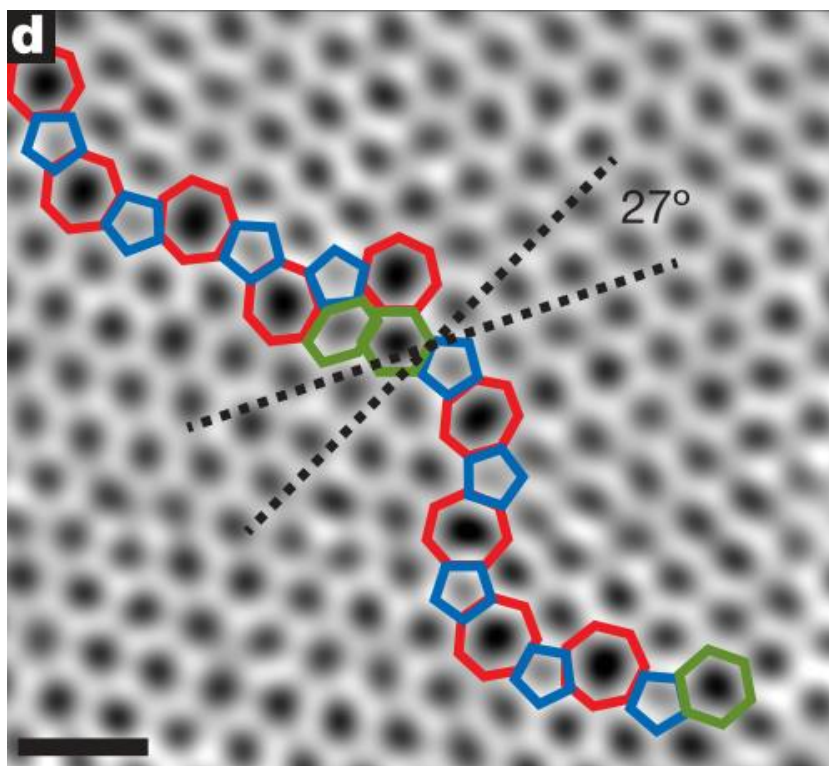
Figure 2-8. Stone-Wales graphene grain boundary observed in high resolution transmission electron microscopy (HR-TEM) image. Grains are mis-aligned with 27 degrees, and grain boundaries consist of penta- and heptagon.
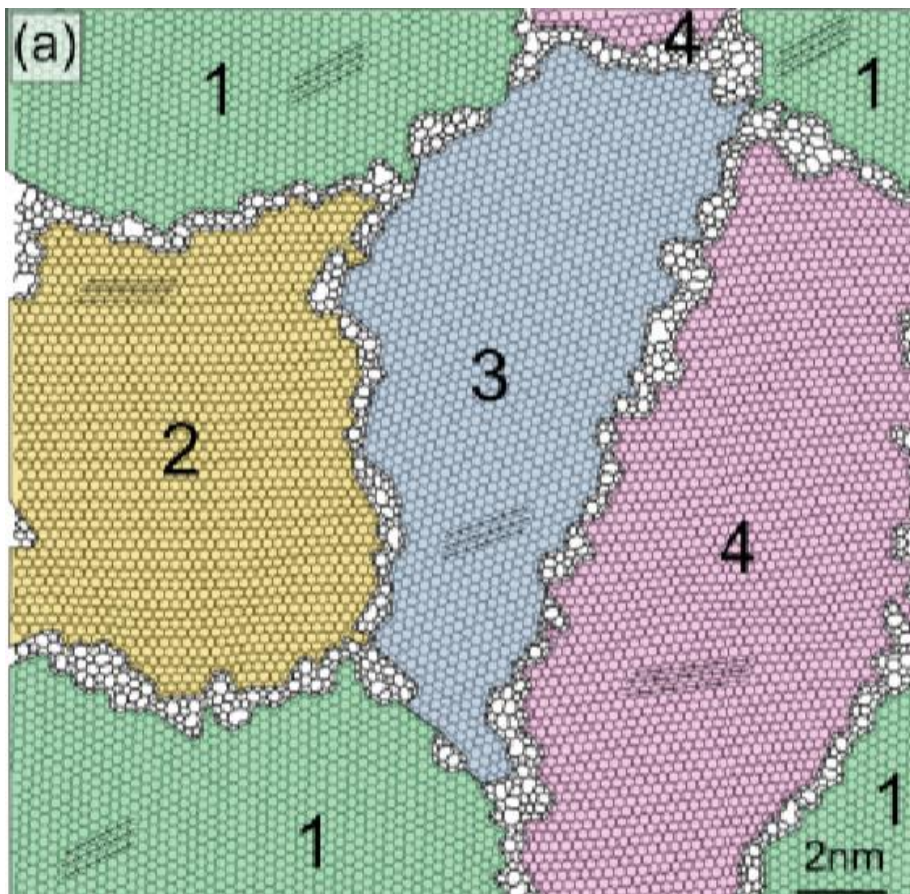
Figure 2-9. Various form of graphene grain boundary in polycrystalline CVD graphene.
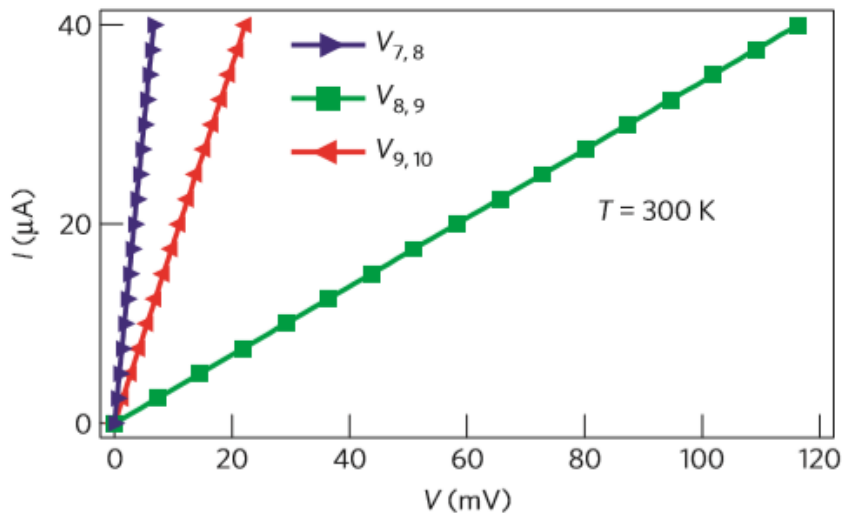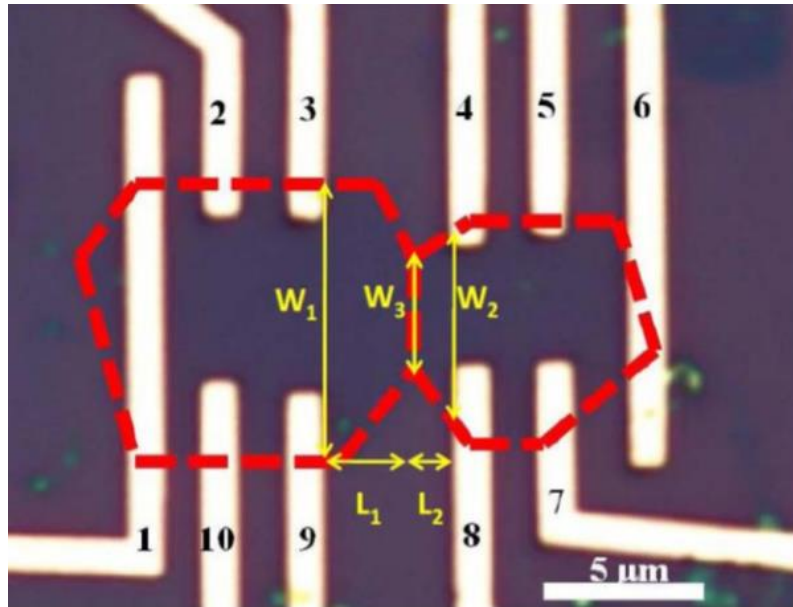
Figure 2-10. Resistance measurement inside of grains, and in between graphene grains. [31]
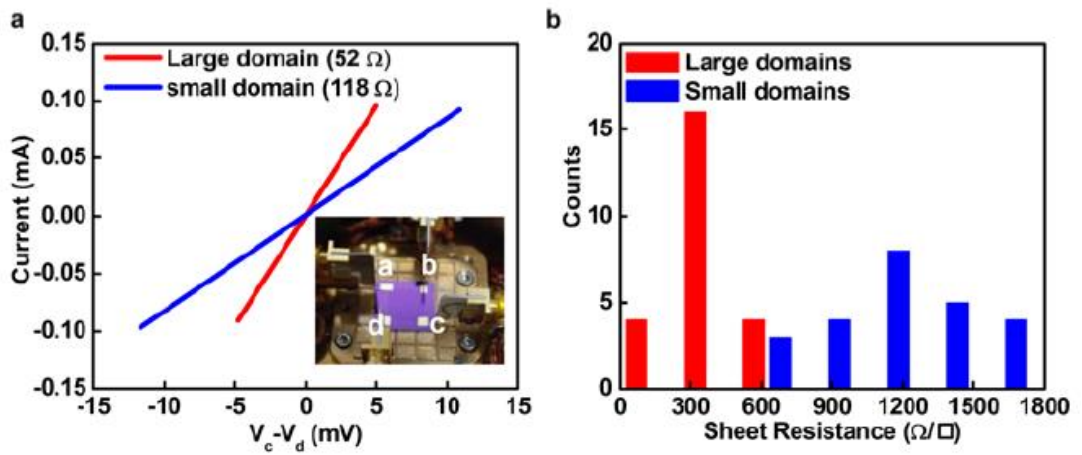
Figure 2-11. (a) The current measurement and (b) the histogram of sheet resistance of graphene with two different grain size. Small domains have 50 um, and large domains has 2 mm size of graphene.
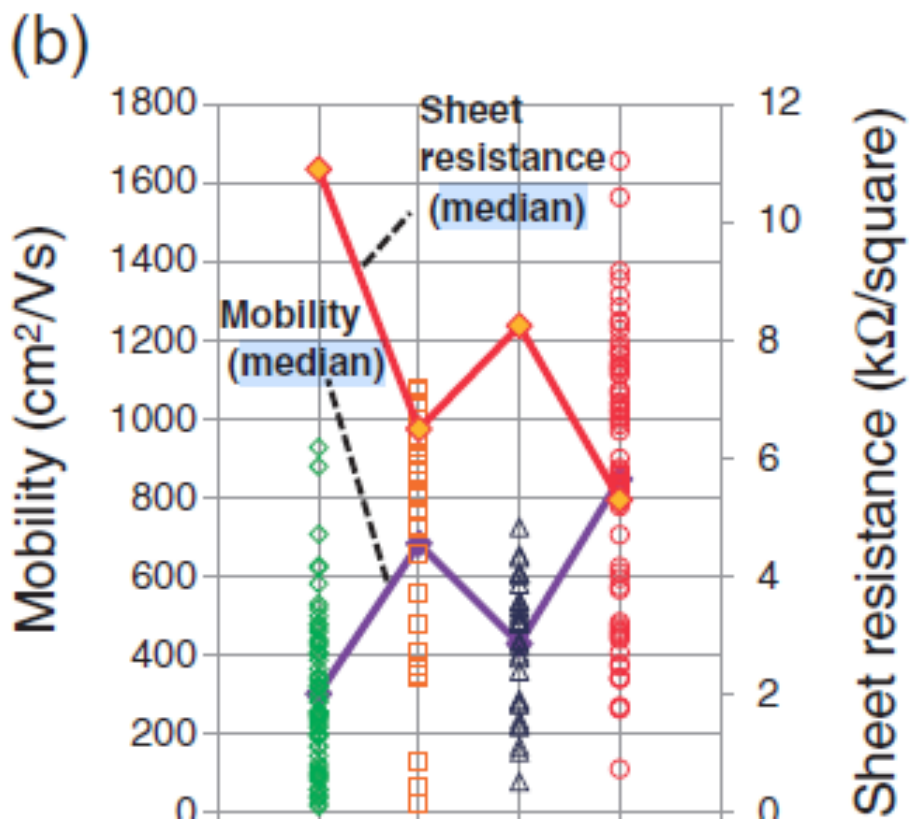
Figure 2-12. Sheet resistance and carrier mobility of graphene with different grain size. In the x-axis, grain size is 0.1, 1.2, 1.2, 4.5 um in sequence.

2.2.4. Other scattering factors

Besides substrate, grain boundary scattering many other scattering factors can exist during CVD growth such as impurity scattering and scattering by other defects. Also, CVD graphene is originally grown on metal catalyst like Cu, as illustrated in **Figure 2-7**, to use graphene as an electrode, transfer process to insulating substrate is required. But the transfer process itself is very complex as **Figure 1-8**[35]. First, graphene grown on Cu foil is spin coated by polymer material such as poly methyl methacrylate (PMMA) and floated in Cu etchant solution. Because of lower density of PMMA (than Cu etchant) and surface tension enable PMMA/graphene/Cu foil float on Cu etchant. After enough process time, Cu foil etched away and only PMMA/graphene layer floated on Cu etchant. Then PMMA/graphene layer scooped by SiO$_2$/Si substrate, and dry PMMA/graphene/SiO$_2$/Si. After dry enough, polymer material removed by acetone solution, transfer process is completed. During transfer process, lots of unwanted damage can be generated during transfer process such as cracks[36] and residue of supporting polymer material[37], and these factors are also act as electrical property degrading ingredient as shown in **Figure 2-13**. Besides those cracks and residues, graphene layer is contaminated by impurities during transfer process and atmospheric environment. And impurities are also one of the strong scattering factors,[38-40]

$$\sigma(n) = Ce \left| \frac{n}{n_{imp}} \right|, \ n_{imp} = \frac{C}{\mu}$$

where, σ is conductivity, C is constant, n is carrier concentration, n_{imp} is concentration of charge impurities and μ is carrier mobility. The concentration of impurity inversely proportional to its carrier mobility as shown in **Figure 2-14**, therefore adsorption of

charged impurities inevitably decreased mobility of graphene and degrade electrical property. In addition to transfer and impurities, defects such as void during graphene growth[41] and wrinkles after transfer process also observed and possibly candidates for lower quality of CVD graphene. (**Figure 2-15**)
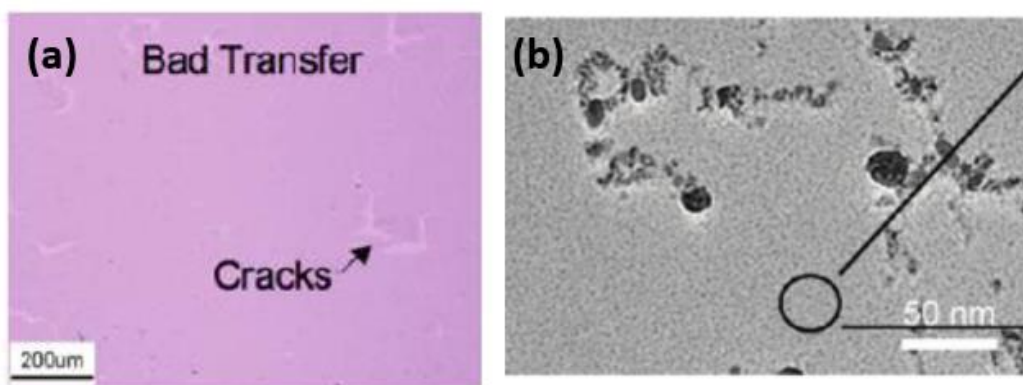
Figure 2-13. (a) optical microscopy image of CVD graphene after transfer process. Cracks are additionally generated and observed after transfer.[36] (b) TEM image of CVD graphene after transfer process, and PMMA residue exist on graphene layer.[37]
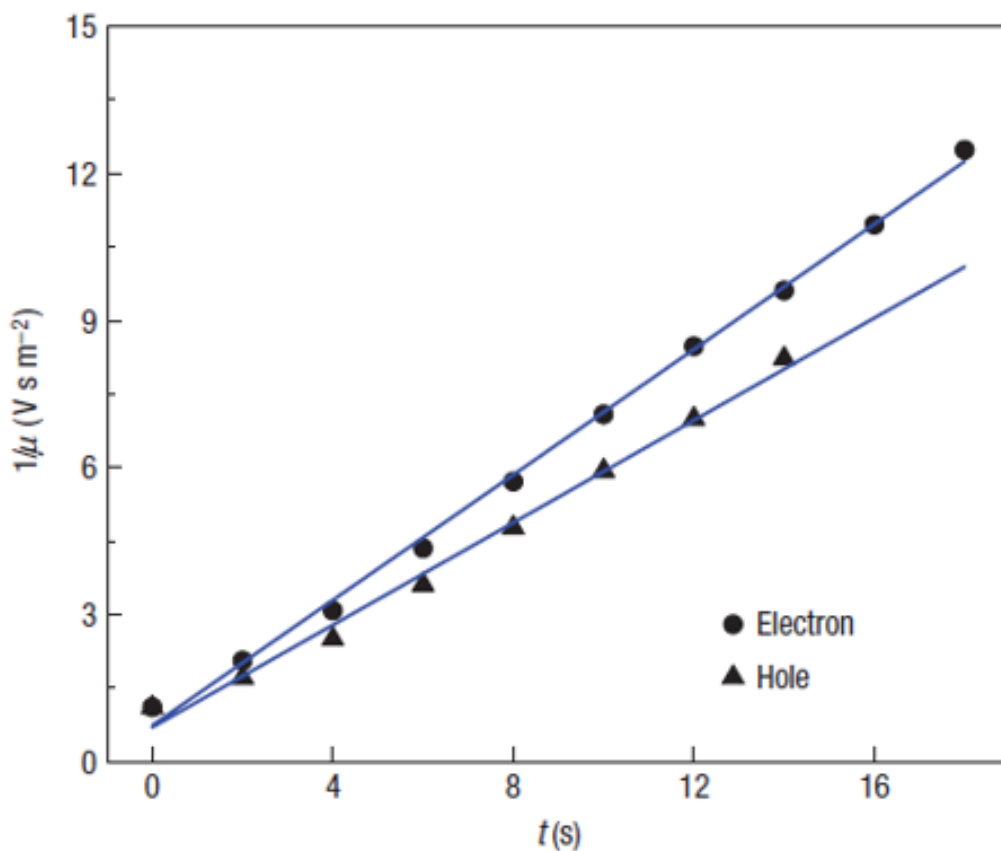
Figure 2-14. 1/μ vs time graph of K atom deposition in UHV system. As the time goes by, K atoms deposited on graphene layer and the carrier mobility decreased with 5×10^{15}/Vs of C.[38]
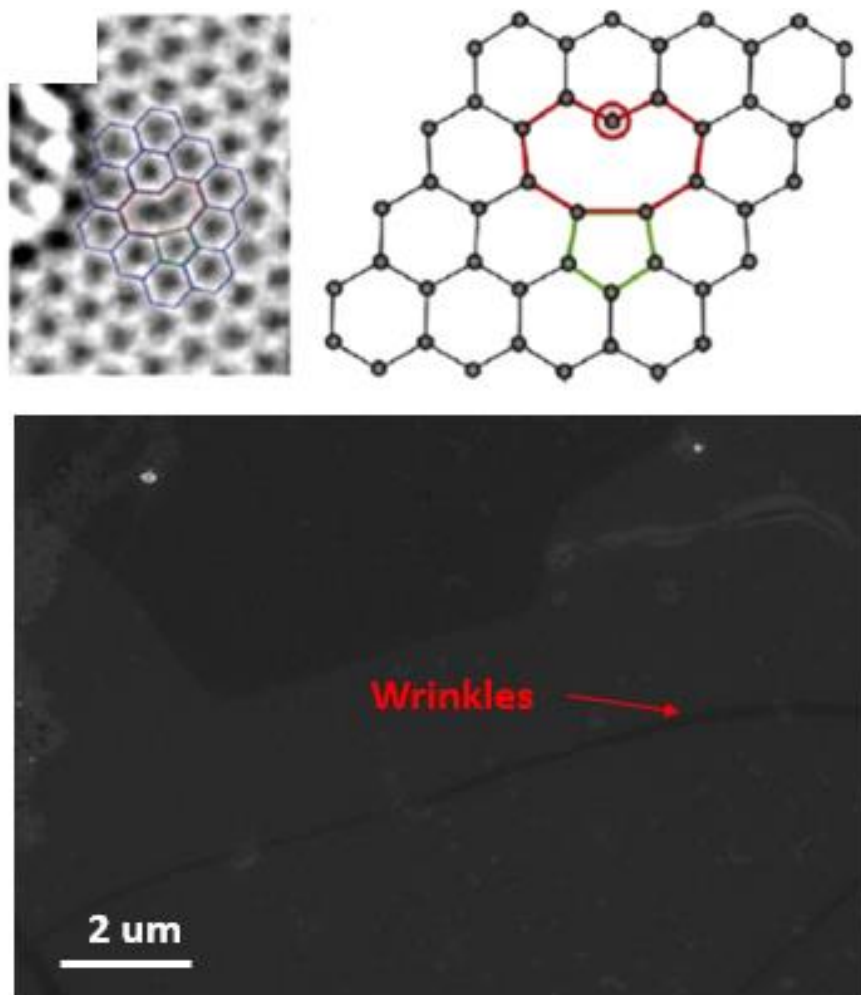
Figure 2-15. HR-TEM image of single void on graphene layer (upper image)[41] and SEM image of wrinkle in graphene layer. (downer image) Hexagonal dark image is additional double layer of graphene in SEM.

2.3. Approaches enhancing electrical property of CVD graphene

   To overcome those electrically limiting factors in CVD graphene, many researches performed in various limiting factors. In the case of RIP scattering (substrate scattering, R_s^{sub}), for example, the carrier mobility decreased from 200,000 cm^2/Vs to 40,000 cm^2/Vs in the presence of SiO$_2$ substrate.[1, 20] When graphene is transfer to different substrate such as hexagonal boron nitride (h-BN) or hexamethyl disilazane (HMDS), the carrier mobility reported to have 15,000 ~ 20,000 cm^2/Vs and 12,000 cm^2/Vs, respectively. [42, 43] Regarding that the suspended graphene (without any substrate) shows 230,000 cm2/Vs[1], existence of substrate cause decrease in carrier mobility, however, choice of substrate could minimize mobility degradation of graphene. Also, to reduce grain boundary scattering of graphene (R_s^{GB}), efforts to increase grain size of graphene was intensively studied. Finally, to minimize damage from transfer process ($R_s^{etc.}$), other transfer or clean transfer process was developed[16, 36, 37, 44, 45] and direct graphene growth process which grow graphene directly on substrate was also reported. [46-52]

   Among lots of efforts were made to overcome limiting factors, two distinguishable method dominantly researched, doping and increase of graphene grain size. Graphene is known to easily doped by electron transfer when it is contact with dopant. Dopant molecular doping by dipping, spin-coating process or metal/metal oxide dopant deposition enable doping of graphene, and a lot of articles report reduced sheet resistance of graphene after doping process as summarized in **Table 2-1**.[16, 53-57] Increase of grain size of graphene was continuously reported since its first CVD growth on Cu foil on 2009 [58] as shown in **Figure 2-16**.[31, 58-72] Recently, sub-centimeter scale of graphene growth is enabled by

smoothing of prepared Cu foil surface and reducing carbon source supply.[62, 64, 67, 71, 72] So far, to minimize graphene grain boundary scattering, grain size is increased up to sub-centimeter scale, and electrical property measurement also intensively studied as summarized in **Table 2-2**. However, electrical property values in **Table 2-2**. are mainly focused on mm scale of large grain itself, not on the graphene grain boundary, the portion of graphene grain boundary is quite unknown. Few articles are reporting the sheet resistance and other electrical properties in the sense of grain size of graphene,[34, 73] these articles are usually having graphene grain size in very short ranges (*i.e.*, from 1 um ~ 2 um). Therefore, to understand effect of graphene grain boundary, relatively large range of grain size needs to analyze (at least few um ~ sub 100 um). The equation of total sheet resistance of graphene as follows,

$$R_S = R_S^{bulk} + R_S^{sub} + R_S^{GB} + R_S^{etc.}$$

$$R_S = [R_S^{bulk} + R_S^{sub} + R_S^{etc.}] + R_S^{GB}$$

$$R_S = R_S^{G} + R_S^{GB}$$

$$R_S^{grain} = [R_S^{bulk} + R_S^{sub} + R_S^{etc.}]$$

R_S^{grain} is divided into grain (R_S^{G}) and grain boundary sheet resistance (R_S^{GB}). And various grain sized graphene was synthesized in Chapter 3, further analysis of graphene grain boundary effect was made in Chapter 4.

Dopant	Method	Rs	Ref.
HNO3	R2R+dipping	125	[16]
AgNO3	Dipping	202	[57]
AuCl3	Spin-coating	500	[54]
MoO3	Film deposition	~600	[55,56]
Ru	ALD	125	[53]

Table 2-1. The summary of graphene doping articles using various dopant and doping method. R2R is roll to roll transfer process.
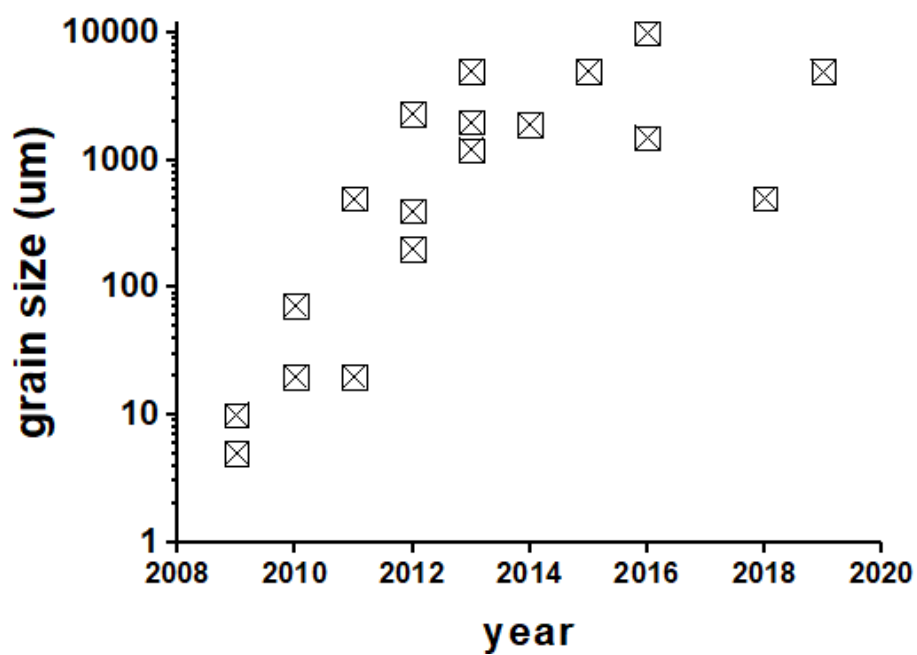
Figure 2-16. The yearly reported CVD graphene grain size.

Grain size	Mobility [cm²/Vs]	Rs	Refer.
2.3 mm	8600	363	[60]
5 mm	11000	284	[64]
2 mm	5200	-	[62]
1.2 mm	6500	-	[61]
1.9 mm	2400	-	[71]
10 mm	4300	-	[63]

Table 2-2. The summary of electrical property of mm size of graphene. The electrical property was made on single grain of graphene.

References

1.   Bolotin, K. I.;   Sikes, K. J.;   Jiang, Z.;   Klima, M.;   Fudenberg, G.;   Hone, J.;   Kim, P.;   Stormer, H. L., Ultrahigh electron mobility in suspended graphene. *Solid State Commun* **2008,** *146* (9-10), 351-355.

2.   Gomez De Arco, L.;   Zhang, Y.;   Schlenker, C. W.;   Ryu, K.;   Thompson, M. E.;   Zhou, C., Continuous, Highly Flexible, and Transparent Graphene Films by Chemical Vapor Deposition for Organic Photovoltaics. *Acs Nano* **2010,** *4* (5), 2865-2873.

3.   Yoon, T.;   Kim, J.-H.;   Choi, J. H.;   Jung, D. Y.;   Park, I.-J.;   Choi, S.-Y.;   Cho, N. S.;   Lee, J.-I.;   Kwon, Y.-D.;   Cho, S.; Kim, T.-S., Healing Graphene Defects Using Selective Electrochemical Deposition: Toward Flexible and Stretchable Devices. *Acs Nano* **2016,** *10* (1), 1539-1545.

4.   Gao, L.;   Ren, W.;   Zhao, J.;   Ma, L.-P.;   Chen, Z.; Cheng, H.-M., Efficient growth of high-quality graphene films on Cu foils by ambient pressure chemical vapor deposition. *Appl Phys Lett* **2010,** *97* (18), 183109.

5.   Kobayashi, T.;   Bando, M.;   Kimura, N.;   Shimizu, K.;   Kadono, K.;   Umezu, N.;   Miyahara, K.;   Hayazaki, S.;   Nagai, S.;   Mizuguchi, Y.;   Murakami, Y.;   Hobara, D., Production of a 100-m-long high-quality graphene transparent conductive film by roll-to-roll chemical vapor deposition and transfer process. *Appl Phys Lett* **2013,** *102* (2), 023112.

6.   Krajewska, A.;   Pasternak, I.;   Sobon, G.;   Sotor, J.;   Przewloka, A.;   Ciuk, T.;   Sobieski, J.;   Grzonka, J.;   Abramski, K. M.; Strupinski, W., Fabrication and applications of multi-layer graphene stack on transparent polymer. *Appl Phys Lett* **2017,** *110* (4), 041901.

7.   Wang, Y.; Chen, X.; Zhong, Y.; Zhu, F.; Loh, K. P., Large area, continuous, few-layered graphene as anodes in organic photovoltaic devices. *Appl Phys Lett* **2009,** *95* (6), 063302.

8.   Park, H. J.; Meyer, J.; Roth, S.; Skakalova, V., Growth and properties of few-layer graphene prepared by chemical vapor deposition. *Carbon* **2010,** *48* (4), 1088-1094.

9.   Lee, S.; Jo, Y.; Hong, S.; Kim, D.; Lee, H. W., Multilayered Graphene Electrode using One-Step Dry Transfer for Optoelectronics. *Curr. Opt. Photon.* **2017,** *1* (1), 7-11.

10.   Zhang, Q.; Di, Y.; Huard, C. M.; Guo, L. J.; Wei, J.; Guo, J., Highly stable and stretchable graphene–polymer processed silver nanowires hybrid electrodes for flexible displays. *Journal of Materials Chemistry C* **2015,** *3* (7), 1528-1536.

11.   Lang, F.; Gluba, M. A.; Albrecht, S.; Rappich, J.; Korte, L.; Rech, B.; Nickel, N. H., Perovskite Solar Cells with Large-Area CVD-Graphene for Tandem Solar Cells. *The Journal of Physical Chemistry Letters* **2015,** *6* (14), 2745-2750.

12.   Griep, M. H.; Sandoz-Rosado, E.; Tumlin, T. M.; Wetzel, E., Enhanced Graphene Mechanical Properties through Ultrasmooth Copper Growth Substrates. *Nano Lett* **2016,** *16* (3), 1657-1662.

13.   Lee, Y.; Bae, S.; Jang, H.; Jang, S.; Zhu, S.-E.; Sim, S. H.; Song, Y. I.; Hong, B. H.; Ahn, J.-H., Wafer-Scale Synthesis and Transfer of Graphene Films. *Nano Lett* **2010,** *10* (2), 490-493.

14.   Reina, A.; Jia, X.; Ho, J.; Nezich, D.; Son, H.; Bulovic, V.; Dresselhaus, M. S.; Kong, J., Large Area, Few-Layer Graphene Films on Arbitrary Substrates by Chemical Vapor Deposition. *Nano Lett* **2008,** *9* (1), 30-35.

15.   Liu, J.;   Yi, Y.;   Zhou, Y.; Cai, H., Highly Stretchable and Flexible Graphene/ITO Hybrid Transparent Electrode. *Nanoscale Res Lett* **2016,** *11* (1), 108.

16.   Bae, S.;   Kim, H.;   Lee, Y.;   Xu, X.;   Park, J.-S.;   Zheng, Y.;   Balakrishnan, J.;   Lei, T.;   Ri Kim, H.;   Song, Y. I.;   Kim, Y.-J.;   Kim, K. S.;   Ozyilmaz, B.;   Ahn, J.-H.;   Hong, B. H.; Iijima, S., Roll-to-roll production of 30-inch graphene films for transparent electrodes. *Nat Nano* **2010,** *5* (8), 574-578.

17.   Wang, C.;   Chen, W.;   Han, C.;   Wang, G.;   Tang, B.;   Tang, C.;   Wang, Y.;   Zou, W.;   Chen, W.;   Zhang, X.-A.;   Qin, S.;   Chang, S.; Wang, L., Growth of Millimeter-Size Single Crystal Graphene on Cu Foils by Circumfluence Chemical Vapor Deposition. *Sci Rep-Uk* **2014,** *4* (1), 4537.

18.   Cvijović, D., The Bloch-Gruneisen function of arbitrary order and its series representations. *Theoretical and Mathematical Physics* **2011,** *166* (1), 37-42.

19.   Efetov, D. K.; Kim, P., Controlling Electron-Phonon Interactions in Graphene at Ultrahigh Carrier Densities. *Phys Rev Lett* **2010,** *105* (25), 256805.

20.   Chen, J.-H.;   Jang, C.;   Xiao, S.;   Ishigami, M.; Fuhrer, M. S., Intrinsic and extrinsic performance limits of graphene devices on SiO2. *Nat Nano* **2008,** *3* (4), 206-209.

21.   Hwang, E. H.; Das Sarma, S., Acoustic phonon scattering limited carrier mobility in two-dimensional extrinsic graphene. *Phys Rev B* **2008,** *77* (11), 115449.

22.   Pietronero, L.;   Strässler, S.;   Zeller, H. R.; Rice, M. J., Electrical conductivity of a graphite layer. *Phys Rev B* **1980,** *22* (2), 904-910.

23.   Stauber, T.;   Peres, N. M. R.; Guinea, F., Electronic transport in graphene: A semiclassical approach including midgap states. *Phys Rev B* **2007,** *76* (20), 205423.

24.   Hess, K.; Vogl, P., Remote polar phonon scattering in silicon inversion layers.

Solid State Commun **1979,** *30* (12), 797-799.

25.   Fratini, S.; Guinea, F., Substrate-limited electron dynamics in graphene. *Phys Rev B* **2008,** *77* (19), 195415.

26.   Fischetti, M. V.;   Neumayer, D. A.; Cartier, E. A., Effective electron mobility in Si inversion layers in metal–oxide–semiconductor systems with a high-κ insulator: The role of remote phonon scattering. *J Appl Phys* **2001,** *90* (9), 4587-4608.

27.   Mattevi, C.;   Kim, H.; Chhowalla, M., A review of chemical vapour deposition of graphene on copper. *J Mater Chem* **2011,** *21* (10), 3324-3334.

28.   Huang, P. Y.;   Ruiz-Vargas, C. S.;   van der Zande, A. M.;   Whitney, W. S.; Levendorf, M. P.;   Kevek, J. W.;   Garg, S.;   Alden, J. S.;   Hustedt, C. J.;   Zhu, Y.; Park, J.;   McEuen, P. L.; Muller, D. A., Grains and grain boundaries in single-layer graphene atomic patchwork quilts. *Nature* **2011,** *469* (7330), 389-+.

29.   Kotakoski, J.; Meyer, J. C., Mechanical properties of polycrystalline graphene based on a realistic atomistic model. *Phys Rev B* **2012,** *85* (19), 195447.

30.   Cummings, A. W.;   Duong, D. L.;   Nguyen, V. L.;   Van Tuan, D.;   Kotakoski, J.;   Barrios Vargas, J. E.;   Lee, Y. H.; Roche, S., Charge Transport in Polycrystalline Graphene: Challenges and Opportunities. *Advanced Materials* **2014**, n/a-n/a.

31.   Yu, Q.;   Jauregui, L. A.;   Wu, W.;   Colby, R.;   Tian, J.;   Su, Z.;   Cao, H.; Liu, Z.;   Pandey, D.;   Wei, D.;   Chung, T. F.;   Peng, P.;   Guisinger, N. P.;   Stach, E. A.;   Bao, J.;   Pei, S.-S.; Chen, Y. P., Control and characterization of individual grains and grain boundaries in graphene grown by chemical vapour deposition. *Nat Mater* **2011,** *10* (6), 443-449.

32.   Zhou, H.;   Yu, W. J.;   Liu, L.;   Cheng, R.;   Chen, Y.;   Huang, X.;   Liu, Y.;

Wang, Y.;   Huang, Y.; Duan, X., Chemical vapour deposition growth of large single crystals of monolayer and bilayer graphene. *Nat Commun* **2013,** *4* (1), 2096.

33.   Yagi, K.;   Yamada, A.;   Hayashi, K.;   Harada, N.;   Sato, S.; Yokoyama, N., Dependence of Field-Effect Mobility of Graphene Grown by Thermal Chemical Vapor Deposition on Its Grain Size. *Jpn J Appl Phys* **2013,** *52* (11).

34.   Isacsson, A.;   Cummings, A. W.;   Colombo, L.;   Colombo, L.;   Kinaret, J. M.; Roche, S., Scaling properties of polycrystalline graphene: a review. *2D Materials* **2016,** *4* (1), 012002.

35.   Kim, K. S.;   Zhao, Y.;   Jang, H.;   Lee, S. Y.;   Kim, J. M.;   Kim, K. S.;   Ahn, J.-H.;   Kim, P.;   Choi, J.-Y.; Hong, B. H., Large-scale pattern growth of graphene films for stretchable transparent electrodes. *Nature* **2009,** *457* (7230), 706-710.

36.   Li, X.;   Zhu, Y.;   Cai, W.;   Borysiak, M.;   Han, B.;   Chen, D.;   Piner, R. D.;   Colombo, L.; Ruoff, R. S., Transfer of Large-Area Graphene Films for High-Performance Transparent Conductive Electrodes. *Nano Lett* **2009,** *9* (12), 4359-4363.

37.   Lin, Y.-C.;   Lu, C.-C.;   Yeh, C.-H.;   Jin, C.;   Suenaga, K.; Chiu, P.-W., Graphene Annealing: How Clean Can It Be? *Nano Lett* **2011,** *12* (1), 414-419.

38.   Chen, J. H.;   Jang, C.;   Adam, S.;   Fuhrer, M. S.;   Williams, E. D.; Ishigami, M., Charged-impurity scattering in graphene. *Nature Physics* **2008,** *4* (5), 377-381.

39.   Trushin, M.; Schliemann, J., Minimum Electrical and Thermal Conductivity of Graphene: A Quasiclassical Approach. *Phys Rev Lett* **2007,** *99* (21), 216602.

40.   Yan, X.-Z.;   Romiah, Y.; Ting, C. S., Electric transport theory of Dirac fermions in graphene. *Phys Rev B* **2008,** *77* (12), 125409.

41.   Meyer, J. C.;   Kisielowski, C.;   Erni, R.;   Rossell, M. D.;   Crommie, M. F.;

Zettl, A., Direct Imaging of Lattice Atoms and Topological Defects in Graphene Membranes. *Nano Lett* **2008,** *8* (11), 3582-3586.

42.   Dean, C. R.;   Young, A. F.;   Meric, I.;   Lee, C.;   Wang, L.;   Sorgenfrei, S.;   Watanabe, K.;   Taniguchi, T.;   Kim, P.;   Shepard, K. L.; Hone, J., Boron nitride substrates for high-quality graphene electronics. *Nat Nanotechnol* **2010,** *5* (10), 722-726.

43.   Lafkioti, M.;   Krauss, B.;   Lohmann, T.;   Zschieschang, U.;   Klauk, H.;   Klitzing, K. v.; Smet, J. H., Graphene on a Hydrophobic Substrate: Doping Reduction and Hysteresis Suppression under Ambient Conditions. *Nano Lett* **2010,** *10* (4), 1149-1153.

44.   Wang, Y.;   Zheng, Y.;   Xu, X.;   Dubuisson, E.;   Bao, Q.;   Lu, J.; Loh, K. P., Electrochemical Delamination of CVD-Grown Graphene Film: Toward the Recyclable Use of Copper Catalyst. *Acs Nano* **2011,** *5* (12), 9927-9933.

45.   Lee, S.;   Lee, S. K.;   Kang, C. G.;   Cho, C.;   Lee, Y. G.;   Jung, U.; Lee, B. H., Graphene transfer in vacuum yielding a high quality graphene. *Carbon* **2015,** *93*, 286-294.

46.   Fanton, M. A.;   Robinson, J. A.;   Puls, C.;   Liu, Y.;   Hollander, M. J.;   Weiland, B. E.;   LaBella, M.;   Trumbull, K.;   Kasarda, R.;   Howsare, C.;   Stitt, J.;   Snyder, D. W., Characterization of Graphene Films and Transistors Grown on Sapphire by Metal-Free Chemical Vapor Deposition. *Acs Nano* **2011,** *5* (10), 8062-8069.

47.   Rümmeli, M. H.;   Bachmatiuk, A.;   Scott, A.;   Börrnert, F.;   Warner, J. H.;   Hoffman, V.;   Lin, J.-H.;   Cuniberti, G.; Büchner, B., Direct Low-Temperature Nanographene CVD Synthesis over a Dielectric Insulator. *Acs Nano* **2010,** *4* (7), 4206-4210.

48.   Chen, J.;   Guo, Y.;   Wen, Y.;   Huang, L.;   Xue, Y.;   Geng, D.;   Wu, B.;

Luo, B.;   Yu, G.; Liu, Y., Two-Stage Metal-Catalyst-Free Growth of High-Quality Polycrystalline Graphene Films on Silicon Nitride Substrates. *Advanced Materials* **2013,** *25* (7), 992-997.

49.   Peng, Z.;   Yan, Z.;   Sun, Z.; Tour, J. M., Direct Growth of Bilayer Graphene on SiO2 Substrates by Carbon Diffusion through Nickel. *Acs Nano* **2011,** *5* (10), 8241-8247.

50.   Yan, Z.;   Peng, Z. W.;   Sun, Z. Z.;   Yao, J.;   Zhu, Y.;   Liu, Z.;   Ajayan, P. M.; Tour, J. M., Growth of Bilayer Graphene on Insulating Substrates. *Acs Nano* **2011,** *5* (10), 8187-8192.

51.   Wei, D.;   Lu, Y.;   Han, C.;   Niu, T.;   Chen, W.; Wee, A. T. S., Critical Crystal Growth of Graphene on Dielectric Substrates at Low Temperature for Electronic Devices. *Angewandte Chemie International Edition* **2013,** *52* (52), 14121-14126.

52.   Kim, J.;   Ishihara, M.;   Koga, Y.;   Tsugawa, K.;   Hasegawa, M.; Iijima, S., Low-temperature synthesis of large-area graphene-based transparent conductive films using surface wave plasma chemical vapor deposition. *Appl Phys Lett* **2011,** *98* (9), 091502.

53.   Kim, M.;   Kim, K.-J.;   Lee, S.-J.;   Kim, H.-M.;   Cho, S.-Y.;   Kim, M.-S.; Kim, S.-H.; Kim, K.-B., Highly Stable and Effective Doping of Graphene by Selective Atomic Layer Deposition of Ruthenium. *Acs Appl Mater Inter* **2017,** *9* (1), 701-709.

54.   Kwon, K. C.;   Choi, K. S.; Kim, S. Y., Increased Work Function in Few-Layer Graphene Sheets via Metal Chloride Doping. *Advanced Functional Materials* **2012,** *22* (22), 4724-4731.

55.   Chen, Z.;   Santoso, I.;   Wang, R.;   Xie, L. F.;   Mao, H. Y.;   Huang, H.; Wang, Y. Z.;   Gao, X. Y.;   Chen, Z. K.;   Ma, D.;   Wee, A. T. S.; Chen, W., Surface transfer hole doping of epitaxial graphene using MoO3 thin film. *Appl Phys Lett* **2010,** *96*

(21), 213104.

56.   Xie, L.;   Wang, X.;   Mao, H.;   Wang, R.;   Ding, M.;   Wang, Y.;   Özyilmaz, B.;   Loh, K. P.;   Wee, A. T. S.;   Ariando; Chen, W., Electrical measurement of non-destructively p-type doped graphene using molybdenum trioxide. *Appl Phys Lett* **2011,** *99* (1), 012112.

57.   Shin, D. H.;   Lee, K. W.;   Lee, J. S.;   Kim, J. H.;   Kim, S.; Choi, S.-H., Enhancement of the effectiveness of graphene as a transparent conductive electrode by AgNO3doping. *Nanotechnology* **2014,** *25* (12), 125701.

58.   Li, X. S.;   Cai, W. W.;   An, J. H.;   Kim, S.;   Nah, J.;   Yang, D. X.;   Piner, R.;   Velamakanni, A.;   Jung, I.;   Tutuc, E.;   Banerjee, S. K.;   Colombo, L.; Ruoff, R. S., Large-Area Synthesis of High-Quality and Uniform Graphene Films on Copper Foils. *Science* **2009,** *324* (5932), 1312-1314.

59.   Wu, Y. A.;   Fan, Y.;   Speller, S.;   Creeth, G. L.;   Sadowski, J. T.;   He, K.;   Robertson, A. W.;   Allen, C. S.; Warner, J. H., Large Single Crystals of Graphene on Melted Copper Using Chemical Vapor Deposition. *Acs Nano* **2012,** *6* (6), 5010-5017.

60.   Yan, Z.;   Lin, J.;   Peng, Z.;   Sun, Z.;   Zhu, Y.;   Li, L.;   Xiang, C.;   Samuel, E. L.;   Kittrell, C.; Tour, J. M., Toward the Synthesis of Wafer-Scale Single-Crystal Graphene on Copper Foils. *Acs Nano* **2012**.

61.   Wu, T.;   Ding, G.;   Shen, H.;   Wang, H.;   Sun, L.;   Jiang, D.;   Xie, X.;   Jiang, M., Triggering the Continuous Growth of Graphene Toward Millimeter-Sized Grains. *Advanced Functional Materials* **2013,** *23* (2), 198-203.

62.   Chen, S.;   Ji, H.;   Chou, H.;   Li, Q.;   Li, H.;   Suk, J. W.;   Piner, R.;   Liao, L.;   Cai, W.; Ruoff, R. S., Millimeter-Size Single-Crystal Graphene by Suppressing

Evaporative Loss of Cu During Low Pressure Chemical Vapor Deposition. *Advanced Materials* **2013,** *25* (14), 2062-2065.

63.   Guo, W.;   Jing, F.;   Xiao, J.;   Zhou, C.;   Lin, Y.; Wang, S., Oxidative-Etching-Assisted Synthesis of Centimeter-Sized Single-Crystalline Graphene. *Advanced Materials* **2016,** *28* (16), 3152-3158.

64.   Chen, X.;   Zhao, P.;   Xiang, R.;   Kim, S.;   Cha, J.;   Chiashi, S.; Maruyama, S., Chemical vapor deposition growth of 5mm hexagonal single-crystal graphene from ethanol. *Carbon* **2015,** *94*, 810-815.

65.   Jacobberger, R. M.; Arnold, M. S., Graphene Growth Dynamics on Epitaxial Copper Thin Films. *Chem Mater* **2013**.

66.   Li, X.;   Magnuson, C. W.;   Venugopal, A.;   Tromp, R. M.;   Hannon, J. B.;   Vogel, E. M.;   Colombo, L.; Ruoff, R. S., Large-Area Graphene Single Crystals Grown by Low-Pressure Chemical Vapor Deposition of Methane on Copper. *Journal of the American Chemical Society* **2011,** *133* (9), 2816-2819.

67.   Wang, H.;   Wang, G.;   Bao, P.;   Yang, S.;   Zhu, W.;   Xie, X.; Zhang, W.-J., Controllable Synthesis of Submillimeter Single-Crystal Monolayer Graphene Domains on Copper Foils by Suppressing Nucleation. *Journal of the American Chemical Society* **2012,** *134* (8), 3627-3630.

68.   Li, X.;   Magnuson, C. W.;   Venugopal, A.;   An, J.;   Suk, J. W.;   Han, B.;   Borysiak, M.;   Cai, W.;   Velamakanni, A.;   Zhu, Y.;   Fu, L.;   Vogel, E. M.;   Voelkl, E.;   Colombo, L.; Ruoff, R. S., Graphene Films with Large Domain Size by a Two-Step Chemical Vapor Deposition Process. *Nano Lett* **2010,** *10* (11), 4328-4334.

69.   Li, X. S.;   Cai, W. W.;   Colombo, L.; Ruoff, R. S., Evolution of Graphene

Growth on Ni and Cu by Carbon Isotope Labeling. *Nano Lett* **2009,** *9* (12), 4268-4272.

70.   Zhou, H.;   Yu, W. J.;   Liu, L.;   Cheng, R.;   Chen, Y.;   Huang, X.;   Liu, Y.;   Wang, Y.;   Huang, Y.; Duan, X., Chemical vapour deposition growth of large single crystals of monolayer and bilayer graphene. *Nat Commun* **2013,** *4*.

71.   Wang, C.;   Chen, W.;   Han, C.;   Wang, G.;   Tang, B.;   Tang, C.;   Wang, Y.;   Zou, W.;   Zhang, X.-A.;   Qin, S.;   Chang, S.; Wang, L., Growth of Millimeter-Size Single Crystal Graphene on Cu Foils by Circumfluence Chemical Vapor Deposition. *Sci. Rep.* **2014,** *4*.

72.   Wu, X.;   Zhong, G.;   D'Arsié, L.;   Sugime, H.;   Esconjauregui, S.;   Robertson, A. W.;   Robertson, J., Growth of Continuous Monolayer Graphene with Millimeter-sized Domains Using Industrially Safe Conditions. *Sci Rep-Uk* **2016,** *6*, 21152.

73.   Duong, D. L.;   Han, G. H.;   Lee, S. M.;   Gunes, F.;   Kim, E. S.;   Kim, S. T.;   Kim, H.;   Ta, Q. H.;   So, K. P.;   Yoon, S. J.;   Chae, S. J.;   Jo, Y. W.;   Park, M. H.;   Chae, S. H.;   Lim, S. C.;   Choi, J. Y.; Lee, Y. H., Probing graphene grain boundaries with optical microscopy. *Nature* **2012,** *490* (7419), 235-239.

CHAPTER 3.

CVD graphene growth with different grain size

3.1. Basic theory of CVD growth of graphene

As described in **Figure 1-7**, CVD graphene process consist of several steps, thermal decomposition of carbon source, surface diffusion of active carbon atom (here, active carbon atom assumed to carbon monomer for simplicity), and nucleation and growth process. Each step is possible to explain classical growth kinetics model, however, steps are inter-related to each other, resulting very complex CVD growth system. For example, changing one growth parameter such as growth temperature effect on thermal decomposition rate, number of stable nuclei, surface diffusion etc., but the only thing that can be measured or observed is just graphene with certain nucleation density and grain size. Therefore, numerous researches are focused on the changing growth parameters and analysis the result as qualitative point of view. And each CVD growth step is analyzed by numerical calculations.

Thermal decomposition of carbon sources

In CVD graphene growth, various carbon-based molecules [1-4] used as carbon sources. Normally, study of graphene CVD growth focused on enlarging its grain size, increasing surface diffusion length is critical because high enough surface diffusion length promote growth process and prohibit nucleation process, consequently, high temperature CVD growth is appropriate. However, higher the temperature, the thermal decomposition rate also increased, then nucleation density can be increased resulting smaller graphene grain size. Generally, it is easier to decompose when carbon molecules have additional CH_x-bonding,[2-4] (it can be decomposed in lower temperature) therefore, the simplest form of

carbon, CH_4, has lower decomposition rate than any other carbon-based molecules. Consequently, CH_4 is typically used in CVD growth of graphene. When CH_4 is used as carbon source, the overall CVD graphene growth reaction is described as following equation.

$$CH_4 \rightarrow C_{graphene} + 2H_2$$
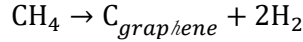
Then, Gibbs free energy would be, (when $\alpha_c=1$)

$$\Delta G = \Delta G^0 + RTln\frac{\alpha_c p_{H_2}^2}{p_{CH_4}^2} = \Delta G^0 + RTln\frac{p_{H_2}^2}{p_{CH_4}^2}$$

The simple numerical calculation of thermodynamics (1 atm assumed) shows that overall reaction starts to have negative ΔG at 600 °C. Even though the overall reaction is possible at 600 °C thermodynamically, numerical calculation tells decomposition process of CH_4 imply lots of intermediate step and require more thermal energy to overcome activation energy of each step as shown in **Figure 3-1**.[5] In experimentally, nucleation of graphene appears at 700 °C with extremely low growth rate, at least 1000 °C is used for CVD graphene growth in the presence of Cu metal catalyst.[1] Without Cu metal catalyst, about 1400 °C is required to decomposed and form graphene for CH_4 gas.[6-8]

Surface diffusion

After CH_4 decomposed, carbon monomer generated (again, active carbon atoms such as monomer, dimer, etc., all assumed to be in the form of monomer) active carbon atoms are generated and the carbon monomer can be formed nuclei, be captured to nuclei (growth process), or be desorb from Cu surface as **Figure 3-2 (a)** [9] through surface diffusion. The surface diffusion length X can be described as,[10]

$$X = \sqrt{2D_s \tau_s}$$

The surface diffusion coefficient, D_s, and remaining time of survival on surface, τ_s, are given by

$$D_s = \frac{1}{2} a_0^2 \nu \, exp\left(-\frac{E_s}{kT}\right)$$

$$\tau_s = \frac{1}{\nu} exp\left(\frac{E_{des}}{kT}\right)$$

Then, X would be

$$X = a_0 \, exp\left(\frac{E_{des} - E_s}{2kT}\right)$$

Here, a_0 is the atomic length, ν is the vibrational frequency of the adatom on the surface, E_s is the activation energy for surface diffusion, E_{des} is the required energy for desorption of adatom. As described above equation surface diffusion length is the function of growth temperature T, increasing growth temperature give a rise of surface diffusion length. Generally, increased X promote nuclei formation process and growth process by carbon monomer attachment, activation energy for nuclei formation is usually higher than that of attachment energy, growth process becomes dominant in high temperature process as **Figure 3-2(b)**.[9, 11]

Nucleation and growth

The initial nucleation and growth process of graphene can be explained as following simple step. After decomposition of CH_4 gas molecules, carbon monomer generated and accumulated in Cu surface as illustrated in **Figure 3-3** graph.[9] The concentration of carbon monomer on Cu surface, C_{Cu}, would be increased as the times goes by, and when C_{Cu}

accumulated enough and supersaturated, graphene nuclei formed at critical carbon monomer concentration, C_{nuc}. Then, the carbon monomer is consumed for nucleation, and its concentration drastically decreased. The carbon monomer is continuously provided by thermal decomposition of CH_4, however, it also consumed by nucleation, attachment to existed nuclei and desorption, therefore, equilibrium state is formed by those processes with the carbon concentration C_{eq}. After initial nucleation process, if the concentration of carbon monomer is high enough to form further nuclei, $C_{Cu} > C_{nuc} > C_{eq}$, nucleation and growth process occurs simultaneously resulting graphene relatively high nucleation density. If the concentration of carbon is higher than that equilibrium but lower than C_{nuc}, $C_{nuc} > C_{Cu} > C_{eq}$, then nucleation is limited and growth process becomes dominant resulting graphene with relatively lower nuclei density. On the other hand, if the concentration of carbon monomer is extremely low, $C_{Cu} < C_{eq}$, then the even growth process cannot be proceeded and full coverage graphene growth is not enabled.[9] The further explanation of graphene growth kinetic would be expressed in chapter 3.2.

Cu metal catalyst

In CVD graphene growth, Cu known to act as two significant roles as a metal catalyst. First, the Cu surface aid the dehydrogenation process of CH. The decomposition process of CH_4 gas has three intermediate states, methyl (CH_3), methylene (CH_2), methylidyne (CH) as illustrated in **Figure 3-1**,[5] and the Cu surface, in the (111) plane for example, the interstitial sites on Cu (111) surface capture dehydrogenated H atoms, lowering its activation energy of each dehydrogenation step as illustrated in **Figure 3-4**.[5] Because the Cu help the thermal decomposition process, growth temperature can be lowered to 1000

°C, [1] in the presence of Cu metal catalyst. Second, without Cu, graphene growth is enabled in high temperature about 1400 °C,[6] the resulting quality of graphene is evidently lower than that of the graphene synthesized by Cu metal catalyst,[6, 8] therefore, it is generally accepted that the Cu surface also helps the crystallization process of graphene. The other various metal such as Ni, Pt, Ru also known to act as metal catalyst for graphene growth, these metals normally have carbon solubility resulting multilayer graphene and uncontrolled grain size, therefore, the Cu becomes representative metal catalyst for CVD graphene growth.
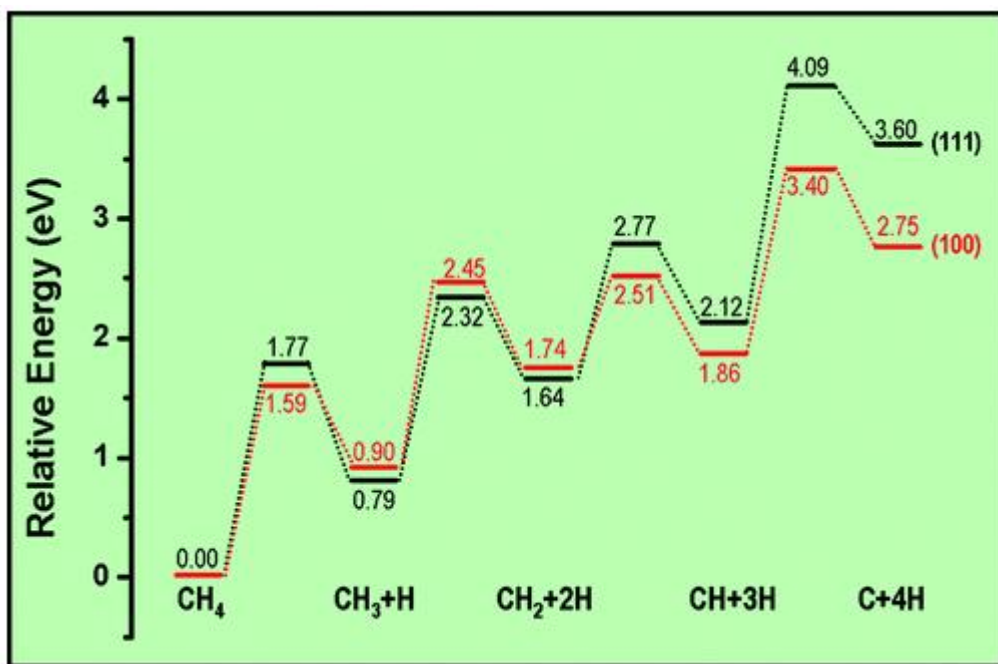
Figure 3-1. Energy profile of dehydrogenation process of CH$_4$ on (111), (100) Cu surfaces.[5]
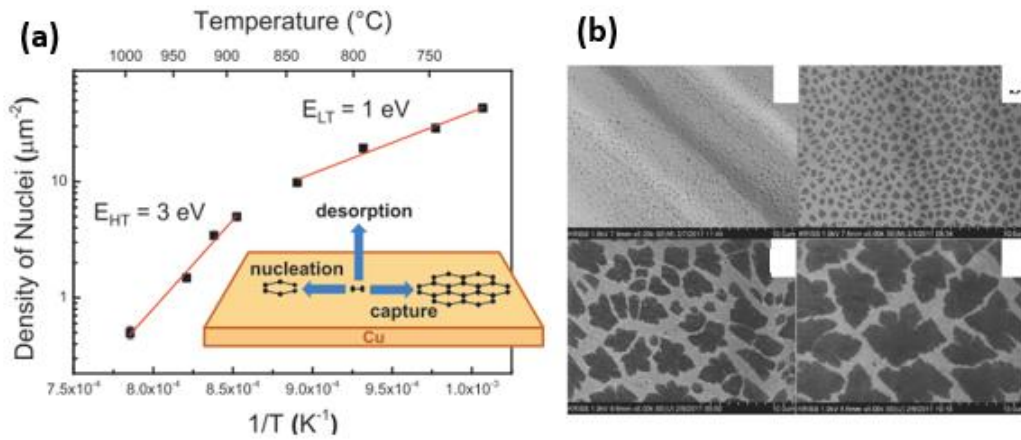
Figure 3-2. (a) density of nuclei vs growth temperature in CVD growth graphene, inset is the illustration of carbon monomer consuming process, nucleation, captured by nuclei, desorption.[9] (b) is the SEM image of CVD graphene on Cu as increasing growth temperature 940, 980, 1000, 1030 °C. The higher growth temperature shows decreased nucleation density.[11]
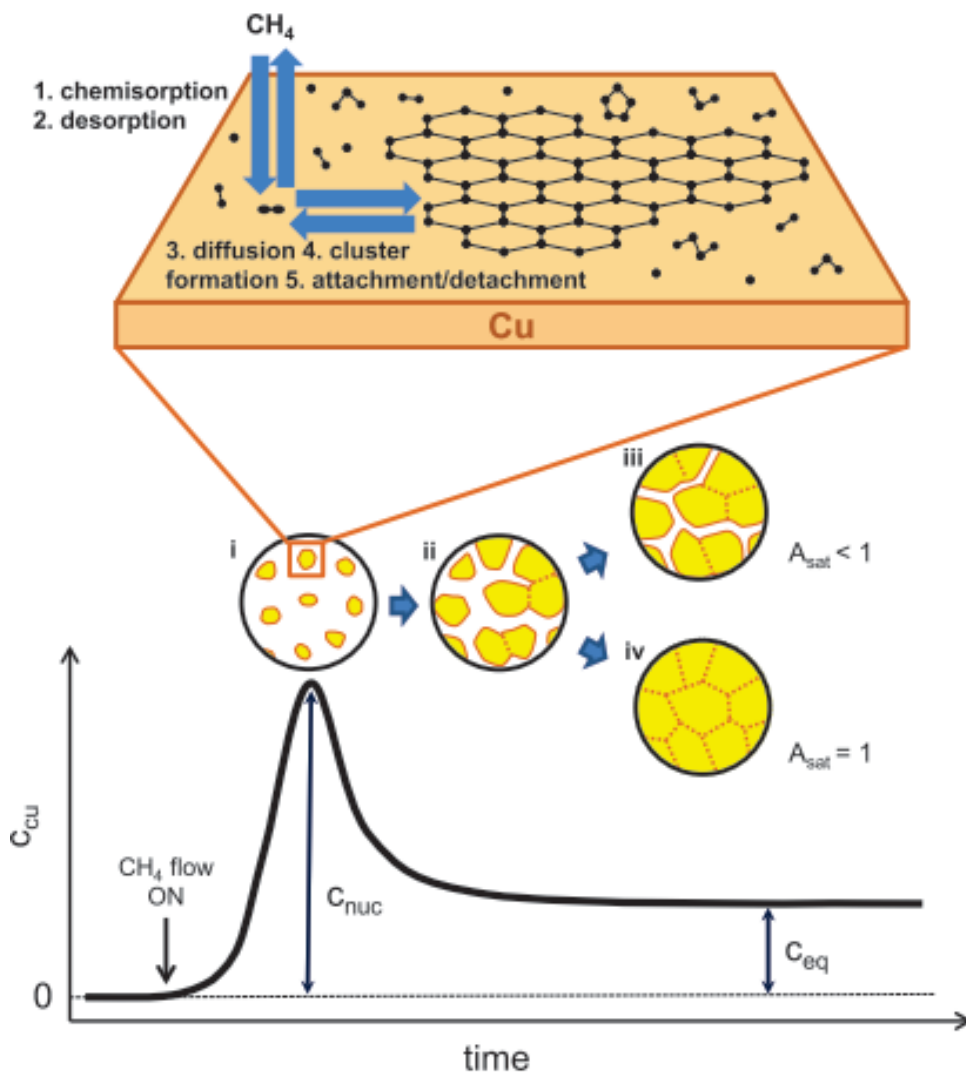
Figure 3-3. The overall illustration of the nucleation growth mechanism of graphene on Cu.[9]
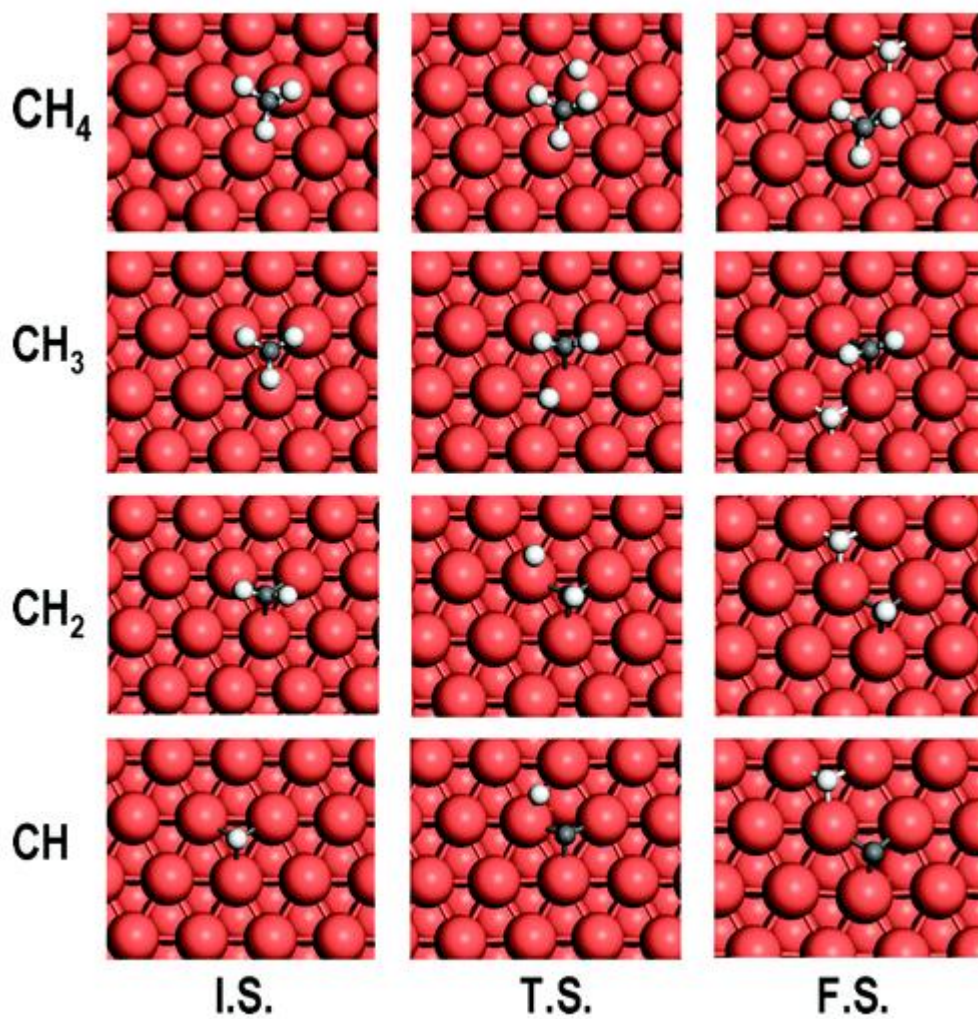
Figure 3-4. The geometric structures of Cu (111) surface in dehydrogenation process of CH$_4$ gas. I.S. is the initial state, T.S. is the transitional state and F.S. is the final state.[5]

3.2. CVD graphene growth

3.2.1. Growth parameter for enlarging grain size of graphene

According to the basic theory of CVD graphene growth, there are three growth parameters that can enlarge the grain size of graphene (or lower its nucleation density). First one is the lowering source carbon supply. As illustrated in **Figure 3-3**, nucleation is proceeded when the concentration of carbon monomer supersaturated and reached critical concentration, C_{nuc}. In the solid thin film theory, for the condensation reaction vapor (v) → solid (s), the chemical free energy per unit volume, ΔG_v, given by [10]

$$\Delta G_v = \frac{kT}{\Omega} ln \frac{p_s}{p_v} = -\frac{kT}{\Omega} ln \frac{p_v}{p_s}$$

where p_s, is vapor pressure of solid, p_v, is the pressure of the supersaturated vapor, Ω is the atomic volume. When the supersaturation ratio S, is defined by $(p_v - p_s)/p_s$ then,

$$\Delta G_v = -\frac{kT}{\Omega} ln(1 + S)$$

From above equation, lowering supersaturation ratio would limits nucleation of graphene and lower final nucleation density of graphene. In **Figure 3-5**, CVD graphene growth is performed with various CH_4 gas flow rate. The lowering source gas supply result in significant decrease in nucleation density of graphene, linearly in logarithmic scale.[12] The Second growth parameter is the growth temperature, and according to the basic theory of CVD graphene growth, there are two contradictorily result expected with increasing the growth temperature. The Gibbs free energy for thermal decomposition and the number of stable nuclei, n^*, can be expressed in following equation,[10, 13]

$$n^* = n_0 \exp\left(-\frac{\Delta G^*}{kT}\right)$$

$$\Delta G = \Delta G^0 + RT ln \frac{p_{H_2}^2}{p_{CH_4}^2}$$

If the growth temperature increased, the number of stable nuclei and the thermal decomposition rate is simultaneously increased, nucleation density is expected to increased. However, the surface diffusion length is also increased, growth dominant (rather than nucleation) process can be proceed. As explained in section 3.1 and **Figure 3-2**, experimental result shows that increasing temperature cause growth dominant process, lowering its nucleation density. Thirdly, overall reaction of graphene is not irreversible process, rather reversible process, [14]

$$CH_4 \leftrightarrow C_{graphene} + 2H_2$$
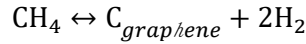
reverse process (etching process) can be proceed by increasing partial pressure of H_2. Etching of graphene by H_2 molecules occurs with several intermediate state as **Figure 3-6** in the presence of Cu metal catalyst.[5, 14, 15] When the grain of graphene is formed, the edge of graphene tends to have thermodynamically stable two different state, zig-zag and armchair shape of edge,[16, 17] and consequently, grain shape has hexagonal shape which is thermodynamically most stable shape. If the growth process is fast, *i.g.*, if carbon source feeding rate is high, the grown graphene grain has dendritic flower shape because of massive attachment of active carbon atoms. However, if source gas feeding rate is low, or partial pressure of H_2 is high, the shape of grain has hexagonal shape because growth and etching process simultaneously occur and thermodynamically stable shape remained even if the net of overall reaction is forward. In **Figure 3-7**, the shape of graphene grain becomes

hexagonal from various shape, and grain size is increased as increase partial pressure of H_2. In summary, controlling growth parameters of CVD graphene growth increasing grain size is enabled.[14] Reducing carbon source supply, increasing growth temperature, and increasing partial pressure of H_2 is possible method to enlarge grain size of graphene.
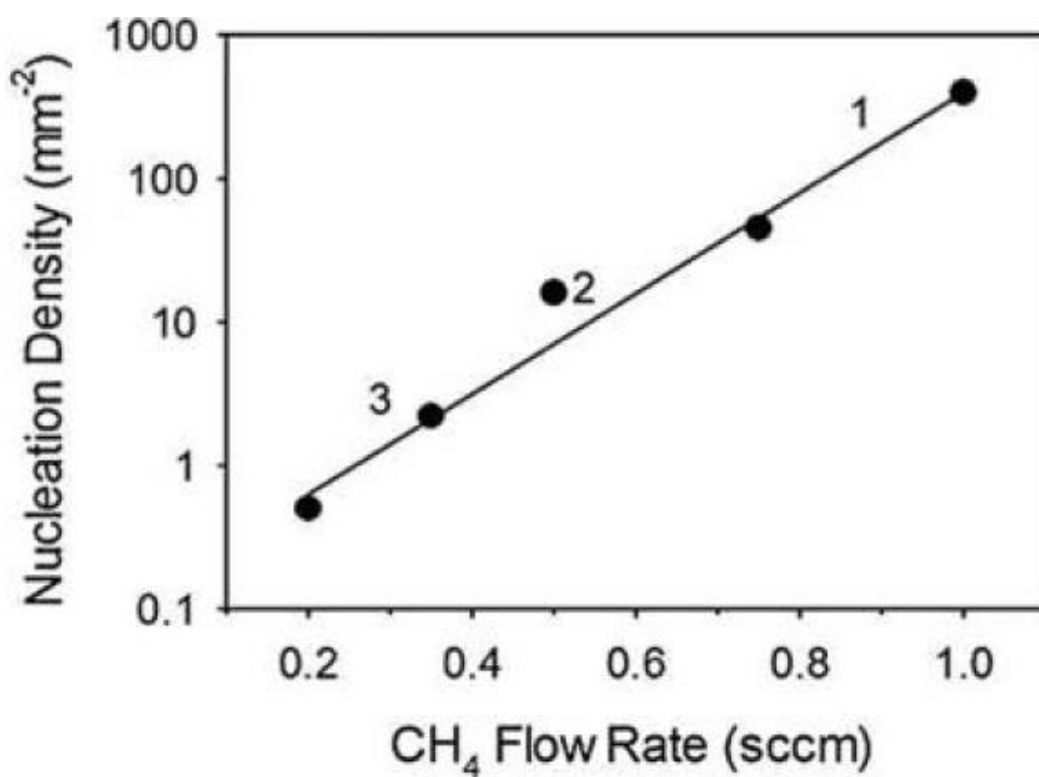
Figure 3-5. (a) density of nuclei vs growth temperature in CVD growth graphene, inset is the illustration of carbon monomer consuming process, nucleation, captured by nuclei, desorption.[12]

$$Cu + H_2 \Leftrightarrow 2H_s \qquad (1)$$

$$Cu + CH_4 \rightarrow (CH_3)_s + H_s \text{ - slow} \qquad (2)$$

$$Cu + CH_4 \Leftrightarrow (CH_4)_s \qquad (3)$$

$$(CH_4)_s + H_s \Leftrightarrow (CH_3)_s + H_2 \qquad (4)$$

$$(CH_3)_s + \text{graphene} \Leftrightarrow (\text{graphene}+C) + H_2 \qquad (5)$$

$$H_s + \text{graphene} \Leftrightarrow (\text{graphene-C}) + (CH_x)_s \qquad (6)$$
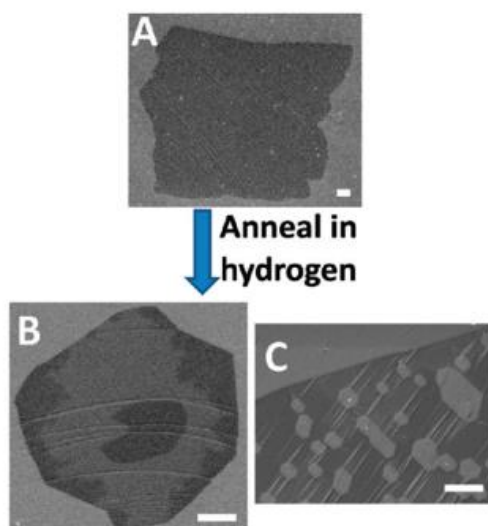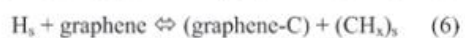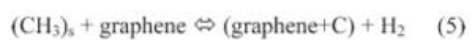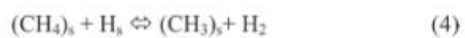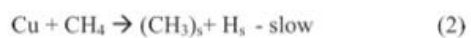
Figure 3-6. The possible scheme for H_2 etching process of graphene on Cu surface, and the SEM image of graphene grain after etching in H_2 environment. The scale bar is 1 um.[14]
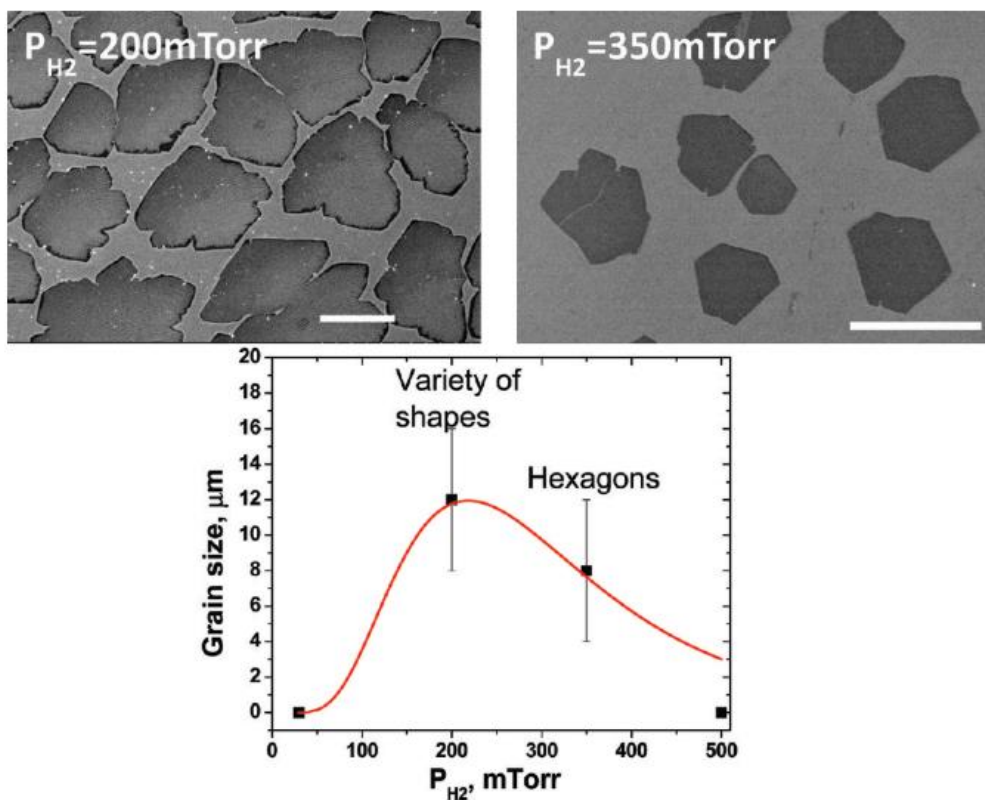
Figure 3-7. The morphology changes of graphene grain as increasing partial pressure of H$_2$. The scale bar is 10 um.[14]

3.2.2. Heterogeneous nucleation of CVD graphene

Since CVD graphene growth use Cu metal catalyst, Cu surface effect important role in nucleation process of graphene. Usually, Cu foil is manufactured by mechanical rolling process, rolling line cause scratches in Cu foil surface and other defects. Also, Cr_2O_3 is coated to protect from formation of native oxide of Cu which possibly acts as impurities during graphene growth.[18] In **Figure 3-8**, it is observed that graphene nucleus formed along with the Cu foil scratch lines, these defects acts as additional nucleation center.[19] In the nucleation theory, the Gibbs free energy for heterogeneous nucleation is expressed as,[10, 13]

$$\Delta G_{hetero} = \Delta G_{homo} \cdot S(\theta)$$

$$\Delta G_{homo} = -\frac{4}{3}\pi r^3 \Delta G_v + 4\pi r^3 \gamma$$

$$S(\theta) = \frac{(2 + cos\theta)(1 - cos\theta)^2}{3}$$

In the case of CVD growth of graphene, n layer of graphene on impurity has angle of θ as shown in **Figure 3-9**. In the CVD graphene synthesis, if heterogeneous nucleation process becomes dominant as **Figure 3-10**, controlling growth parameter may enlarge homogeneous nucleation density, but experimental result would be converged to heterogeneous nucleation. Therefore, before synthesize the graphene by controlling growth parameter, Cu surface needs to be treated to minimize heterogeneous nucleation effect. The several methods were introduced to remove surface defects of Cu surface, pre-heating in high temperature[20] is simplest way of it, and the chemical mechanical polishing[19] and electropolishing[18] also introduced to minimize heterogeneous nucleation of graphene. grain size of graphene. Before the graphene growth with different grain size, electropolishing was selected for Cu surface treatment, and optical microscopy image of

graphene synthesis before and after electropolishing was on **Figure 3-11**.

Experimental details of electropolishing

Solution : 100 mL of DI water, 50 mL of orthophosphoric acid, 50 mL of ethanol, 10 mL of IPA

Condition : 5 V of applied voltage, 2 A of current, 2 min of time
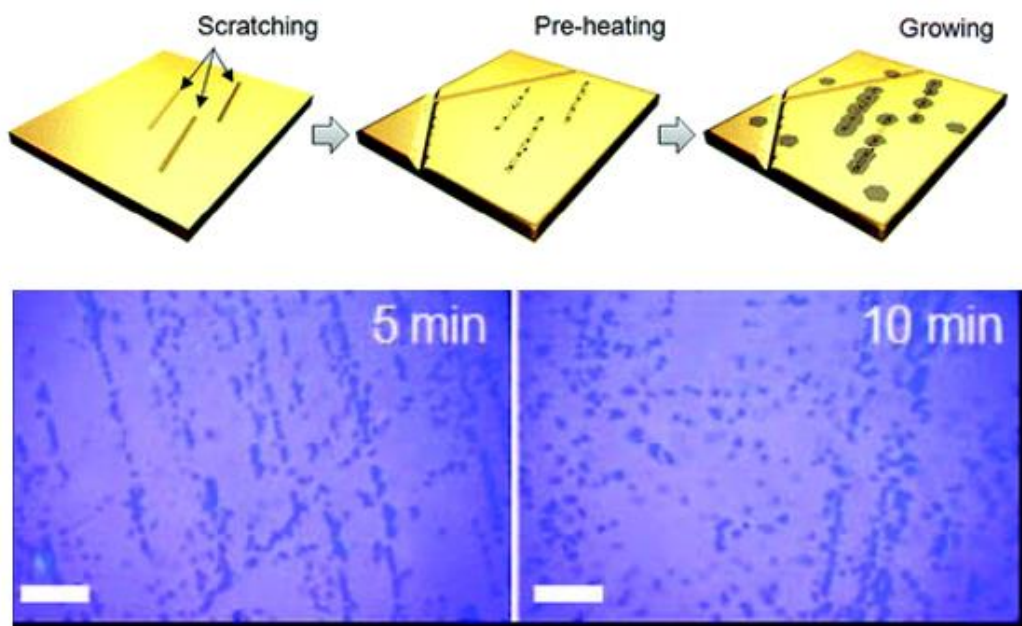
Figure 3-8. The schematics if nuclei formation of graphene on Cu surface scratches and optical image of graphene after transferred on SiO_2/Si substrate. The scale bar is 10 um.[19]

$$\theta_n = \cos^{-1}\left(\frac{r - nt_{gr}}{r}\right)$$
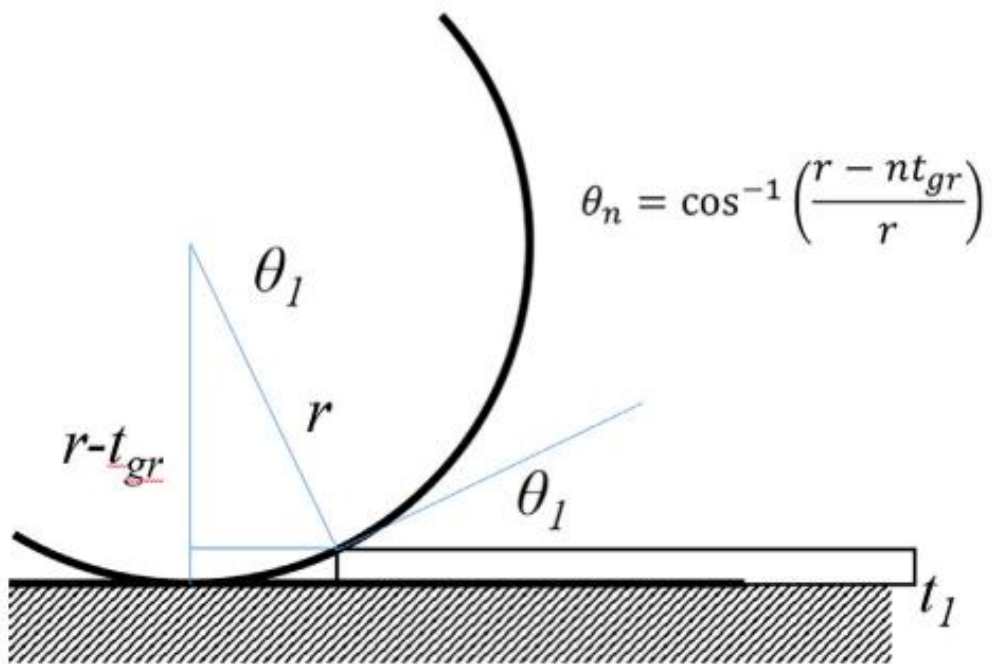
Figure 3-9. The diagram of angle between graphene layer and impurity. n is the number of layers of graphene and t is the thickness of graphene.
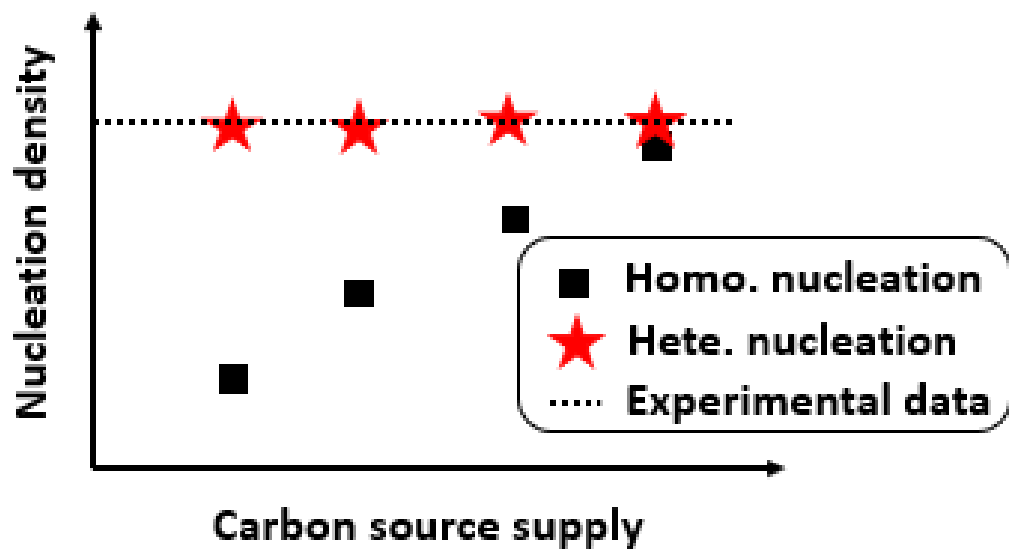
Figure 3-10. The schematic graph of nucleation density of heterogeneous and homogeneous nucleation.
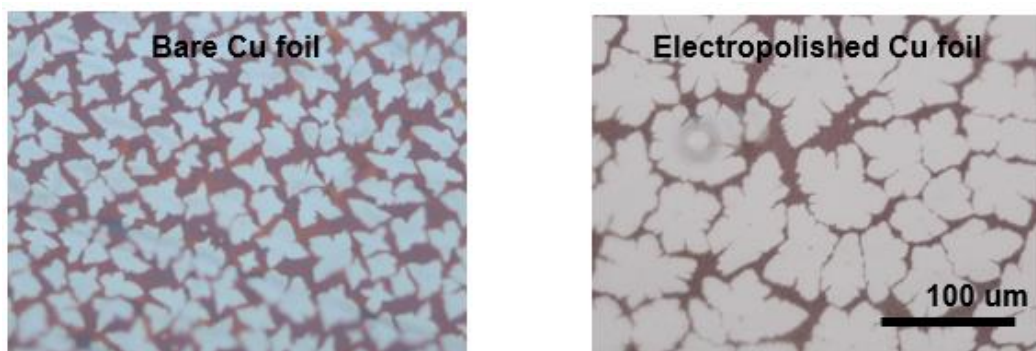
Figure 3-11. Optical microscope image of graphene grown on Cu foil with same condition. The bare Cu foil (before electropolishing, left image) has higher nucleation density than that of electropolished Cu foil (right image).

3.2.3. JMAK growth kinetics of CVD graphene

In section 3.1, growth dominant process is proceeded when the concentration of carbon monomer is less than C_{nuc}, however, the Cu act as metal catalyst for dehydrogenation of CH$_4$, exposed Cu surface is reduced and generated carbon monomer becomes depleted even though same carbon source feeding rate is same. If the remained carbon monomer concentration on Cu surface is more than the 2D density of graphene, $\frac{C_{nuc} - C_{eq}}{\rho_G} = 1$, full covered graphene can be synthesized after long enough of growth time. But if remained carbon monomer concentration is less than the 2D density of graphene, $\frac{C_{nuc} - C_{eq}}{\rho_G} < 1$, full covered graphene cannot be formed and unfilled gap exist after graphene synthesis as illustrate in **Figure 3-3**.[9] The John-Mehl-Avrami-Kolmogorov (JMAK) equation is the model explaining phase transformation growth kinetics which α phase transforming to β phase by consuming α phase in give volume V. Since the β phase formed by consuming α phase and increment of β phase is proportional to remained α phase therefore growth rate becomes decreased as the time increased, its growth kinetics is very similar to that of CVD graphene, which the carbon monomer generation is decreased as the exposed Cu surface area becomes smaller. When the α phase transformed into β phase, the general form of JMAK is given by[21-23]

$$Y = 1 - \exp(-kt^n)$$

Where, Y is volume fraction of β phase, k is the transformation related constant, t is the time, and n is the dimensional parameter. In ideal case, when β phase is formed to round (round in 2D, sphere in 3D) shape, 2, 3 and 4 of n corresponding to the 1D, 2D and 3-dimensional growth. In many cases, especially in graphene, the shape of β phase doesn't

have the round shape, rather, nonideal shape is observed. Then the shape parameter n can be expressed further, n=b+pm, b is the time-dependent nucleation rate, p is the growth mode, m is dimensional parameter. [9, 24] The specific description of these parameters is summarized in **Table 3-1**, here, instant nucleation means nucleation process initially occurs only and further nucleation is limited, linear growth means ideal growth (such as round shape), and non-linear growth is the growth except ideal shape. Typically, since the graphene growth is focused on enlarging grain size, the carbon source supply is minimized and growth dominant process occurs, therefore, the time-dependent nucleation rate, b, normally have zero value, nucleation occurs only initial stage of graphene growth (b≈0). The most low-pressure CVD (LPCVD) graphene has high growth rate, shape of graphene is dendritic as **Figure 3-11**, the growth mode normally less than 1, p < 1, in atmospheric pressure CVD (APCVD), the most of partial pressure is filled with H_2 gas, growth rate is extremely slow and shape of graphene becomes ideal, p≈ 1.[25, 26] Therefore, the typical graphene growth, the expected shape factor n becomes 1~1.5 (b≈0, p<1, m=2).

The graphene synthesis is performed for various carbon source feeding rate using electropolished Cu foil, and JMAK growth kinetics analyzed, the growth parameter is summarized in **Table 3-2**. To estimate coverage of graphene, partial covered graphene was obtained by optical microscopy and the coverage of graphene were collected by image analysis using IMAGE PRO program. The growth time vs coverage data was evaluated by fitting JMAK equation with various n value in **Figure 3-12**. The graph is well fitted with the 1.5 of n value, like typical LPCVD graphene case, it seems that each parameter has value b≈0, p<1, m=2.

Parameter	Value	Significance
b	>1	Increasing nucleation rate
	0	Instant nucleation
	<1	Decreasing nucleation rate
p	1	Linear growth
	<1	Non-linear growth
m	1	1D growth
	2	2D growth
	3	3D growth

Table 3-1. The parameters of shape factor n and its significance.[9]

Pressure & temperature	Growth condition	Growth time
	Ar 50 sccm, H_2 30 sccm / CH_4 10 sccm	2 min
0.5~0.8 Torr	Ar 50 sccm, H_2 30 sccm / CH_4 5 sccm	5 min
1030 °C	Ar 50 sccm, H_2 12 sccm / CH_4 0.5 sccm	30 min
	H_2 12 sccm / CH_4 0.1 sccm	4 hours

Table 3-2. The growth parameters of CVD graphene to synthesize different grain size.
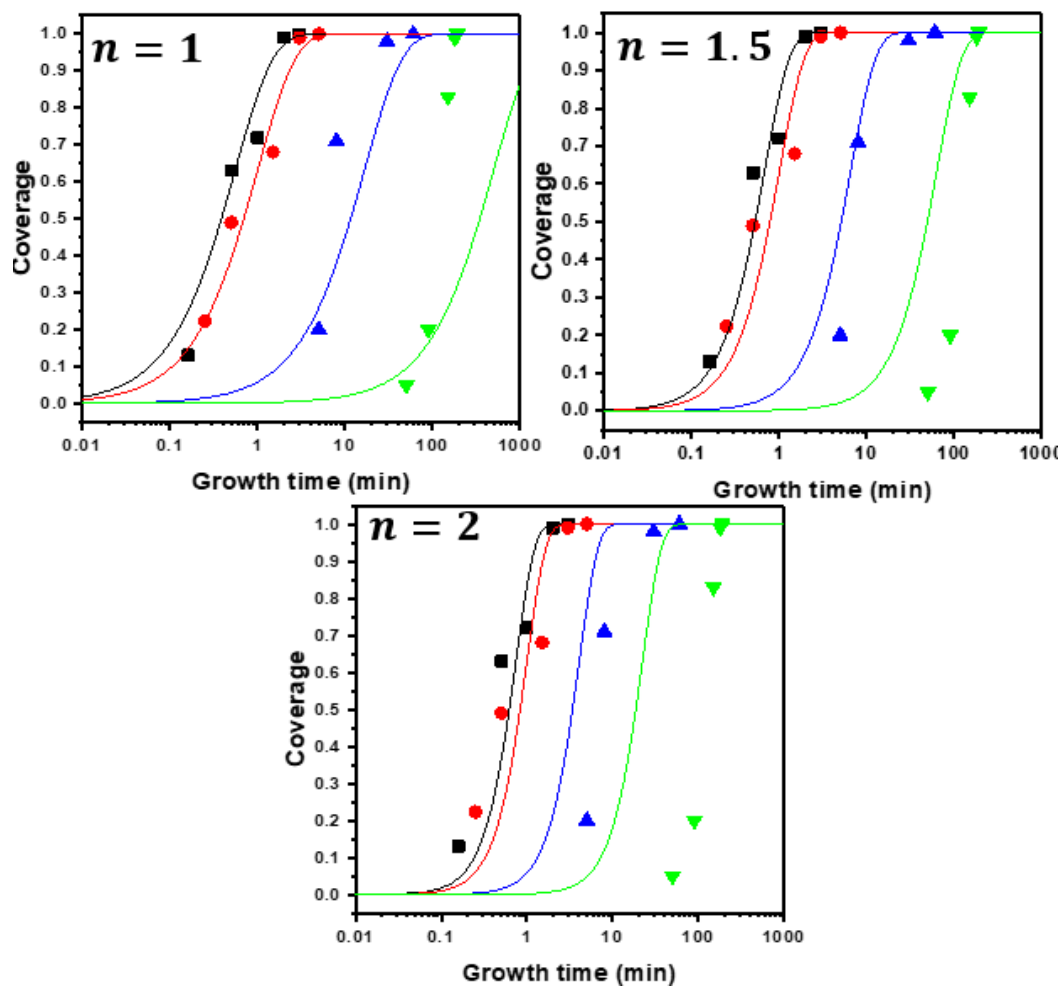
Figure 3-12. The JMAK fitting of synthesized graphene with growth condition in **Table 3-2**. 10 sccm (black, square), 5 sccm (red, circle), 0.5 sccm (blue, upper triangle), 0.1 sccm (green, downer triangle).

3.2.4. Growth of CVD graphene with different grain size

The 4 different grain size of graphene synthesized with the growth condition in **Table 3-2**, the optical microscopy image is in the **Figure 3-13**. The grain size was measure with analysis its partial coverage sample. Image process was conducted on partial covered graphene sample, after measuring domain area, the grain size was calculated assuming domain area is circle. The measured domain size is 17, 25, 52, 78 um, respectively. The **Figure 3-14** is the optic and SEM image of 0.5 sccm, in optic image, it seems that clean, full covered graphene is synthesize, however, in SEM image unfilled gap between graphene grains are observed. As the growth time increased, the growth rate is decreased showing JMAK growth behavior, lack of carbon monomer concentration on Cu surface result unfilled graphene area between grains. The sample with 0.1 sccm also similar phenomena was observed, and these unfilled gaps may effect on the electrical property measurement, misguiding grain boundary effect of graphene. there are two solution for gap problem, increasing growth temperature and applying additional carbon source supply. In both ways, the carbon concentration on Cu surface increased by increasing thermal decomposition and applying more carbon sources, the increasing carbon source feeding rate is more simple way in practically, this method was selected for unfilled gap solution. The modified growth condition for the sample with 0.5 sccm and 0.1 sccm summarized in **Table 3-3**, two-step growth was conducted,[27, 28] after growing graphene with condition in **Table 3-2** with almost full coverage, additional carbon source supply was introduced to fill the gap between graphene grains.
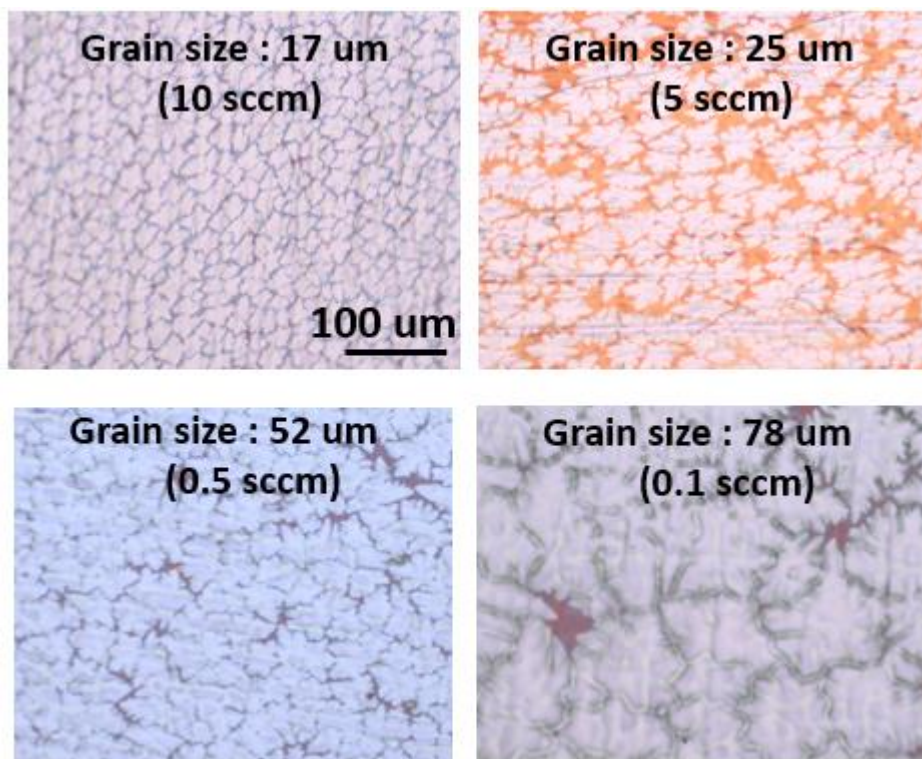
Figure 3-13. The optical microscopy image of grown graphene with the condition **Table 3-2**.
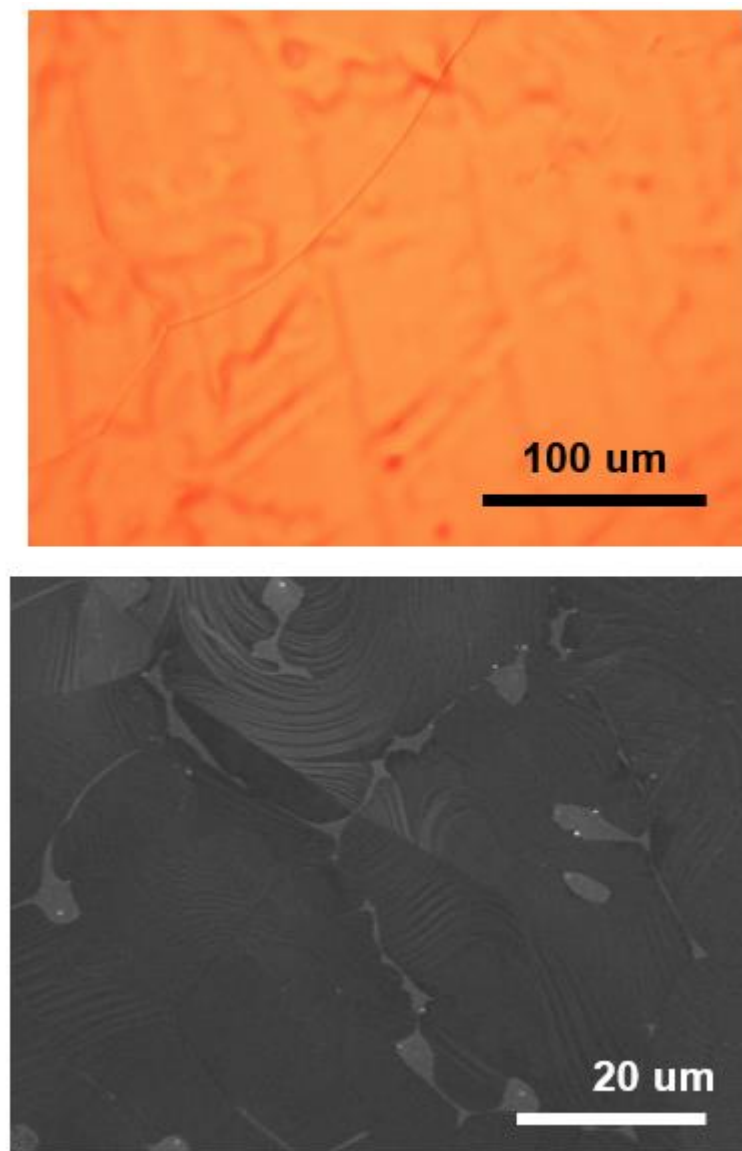
Figure 3-14. The optical microscopy image (up) and SEM image (down) of 0.5 sccm sample.

Pressure & temperature	Growth condition	Growth time
	1st step : Ar 50 sccm, H_2 12 sccm / CH_4 0.5 sccm	30 min
0.5~0.8 Torr	2nd step : Ar 50 sccm, H_2 12 sccm / CH_4 1 sccm	30 min
1030 ^{o}C	1st step : H_2 12 sccm / CH_4 0.1 sccm	4 hours
	2nd step : H_2 12 sccm / CH_4 1 sccm	1 hour

Table 3-3. The two-step growth condition for filling graphene gap.

References

1.   Li, X. S.;   Cai, W. W.;   An, J. H.;   Kim, S.;   Nah, J.;   Yang, D. X.;   Piner, R.;   Velamakanni, A.;   Jung, I.;   Tutuc, E.;   Banerjee, S. K.;   Colombo, L.; Ruoff, R. S., Large-Area Synthesis of High-Quality and Uniform Graphene Films on Copper Foils. *Science* **2009,** *324* (5932), 1312-1314.

2.   Zhang, B.;   Lee, W. H.;   Piner, R.;   Kholmanov, I.;   Wu, Y.;   Li, H.;   Ji, H.; Ruoff, R. S., Low-Temperature Chemical Vapor Deposition Growth of Graphene from Toluene on Electropolished Copper Foils. *Acs Nano* **2012,** *6* (3), 2471-2476.

3.   Guermoune, A.;   Chari, T.;   Popescu, F.;   Sabri, S. S.;   Guillemette, J.; Skulason, H. S.;   Szkopek, T.; Siaj, M., Chemical vapor deposition synthesis of graphene on copper with methanol, ethanol, and propanol precursors. *Carbon* **2011,** *49* (13), 4204-4210.

4.   Wassei, J. K.;   Mecklenburg, M.;   Torres, J. A.;   Fowler, J. D.;   Regan, B. C.; Kaner, R. B.; Weiller, B. H., Chemical Vapor Deposition of Graphene on Copper from Methane, Ethane and Propane: Evidence for Bilayer Selectivity. *Small* **2012,** *8* (9), 1415-1422.

5.   Zhang, W.;   Wu, P.;   Li, Z.; Yang, J., First-Principles Thermodynamics of Graphene Growth on Cu Surfaces. *The Journal of Physical Chemistry C* **2011,** *115* (36), 17782-17787.

6.   Fanton, M. A.;   Robinson, J. A.;   Puls, C.;   Liu, Y.;   Hollander, M. J.; Weiland, B. E.;   LaBella, M.;   Trumbull, K.;   Kasarda, R.;   Howsare, C.;   Stitt, J.; Snyder, D. W., Characterization of Graphene Films and Transistors Grown on Sapphire by Metal-Free Chemical Vapor Deposition. *Acs Nano* **2011,** *5* (10), 8062-8069.

7.   Rümmeli, M. H.; Bachmatiuk, A.; Scott, A.; Börrnert, F.; Warner, J. H.; Hoffman, V.;   Lin, J.-H.;   Cuniberti, G.; Büchner, B., Direct Low-Temperature Nanographene CVD Synthesis over a Dielectric Insulator. *Acs Nano* **2010,** *4* (7), 4206-4210.

8.   Chen, J.; Guo, Y.; Wen, Y.; Huang, L.; Xue, Y.; Geng, D.; Wu, B.; Luo, B.;   Yu, G.; Liu, Y., Two-Stage Metal-Catalyst-Free Growth of High-Quality Polycrystalline Graphene Films on Silicon Nitride Substrates. *Advanced Materials* **2013,** *25* (7), 992-997.

9.   Kim, H.; Mattevi, C.; Calvo, M. R.; Oberg, J. C.; Artiglia, L.; Agnoli, S.;   Hirjibehedin, C. F.;   Chhowalla, M.; Saiz, E., Activation Energy Paths for Graphene Nucleation and Growth on Cu. *Acs Nano* **2012,** *6* (4), 3614-3623.

10.   Ohring, M., *The materials science of thin films*. Academic Press: Boston, 1992; p xx, 704 p.

11.   Hwang, C.; Yoo, K.; Kim, S. J.; Seo, E. K.; Yu, H.; Biró, L. P., Initial Stage of Graphene Growth on a Cu Substrate. *The Journal of Physical Chemistry C* **2011,** *115* (45), 22369-22374.

12.   Eres, G.; Regmi, M.; Rouleau, C. M.; Chen, J.; Ivanov, I. N.; Puretzky, A. A.; Geohegan, D. B., Cooperative Island Growth of Large-Area Single-Crystal Graphene on Copper Using Chemical Vapor Deposition. *Acs Nano* **2014,** *8* (6), 5657-5669.

13.   Callister, W. D., *Materials science and engineering : an introduction*. 4th ed.; John Wiley & Sons: New York, 1997; p xx, 852 p., 4 p. of plates.

14.   Vlassiouk, I.; Regmi, M.; Fulvio, P.; Dai, S.; Datskos, P.; Eres, G.; Smirnov, S., Role of Hydrogen in Chemical Vapor Deposition Growth of Large Single-

Crystal Graphene. *Acs Nano* **2011,** *5* (7), 6069-6076.

15. Kharlamova, T.; Pavlova, S.; Sadykov, V.; Krieger, T.; Alikina, G.; Argirusis, C., Catalytic properties and coking stability of new anode materials for internal methane reforming in the intermediate temperature solid oxide fuel cells. *Catal Today* **2009,** *146* (1), 141-147.

16. Vo, T. H.; Shekhirev, M.; Kunkel, D. A.; Orange, F.; Guinel, M. J. F.; Enders, A.; Sinitskii, A., Bottom-up solution synthesis of narrow nitrogen-doped graphene nanoribbons. *Chem Commun* **2014,** *50* (32), 4172-4174.

17. Cai, J.; Ruffieux, P.; Jaafar, R.; Bieri, M.; Braun, T.; Blankenburg, S.; Muoth, M.; Seitsonen, A. P.; Saleh, M.; Feng, X.; Müllen, K.; Fasel, R., Atomically precise bottom-up fabrication of graphene nanoribbons. *Nature* **2010,** *466* (7305), 470-473.

18. Cho, S.-Y.; Kim, M.; Kim, M.-S.; Lee, M.-H.; Kim, K.-B., Effect of Cu surface treatment in graphene growth by chemical vapor deposition. *Materials Letters* **2019,** *236*, 403-407.

19. Han, G. H.; Güneş, F.; Bae, J. J.; Kim, E. S.; Chae, S. J.; Shin, H.-J.; Choi, J.-Y.; Pribat, D.; Lee, Y. H., Influence of Copper Morphology in Forming Nucleation Seeds for Graphene Growth. *Nano Lett* **2011,** *11* (10), 4144-4148.

20. Wang, H.; Wang, G.; Bao, P.; Yang, S.; Zhu, W.; Xie, X.; Zhang, W.-J., Controllable Synthesis of Submillimeter Single-Crystal Monolayer Graphene Domains on Copper Foils by Suppressing Nucleation. *Journal of the American Chemical Society* **2012,** *134* (8), 3627-3630.

21. Avrami, M., Kinetics of Phase Change. I General Theory. *The Journal of Chemical Physics* **1939,** *7* (12), 1103-1112.

22.   Avrami, M., Kinetics of Phase Change. II Transformation-Time Relations for Random Distribution of Nuclei. *The Journal of Chemical Physics* **1940,** *8* (2), 212-224.

23.   Avramov, I., Kinetics of distribution of infections in networks. *Physica A: Statistical Mechanics and its Applications* **2007,** *379* (2), 615-620.

24.   Earnshaw, A.; Harrington, T. J., *The chemistry of the transition elements*. Clarendon Press: Oxford,, 1973; p 101 p.

25.   Yan, Z.;   Lin, J.;   Peng, Z.;   Sun, Z.;   Zhu, Y.;   Li, L.;   Xiang, C.;   Samuel, E. L.;   Kittrell, C.; Tour, J. M., Toward the Synthesis of Wafer-Scale Single-Crystal Graphene on Copper Foils. *Acs Nano* **2012**.

26.   Wang, C.;   Chen, W.;   Han, C.;   Wang, G.;   Tang, B.;   Tang, C.;   Wang, Y.;   Zou, W.;   Zhang, X.-A.;   Qin, S.;   Chang, S.; Wang, L., Growth of Millimeter-Size Single Crystal Graphene on Cu Foils by Circumfluence Chemical Vapor Deposition. *Sci. Rep.* **2014,** *4*.

27.   Li, X.;   Magnuson, C. W.;   Venugopal, A.;   An, J.;   Suk, J. W.;   Han, B.;   Borysiak, M.;   Cai, W.;   Velamakanni, A.;   Zhu, Y.;   Fu, L.;   Vogel, E. M.;   Voelkl, E.;   Colombo, L.; Ruoff, R. S., Graphene Films with Large Domain Size by a Two-Step Chemical Vapor Deposition Process. *Nano Lett* **2010,** *10* (11), 4328-4334.

28.   Cho, S.-Y.;   Kim, M.-S.;   Kim, M.;   Kim, K.-J.;   Kim, H.-M.;   Lee, D.-J.;   Lee, S.-H.; Kim, K.-B., Self-assembly and continuous growth of hexagonal graphene flakes on liquid Cu. *Nanoscale* **2015,** *7* (30), 12820-12827.

CHAPTER 4.

Grain size dependence of electrical property of graphene

4.1. The electrical property of 4 different domain sized graphene

The single crystal graphene has remarkable mobility with 230,000 cm²/Vs at R.T. condition and corresponding sheet resistance of graphene is calculated about 30 ohm/sq.[1, 2] However, the polycrystalline CVD graphene has about 500 ohm/sq by various limiting factors described in chapter 2, as numerical formula, $R_S = R_S^{bulk} + R_S^{sub} + R_S^{GB} + R_S^{etc.}$. To evaluate the grain boundary effect on electrical property of graphene, this numerical formula can be simplified as

$$R_S = R_S^{bulk} + R_S^{sub} + R_S^{GB} + R_S^{etc.}$$

$$R_S = R_S^G + R_S^{GB}$$

$$R_S^G = R_S^{bulk} + R_S^{sub} + R_S^{etc.}$$

Here, R_S^G is the sheet resistance of graphene grain, therefore, the total sheet resistance of graphene can be divided into two important term, the graphene grain sheet resistance, R_S^G, the graphene grain boundary sheet resistance, R_S^{GB}. Using graphene samples which synthesized in chapter 3, the grain boundary effect on electrical property was performed in this chapter.

4.1.1. Experimental scheme

The experimental scheme of this chapter is illustrated in **Figure 4-1**. The prepared samples in chapter 3 was wet transferred on polyethylene terephthalate (PET) substrate using ammonium persulfate (APS, $(NH_4)_2S_2O_8$) Cu etching solution. To measure electrical property of graphene, the transferred samples were measured by Hall measurement system

(HL 5500PC, BIO-RAD) with the square Van der Pauw structure. The contact pad with 1 mm by 1 mm were made on each corner of sample by sequential evaporation of Ti and Au (3 nm, 50 nm respectively). The size of sample was determined with the 10 mm by 10 mm, which is far larger than graphene grain size to maximize its reliability of grain boundary effect. The grain size of graphene is 17, 25, 52, 78 um as synthesized in chapter 3 and each grain size, 9~12 sample were Hall measured. After electrical property measurement of undoped graphene, all graphene samples were dipped into benzimidazole (BZ) based p-type doping solution (H_2SO_4+H_2O_2+BZ), to investigate doping effect on various grain size of graphene. The BZ is known to have high electron withdrawing molecule with high electronegativity typically used to dope carbon nanotube (CNT) and graphene.[3-5] After doping process, electrical property of all samples was evaluated again, using Hall measurement system
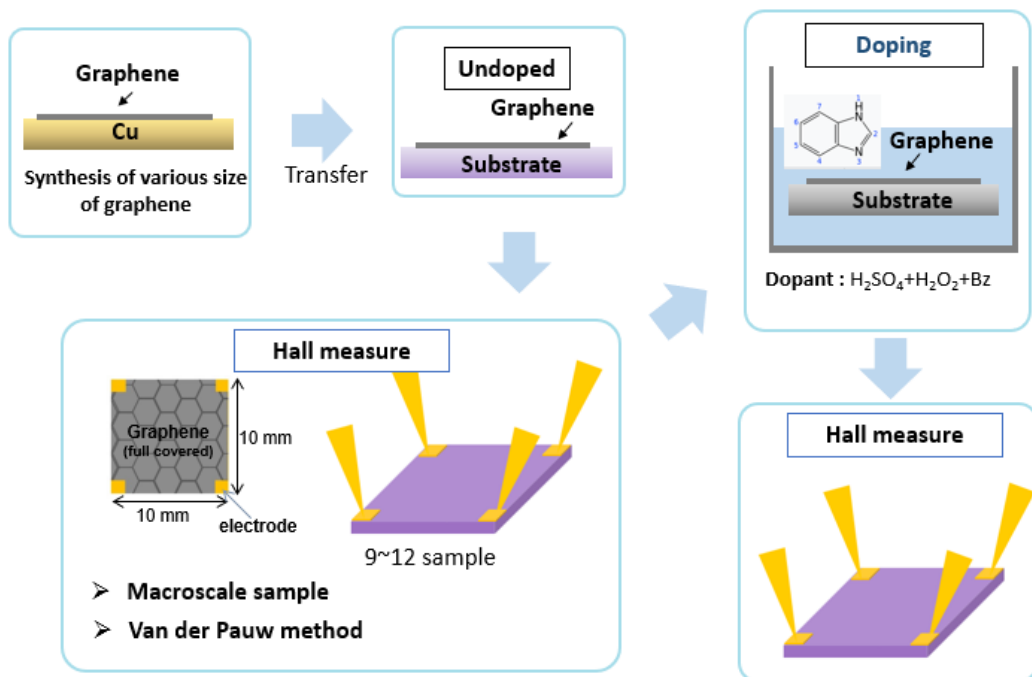
Figure 4-1. The schematic illustration of experimental scheme to evaluate the graphene grain boundary and doping effect on electrical property of graphene.

4.1.2. The electrical property of undoped/doped graphene

The electrical property of undoped graphene were evaluated by Hall measurement, and the result is in **Figure 4-2**. The sheet resistance of graphene decreased from about 480 ohm/sq to 400 ohm/sq as the average graphene grain size increased. The carrier concentration is relatively constant with 8.5×10^{12} /cm^2, the carrier mobility is increased from 1500 to 1800 cm^2/Vs as the average grain size increased. The electrical property result is corresponding to the previous reported result, as the grain size of graphene increased, the sheet resistance of graphene is reduced because the mobility scattering in grain boundary decreased causing increase its mobility. The doped graphene also has similar electrical property behavior. As the grain size increased the sheet resistance of graphene reduced since the carrier mobility increased and the carrier concentration relatively stays constant as **Figure 4-3**. However, because the graphene is doped, the carrier concentration is increased from 8.5×10^{12} /cm^2 to 2.1×10^{13} /cm^2 and the sheet resistance of graphene is reduced from 400~500 to 200~250 ohm/sq over 10~80 um of grain size. The carrier mobility is also increased in doped graphene as the average grain size is increased as **Figure 4-3(c)**, it is in the range of 1200~1400 cm^2/Vs which less than undoped graphene case, since the additional charge impurity scattering arises from dopant element. From the numerical formula $R_S = R_S^G + R_S^{GB}$, as the average grain size is increased the portion of the grain boundary sheet resistance, R_S^{GB}, decreased and in extreme case, when the graphene grain size is increased extremely like single crystal graphene, then $R_S \approx R_S^G$ as **Figure 4-2** left graph downer dash lines. Then, the gap between the experimental sheet resistance data (or total sheet resistance R_S) and R_S^G would be the R_S^{GB}. In the same manner, the carrier mobility converges to the mobility of

grain, μ_G, as the grain size increased and the grain boundary mobility, μ_{GB}, show some far below value than μ_G as **Figure 4-2**. It is noted that the carrier concentration and carrier mobility both positive with major carrier is hole. Typically, the transferred CVD graphene has major hole carrier because of electron capturing from SiO_2 substrate, and p-type doping effect of oxygen-based molecules from air environment contamination.[1, 6, 7] Even though graphene is transferred on PET substrate, similar phenomena seem to occurs on prepared graphene samples.

To extract R_S^G, R_S^{GB} and μ_G, μ_{GB} terms, and evaluate electrical property of graphene grain boundary, two different method were performed, extracting grain boundary property from simple numerical formula, ohmic scaling model, and considering graphene grain boundary as a scattering center in the point of view of transport dynamics, using Mayadas-Shatzkes model.
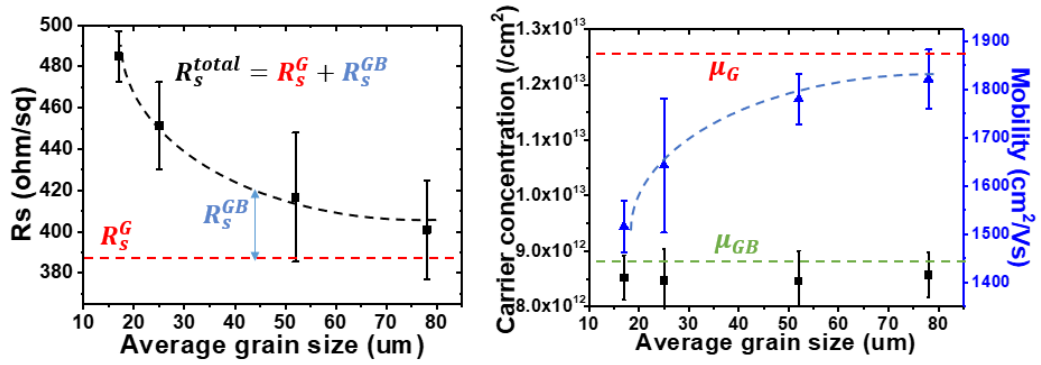
Figure 4-2. The electrical property of undoped graphene with various grain size measured by Hall measurement system. The sheet resistance (left graph), carrier concentration (right graph, left side of vertical axis with black square) and carrier mobility (right graph, right side of vertical axis with upper triangle).
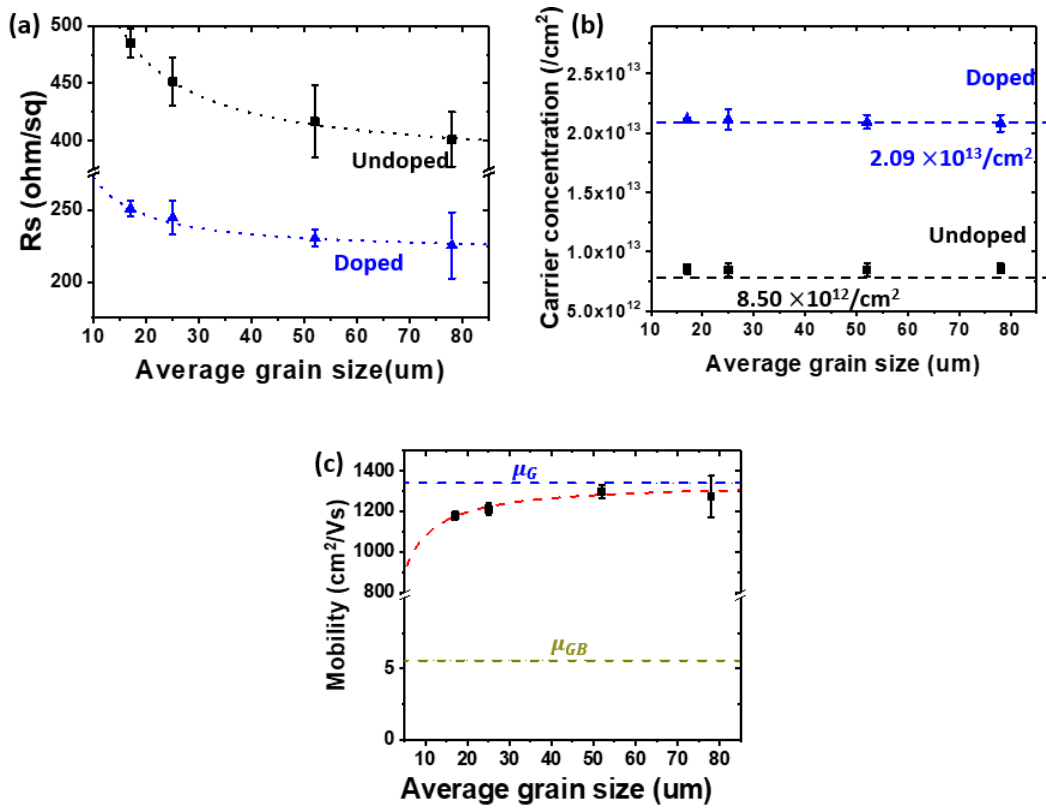
Figure 4-3. The electrical property of undoped/dope graphene with various grain size. (a) the sheet resistance of undoped (square) and doped (upper triangle) graphene with average grain size. (b) the carrier concentration of undoped/doped graphene. (c) the carrier mobility of doped graphene.

4.2. Ohmic scaling model

4.2.1. Ohmic scaling model

If grain boundary graphene is considered to the another 2-D bulk material same as graphene grains, electrical property of grain boundary can be extracted by simple numerical calculation. An ohmic scaling model was proposed for 1-D numerical calculation model for graphene grain and grain boundary.[8, 9] There are 3 major assumption is made in the ohmic scaling model, first, the graphene grain and grain boundary are bulk material which have resistance value. Second, the graphene grain exist as rectangular shape and grain boundary is straight line between graphene grains. Lastly, each grains and grain boundary has same electrical property. The principle and derivation of the ohmic scaling model is described in **Figure 4-4**. The derivation of the ohmic scaling model is follows in detail. Since the grain and grain boundary are both bulk materials having resistance, the total resistance of graphene, R, can be expressed,

$$R = R_1^G + R_1^{GB} + R_2^G + R_2^{GB} + R_3^G + R_3^{GB} \cdots + R_n^G + R_n^{GB}$$

R_i^G is the resistance of graphene grain, R_i^{GB} is the resistance of graphene grain boundary. Since each grain and grain boundary have same electrical property respectively from assumption, and resistance $R = \rho \frac{L}{Wt}$, therefore,

$$R = \sum_{i=1}^{n} R_i^G + \sum_{i=1}^{n} R_i^{GB}$$

$$R = \sum_{i=1}^{n} [R_S^G] \frac{L_i}{W} + \sum_{i=1}^{n} [R_S^{GB}] \frac{L_{GB}^*}{W}$$

R_S^G, R_S^{GB} is the sheet resistance of graphene grain and grain boundary, and L_i is the length of ith grain, L_{GB}^* is the length of grain boundary. Since, $\sum L_i \approx L$ (neglecting L_{GB}^* value) and L_{GB}^* is constant,

$$R = R_S^G \frac{L}{W} + nR_S^{GB} \frac{L_{GB}^*}{W}$$

$$\rho \frac{L}{Wt} = R_S^G \frac{L}{W} + nR_S^{GB} \frac{L_{GB}^*}{W}$$

$$R_s \frac{L}{W} = R_S^G \frac{L}{W} + nR_S^{GB} \frac{L_{GB}^*}{W}$$

$$R_s = R_S^G + [R_S^{GB} L_{GB}^*] \frac{n}{L}$$

$$R_s = R_S^G + \rho^{GB} \frac{1}{L_G}$$

$$\rho^{GB} = R_S^{GB} L_{GB}^*, \quad and \quad \frac{n}{L} = \frac{1}{L_G}$$

ρ^{GB} is defined by the resistivity of grain boundary (having unit of $k\Omega \cdot \mu m$), and L_G is the average grain size by definition. From above equation, the total sheet resistance (or measured sheet resistance) of graphene is inversely proportional to the its grain size since R_S^G, and ρ^{GB} is constant, and the value of ρ^{GB} is reported about 0.1~10 $k\Omega \cdot \mu m$.[8-11] To extract and calculate grain boundary property of mobility and carrier concentration, the ohmic scaling model is modified. Re-considering grain and grain boundary length,

$$\sum_{i=1}^{n} L_i = L_{grain}$$

$$\sum_{i=1}^{n} L_{GB}^* = nL_{GB}^* = L_{GB}$$

$$L_{grain} + L_{GB} = L$$

Then the sheet resistance of graphene can be expressed as follows,

$$R_S = \frac{L_{grain}}{L} R_S^G + \frac{L_{GB}}{L} R_S^{GB}$$

And if $\frac{L_{GB}}{L} = \chi$,

$$R_S = (1 - \chi) R_S^G + \chi R_S^{GB}$$

Then, R_S is the sum of R_S^G and R_S^{GB} with multiplied by each portion of length. Since the $L \gg L_{GB}$,

$$R_S = R_S^G + \chi R_S^{GB}$$

The carrier concentration can be explained similar method as shown in **Figure 4-5**. The total carrier concentration is given by,

$$N = Wt \sum_{i=1}^{n} n^G L_i + Wt \sum_{i=1}^{n} n^{GB} L_{GB}^*$$

$$N = Wt n^G L_{grain} + Wt n^{GB} L_{GB}$$

$$N \frac{1}{WtL} = n = \frac{L_{grain}}{L} n^G + \frac{L_{GB}}{L} n^{GB}$$

$$n_s = \frac{L_{grain}}{L} n_s^G + \frac{L_{GB}}{L} n_s^{GB}$$

$$n_s = (1 - \chi) n_s^G + \chi n_s^{GB}$$

In the same reason, $L \gg L_{GB}$,

$$n_s = n_s^G + \chi n_s^{GB}$$

Here, N is the total number of carrier (with unit /cm^3) and n_s is the sheet carrier concentration. Without further notice, the carrier concentration of graphene normally means the sheet carrier concentration. From the experimental result of the carrier concentration on undoped/doped graphene in **Figure 4-2** (right graph) and **Figure 4-3(b)**,

there is no significant deviation or trends of the carrier concentration over grain size of graphene, and also χ is in the order of $\sim 10^{-5}$. Therefore, if n_S^{GB} is not extremely larger than n_s, $i.g.$, $\sim 10^{15}$ /cm^2, the term χn_S^{GB} becomes negligible. The carrier mobility can be calculated from equations, $R_s = R_S^G + \chi R_S^{GB}$ and $R_s = \frac{1}{n_s q \mu}$,

$$R_s = R_S^G + \chi R_S^{GB}$$

$$\frac{1}{n_s \mu} = \frac{1}{n_S^G \mu_G} + \chi \frac{1}{n_S^{GB} \mu_{GB}}$$

Here, if $n_S^G \approx n_S^{GB}$ is assumed, (further detail of this assumption will be described in section 4.2.3 and 4.4.1) then $n_s \approx n_S^G \approx n_S^{GB}$, so,

$$\frac{1}{\mu} = \frac{1}{\mu_G} + \chi \frac{1}{\mu_{GB}}$$

Therefore, the sheet resistance, carrier concentration and the carrier mobility can be expressed as following simple equations,

$$R_s = R_S^G + \chi R_S^{GB}$$

$$n_s = n_S^G + \chi n_S^{GB}$$

$$\frac{1}{\mu} = \frac{1}{\mu_G} + \chi \frac{1}{\mu_{GB}}$$
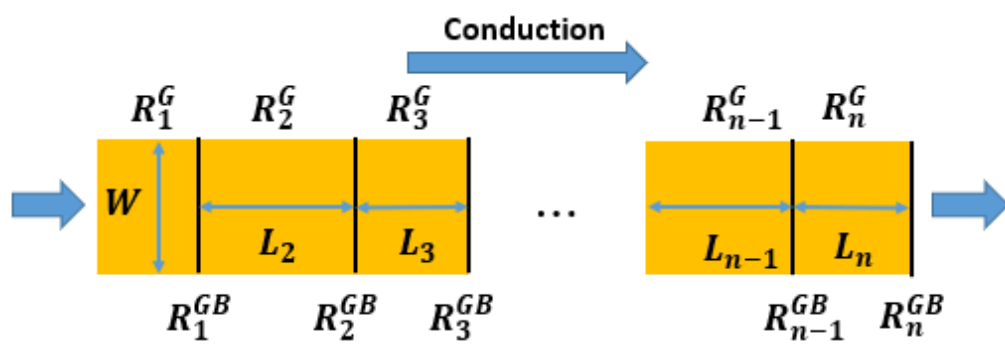
Figure 4-4. The principle and derivation of the ohmic scaling model.

Figure 4-5. The principle of calculating total carrier concentration using ohmic scaling model.

4.2.2. Application of ohmic scaling model

The sheet resistance of undoped graphene in **Figure 4-2** can be fitted by the equation $R_s = R_S^G + \chi R_S^{GB}$ and the result is in the **Figure 4-6**. The R_S^G is fitted to 379 ohm/sq, meaning that the single grain of graphene have average 379 ohm/sq of the sheet resistance, and if the grain size is extremely enlarged the sheet resistance converged to 379 ohm/sq. The ρ^{GB} is fitted to 1808 $k\Omega \cdot \mu m$ which is similar to the previously reported ρ^{GB}. For clear view of the grain boundary portion in sheet resistance of graphene, the sheet resistance is expressed in columnar graph as shown in **Figure 4-7**. In the case of 17 um of grain size, the χR_S^{GB}, the portion of grain boundary is 22 % which is incredibly large. Comparing with the thin-film metal, the graphene has more than 10 um of grain size but considering typical thin film has few hundreds of grain size. Even though graphene has about 100 times larger grain size, 22% of the sheet resistance arises because of grain boundary itself. From the fitted value the grain and grain boundary mobility can be calculated with following equations,

$$\mu_G = \frac{1}{q n_s^G R_S^G}$$

$$\mu_{GB} = \frac{1}{q n_s^{GB} R_S^{GB}}$$

To determine R_S^{GB}, the single grain boundary length L_{GB}^* required to define. The most stable grain boundary, Stone-Wales grain boundary in **Figure 2-8**,[12] the length of grain boundary is about 0.3~0.4 nm. However, the grain boundary in polycrystalline graphene has not only Stone-Wales grain boundary which consisted of penta-, heptagon of carbon rings, but also has polygons, voids as **Figure 2-9**.[13] Therefore, L_{GB}^* is determined from

polycrystalline graphene grain boundary in **Figure 2-9** with about 0.7 nm. The mobility of grain and grain boundary is calculated as follows,

$$\mu_G = \frac{1}{qn_s^G R_S^G} = 1940 \ \text{cm}^2/\text{Vs}$$

$$\mu_{GB} = \frac{1}{qn_s^{GB} R_S^{GB}} = 2.85 \times 10^{-1} \ \text{cm}^2/\text{Vs}$$

The grain mobility is calculated to 1940 cm²/Vs, and the carrier mobility of graphene considered to converges to the value 1940 cm²/Vs. This value is far from the carrier mobility of single crystal graphene, 200,000 cm²/Vs, [2] and that single crystal graphene is typically measured FET device or Hall bar system, in very clear environment, (*i.g.*, including degassing process to remove contaminations, and measuring UHV environment to prevent further contamination from air), with suspended condition (removing substrate scattering effect), without wet transfer process (typically sample is prepared by mechanical cleavage method).[1, 2, 14] The grain boundary mobility was calculated below 1, which means that grain boundary act as strong scattering center, and one of the dominant factors for limiting electrical property of graphene. Using equation $\frac{1}{\mu} = \frac{1}{\mu_G} + \chi \frac{1}{\mu_{GB}}$, calculated the total mobility denoted on **Figure 4-8**, and experimental data is well fitted by mobility equation.

The doped graphene also evaluated by ohmic scaling model and very similar behavior was observed. The calculated various terms are summarized in **Table 4-1** at 17 um size of graphene. The sheet resistance of grain, R_S^G, is reduced from 379 to 220 ohm/sq, the μ_G is decreased in doped graphene about 0.7 times because of charge impurity scattering, the carrier concentration is 2.5 times increased by doping process. The calculated μ_{GB} is

about 0.4 cm^2/Vs in doped graphene, it is clearly showing that the mobility of grain boundary is relatively low regardless of doping effect.

$$R_s = R_s^G + [R_s^{GB} L_{GB}^*] \cdot \frac{1}{L_G}$$
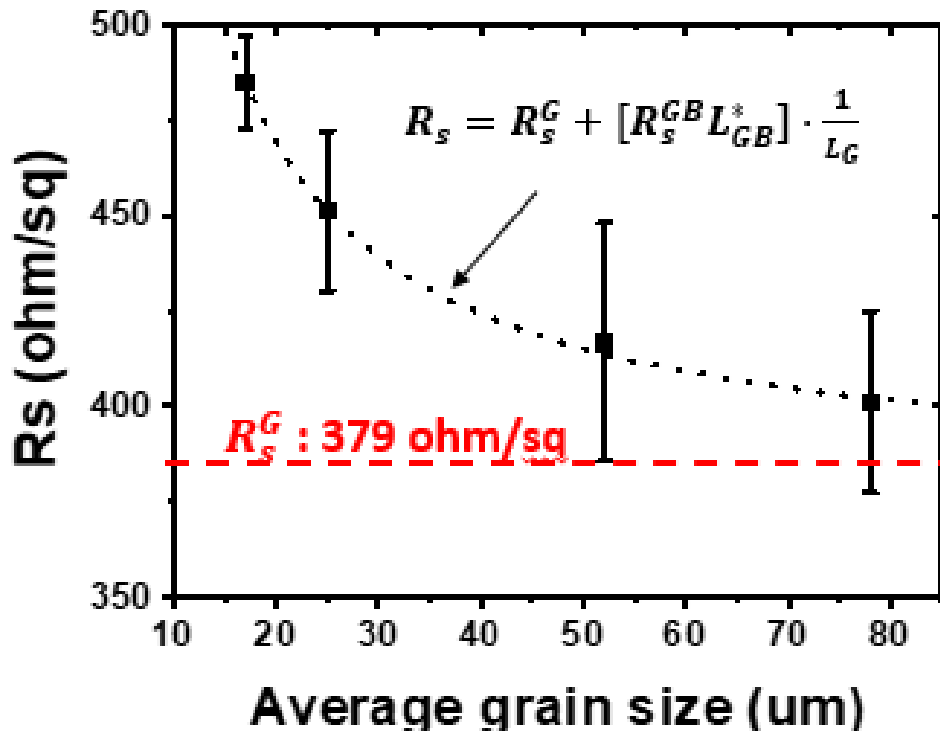
$R_S^G : 379$ ohm/sq

Figure 4-6. The fitted sheet resistance of undoped graphene (dot), the dashed line represents the R_S^G value.
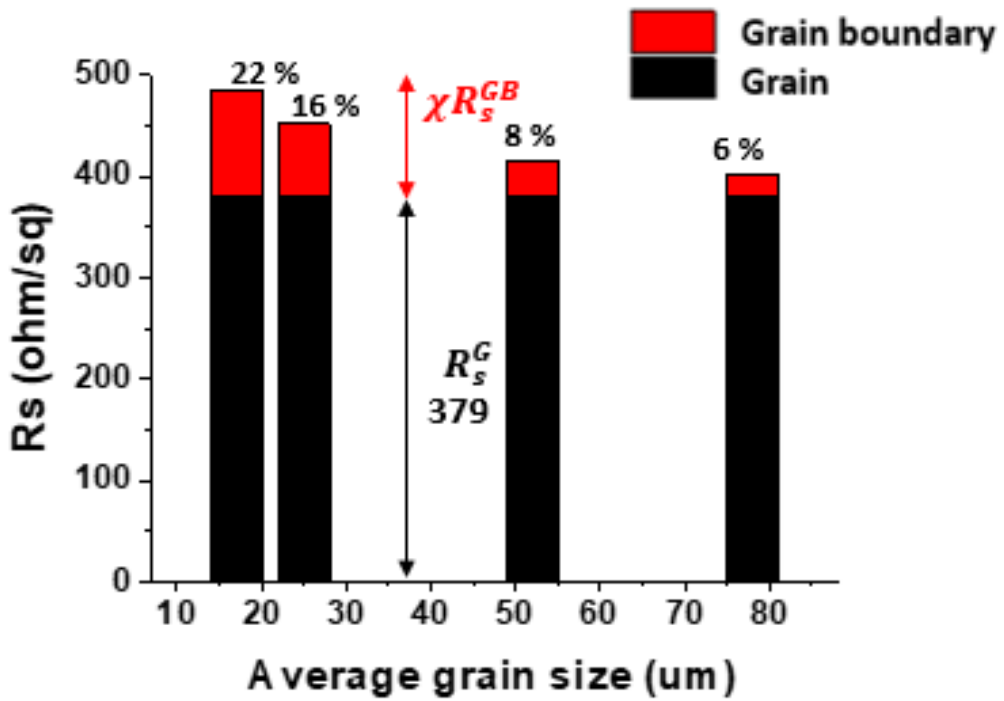
Figure 4-7. The column graph of the sheet resistance of graphene with various grain size. The portion of graphene grain is 379 ohm/sq (down side of column) and the portion of grain boundary is denoted on upside of the column.
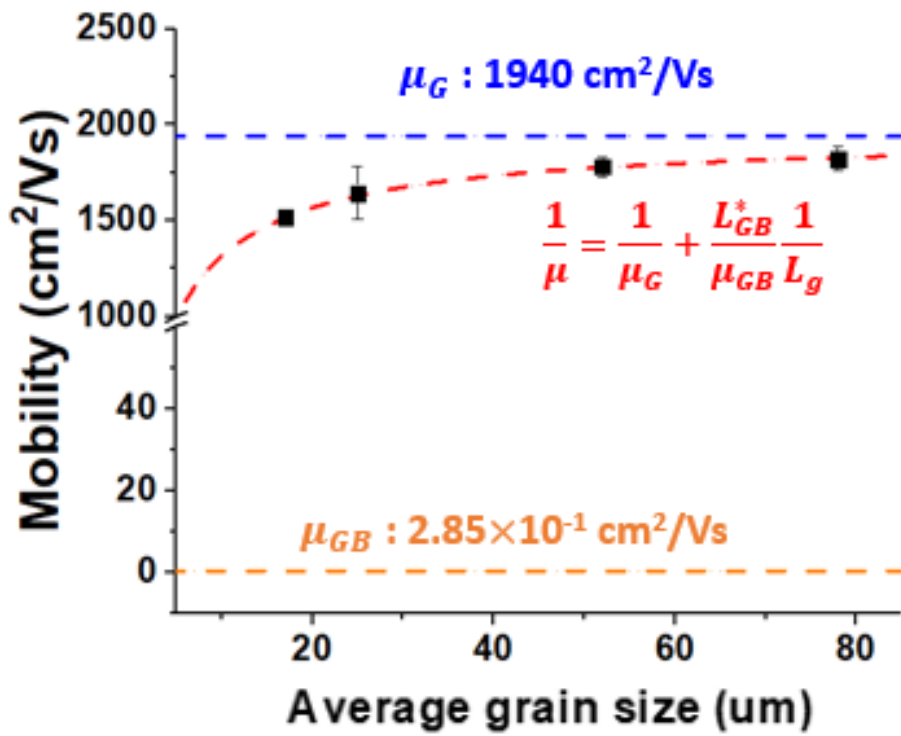
Figure 4-8. The carrier mobility of undoped graphene with various grain size (square), and the calculated grain mobility, total mobility, grain boundary mobility is expressed as dashed lines.

Terms	Undoped	Doped
R_S^G [ohm/sq]	379	220
χR_S^{GB} [ohm/sq]	106	31
n_s [/cm^2]	8.5×10^{12}	2.1×10^{13}
μ_G [cm$_2$/Vs]	1940	1360
μ_{GB} [cm$_2$/Vs]	2.9×10^{-1}	4.0×10^{-1}

Table 4-1. The summary of electrical property of undoped/doped graphene with 17 um size using ohmic scaling model.

4.2.3. Limitation of ohmic scaling model

Using ohmic scaling model, the sheet resistance of graphene grain boundary was successfully extracted and mobility also calculated. The terms ρ^{GB} is generally accepted in graphene articles,[8, 9] however, other terms such as μ_{GB} , n_s^{GB}, L_{GB}^* are not yet used term in the field of graphene and uncertainty is exist considering those terms. The L_{GB}^*, for example, it is hard to define the grain boundary length itself which have various conditions and status. In this chapter, 0.7 nm was used from statistical data from **Figure 2-9**, more variation can be occurred by various growth condition of CVD graphene. In **Figure 4-9**, the μ_{GB} is calculated from various L_{GB}^*, and as the L_{GB}^* increased, the μ_{GB} is also increased proportionally. Also, during derivation of mobility equation in section 4.2.1, the carrier concentration is assumed as $n_s^G \approx n_s^{GB}$. The value of n_s^G is seem to be reasonable in logically and experimentally, defining n_s^{GB} is very difficult and hard to know its value. Generally, the grain boundary is defined into two different point of view, as a charge trapping potential barrier in semiconductor, and as a scattering center in carrier transport dynamics in typical metal as shown in **Figure 4-10**. The former case, grain boundary acts as charge trapping site and forming depletion layer, and considered to the potential barrier for electric conduction. The latter case, grain boundary doesn't act as charge trapping site, rather just scattering center for carrier transport. It is hard to judge which is the case in graphene grain boundary but graphene grain boundary is rather act as carrier generating site from doping, and most of electrical property is similar to the metal electrical property. Therefore, from ohmic scaling model, it is hard to clearly accept the value of μ_{GB}, n_s^{GB}, L_{GB}^*, quantitively, it is certain and assured by ohmic scaling model that graphene grain boundary act as strong scattering center qualitatively. To complement the limitation of

ohmic scaling model which extract grain boundary property by simple numerical calculation, Madayas-Shatzkes model was used to analyze grain boundary property of graphene which is classical model of grain boundary carrier transport.
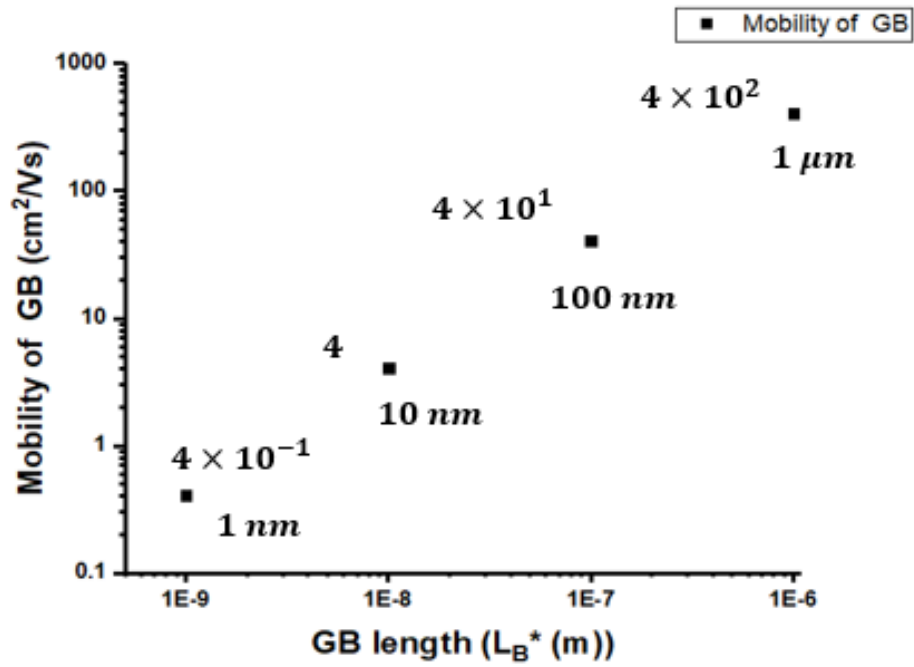
Figure 4-9. The calculated grain boundary mobility in the function of grain boundary length.

Semiconductor
GB as a potential barrier by charge trap
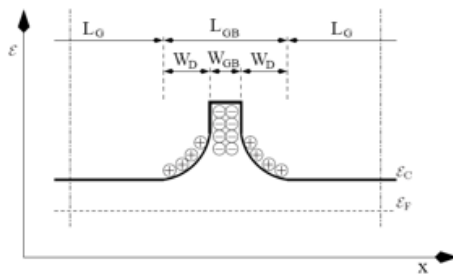
Metal
GB as a scattering center
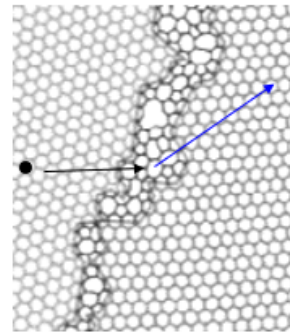
Figure 4-10. Two different classical point of view considering grain boundary. [13, 15]

4.3. Mayadas-Shatzkes model

4.3.1. Mayadas-Shatzkes model

 In classical model for metal thin film, the resistivity of metal thin film can be described as follows,

$$\rho_{totoal} = \rho_0 + \rho_{FS} + \rho_{MS}$$

The ρ_{totoal} is the total resistivity of metal thin film, the ρ_0 is the bulk resistivity, the ρ_{FS} is the resistivity by surface scattering with Fuch-Sonheimer (FS) model (or Fuch size effect),[16] the ρ_{MS} is the resistivity by grain boundary scattering with MS model.[17] On 1970s, during the thin-film technology arises, people found out that lower film thickness result increased ρ_{totoal} of thin film, and Fuch *et al.* postulated that surface scattering factor act an important role in metal thin film, as follows,[16]

$$\rho_{FS} = \rho_i \left[1 - \left(\frac{3}{2k} \right)(1-p) \int_1^\infty \left(\frac{1}{t^3} - \frac{1}{t^5} \right) \frac{1-\exp(-kt)}{1-p\cdot\exp(-kt)} dt \right]^{-1}$$

$$k = a/l_i$$

The a is thin film thickness, l_i is the intrinsic mean free path, p is the probability of electron scattering at surface, ρ_i is the thickness independent resistivity of metal which does not consider grain boundary scattering. After massive study on surface scattering of thin films, people also found out that the single crystal film and polycrystalline film have different ρ_i value which is constant material property.[18] Mayadas *et al.* have found that in evaporated Al films ρ_i is increased with decreasing film thickness, and the fact that the film thickness and grain diameter is very similar is also found out.[19, 20] Mayadas *et al.* claimed that grain boundary act as a scattering center in thin film, and MS model was

established. In MS model, the grain boundary is denoted as potential barrier as the δ function with strength s, and the background scattering (scattering in grain *i.g.*, lattice phonon scattering) is set as point defects and phonon as illustrated in **Figure 4-11**. The position of grain boundary is distributed by Gaussian distribution. The carrier transport equation is carried out by Boltzman equation for the geometry on **Figure 4-11** is given by,[17]

$$eE_{v_x}\frac{\partial f_0(\mathbf{k})}{\partial \epsilon} = \int P(\mathbf{k},\mathbf{k}')[\Phi(\mathbf{k}) - \Phi(\mathbf{k}')]d\mathbf{k} + \frac{\Phi(\mathbf{k})}{\tau}$$

The E is the electrical field, $P(\mathbf{k},\mathbf{k}')$ is the transition probability for an electro in state $\mathbf{k}$ to be scattered to $\mathbf{k}'$, $\Phi(\mathbf{k}) - \Phi(\mathbf{k}')$ is the deviation of the distribution function $f(\mathbf{k})$ from its equilibrium value $f_0(\mathbf{k})$, v_x is the x component of velocity, ϵ is the electron energy. The resultant resistivity considering grain boundary scattering is as follows,[17]

$$\rho_{GB} = \rho_0\left[1 - \frac{3}{2}\alpha + 3\alpha^2 - 3\alpha^3\ln\left(1 + \frac{1}{\alpha}\right)\right]$$

$$\alpha = \left[\left(\frac{\lambda}{g}\right)\left(\frac{R}{1-R}\right)\right]$$

here, λ is the mean free path, g is the grain size and R is reflection coefficient ($0 < R < 1$) which is the experimental factor. The reflection coefficient factor is the index of grain boundary scattering which is extracted by experimental data, high R means that scattering effect is very strong at grain boundary, and low R means that relatively weak scattering effect at grain boundary as shown in **Figure 4-12**.
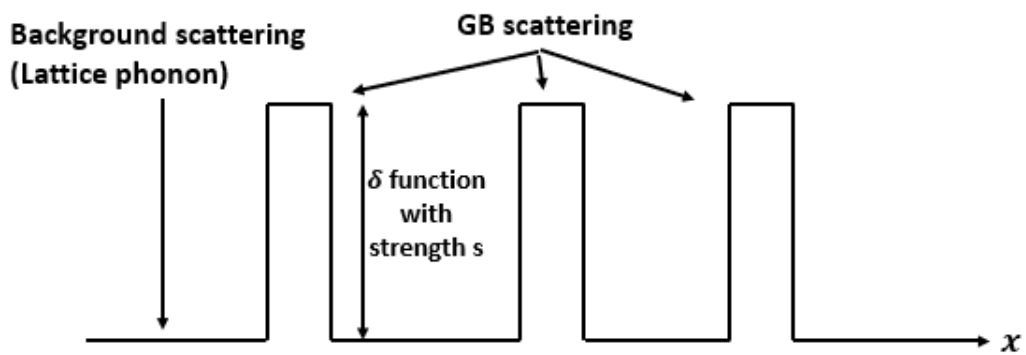
Figure 4-11. Model for calculating ρ_{GB} including grain boundary scattering and background scattering on grain.
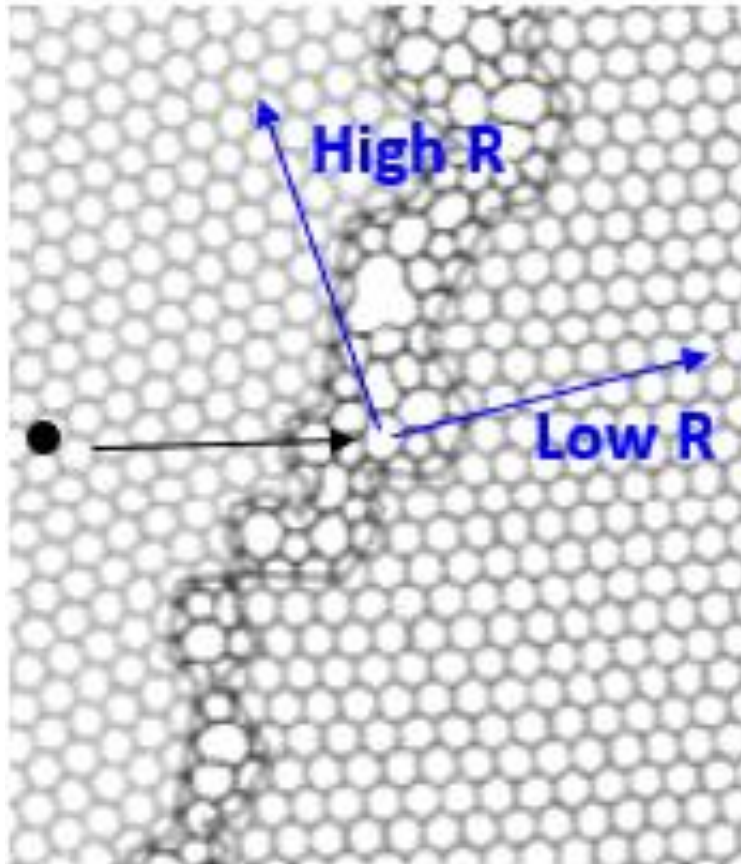
Figure 4-12. The schematic illustration of reflection coefficient on grain boundary scattering.[13]

4.3.2. Application of MS model

Prior to apply MS model in undoped graphene, ρ_{GB} equation should be altered in R_s^{GB} form as follows, [17, 21, 22]

$$R_s = R_s^G + R_s^{GB}$$

$$R_s^{GB} = R_s^{bulk}\left[\left\{1 - \frac{3}{2}\alpha + 3\alpha^2 - 3\alpha^3\ln\left(1 + \frac{1}{\alpha}\right)\right\}^{-1} - 1\right]$$

For the calculation of MS model application, R_s^G value is collected from ohmic scaling model as 379 ohm/sq, and the mean free path of graphene was 3.8 um which is reported from articles. [23, 24] The reflection coefficient is extracted from fitting the graph in **Figure 4-2**, and the fitting is as shown in **Figure 4-13**. The sheet resistance of graphene is well fitted by MS model (the dashed line) and ohmic scaling model (the dot line), corresponding R value is 0.92 in undoped graphene. To compare R value from metals, representative metal's R value is summarized in **Table 4-2**.[17, 18, 21, 25-27] As it can be seen in **Table 4-2**, most of metal have 0.2~0.5 of R value, however, the undoped graphene has significantly large R value which postulate that grain boundary is act as strong scattering center. The application of MS model in doped graphene is shown in **Figure 4-14**. The resultant R in doped graphene is 0.76, and R value is decreased from undoped graphene, still very high comparing other metals. The reason for reduce of R in doped graphene is unclear, one of the possible reasons is that grain boundary oriented doping effect on graphene,[28] the carrier generation is more efficient on the grain boundary of graphene resulting reducing the sheet resistance of graphene on grain boundary.
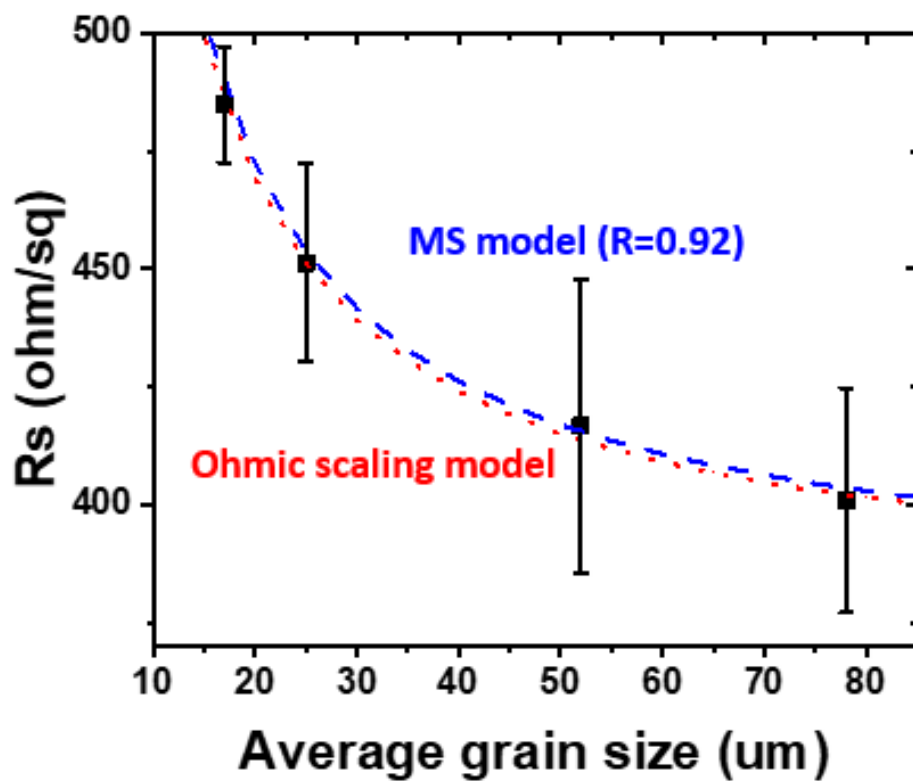
Figure 4-13. The fitting of MS model and ohmic scaling model on the sheet resistance of undoped graphene with various grain size. The dashed line is MS model, and the dot line is ohmic scaling model.

Materials	Undoped
Ni	0.41
Ti	0.45
Pt	0.46
Cu	0.27
Ag	0.35
Al	0.22

Table 4-2. The reflection coefficient of metals.
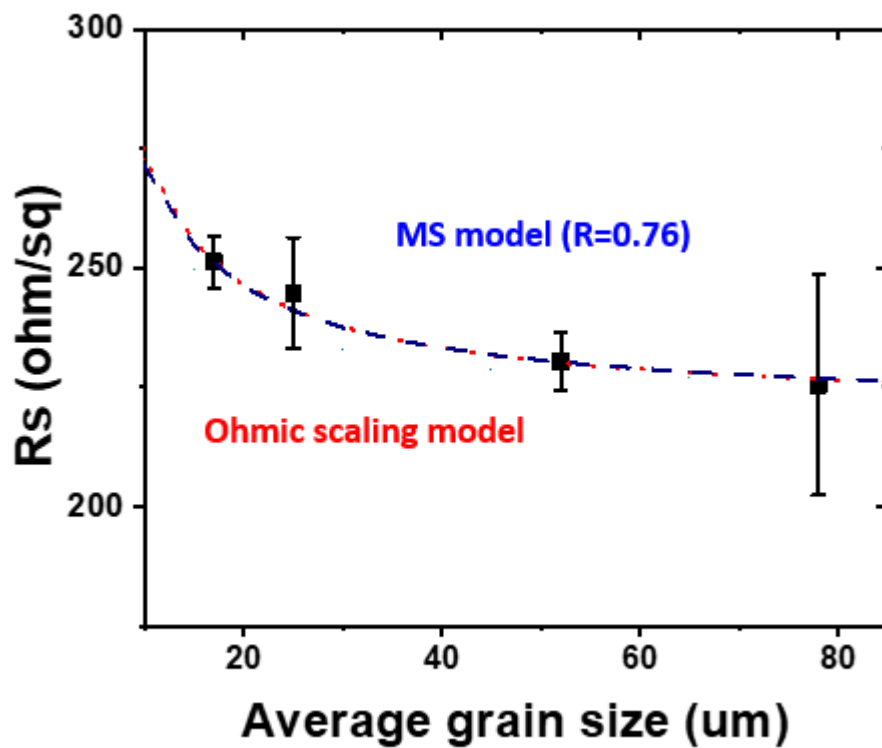
Figure 4-14. The fitting of MS model and ohmic scaling model on the sheet resistance of doped graphene with various grain size. The dashed line is MS model, and the dot line is ohmic scaling model.

4.4. Approaches to overcome electrical property limiting factor of CVD graphene

4.4.1. The doping and the enlarging grain size

The approaches to overcome electrical property of CVD graphene is various, as mentioned in section 2.3, doping and increasing graphene grain size is major approaches for enhancing electrical property of CVD graphene. In this chapter, both major methods were evaluated and it is possible to compare which method is more efficient in ideally, or in practically. First, considering doping effect, the efficiency of doping can be expressed as,

$$\eta = \left| \frac{(R_{s,doped} - R_{s,undoped})}{R_{s,undoped}} \times 100 \ (\%) \right|$$

Here, η is the doping efficiency of doped graphene and it is shown in **Figure 4-15(a)** based on the ohmic scaling model. The experimental grain size range 17~78 um, η is about 45 % relatively constant. Even though η becomes higher at the small size of graphene grain, the sheet resistance cannot be inverse because undoped graphene at the small grain size much larger as shown in **Figure 4-15(b)**. Interestingly, the doping efficiency tends to increase as the average grain size decreased, implying that the density of grain boundary affects doping effect. In other words, larger grain boundary density shows higher doping efficiency, doping is promoted more on graphene grain boundary. From the value in **Table 4-1**, R_s^G is reduced about 1/2 times after doping, however, R_s^{GB} is reduced about 1/3 after doping, the electrical property grain boundary is more enhanced after doping than that of the graphene grain. This phenomenon is contradictory to the

assumption in carrier concentration part of ohmic scaling model, $n_s^G \approx n_s^{GB}$, rather, the efficiency graph implying that $n_s^G < n_s^{GB}$. Considering $n_s^G < n_s^{GB}$, the carrier concentration on doped graphene can be re-written as following equations,

$$n_s = n_s^G + \chi n_s^{GB}$$

$$\chi = \frac{L_{GB}}{L} = \frac{nL_{GB}^*}{L} = \frac{L_{GB}^*}{L_G}$$

$$n_s = n_s^G + n_s^{GB} \cdot \frac{L_{GB}^*}{L_G}$$

Here, n_s^G, n_s^{GB}, L_{GB}^*, is constant, therefore, n_s is the function of L_G and the carrier concentration of doped graphene can be fitted as **Figure 4-16**. From the fitting, calculated n_s^G and n_s^{GB} are 2.1×10^{13} /cm² and 5.8×10^{14} /cm² respectively, the carrier concentration is higher on the graphene grain boundary. The mobility equation also can be re-written as follows,

$$\frac{1}{n_s \mu} = \frac{1}{n_s^G \mu_G} + \chi \frac{1}{n_s^{GB} \mu_{GB}}$$

$$\frac{1}{\mu} = \frac{1}{\gamma_1 \mu_G} + \chi \frac{1}{\gamma_2 \mu_{GB}}$$

$$\gamma_1 = n_s^G / n_s \quad and \quad \gamma_2 = n_s^{GB} / n_s$$

Using above equation, calculated graphene mobility is shown in **Figure 4-17**. As it can be seen in **Figure 4-17**, the calculated mobility well matched with experimental data. In both cases, $n_s^G \approx n_s^{GB}$ and $n_s^G < n_s^{GB}$, the mobility fitting is well matched and the decrease of carrier concentration is relatively small compared with the its deviation, it is hard to judge which assumption is appropriate in electrical property of grain boundary. The grain boundary oriented doping effect is further analyzed on chapter 5 by selective Ru ALD on

graphene grain boundaries.[28]

  Increasing grain size is readily studied in section 4.2.2 and based on the graphene with 17 um of grain size, about 20 % of the sheet resistance reduce expected by increasing grain size. In the view point of effectiveness of reducing the sheet resistance, the doping process has about 45 % and the enlarging grain size has about 20 % of the sheet resistance reduce. In practically, the doping process such as dipping, spin coating, and deposition of dopant (by PLD, ALD) is simple, however, growing larger size of grain requires high cost and long process time. In **Table 4-3**,[29-31] the process time and corresponding grain size is summarized. To increase grain size of graphene, extremely reducing carbon source supply required and therefore, process time should be longer. Considering CVD graphene process conducted on 1000 °C of high temperature, the cost also becomes higher as the process times becomes longer. Therefore, in the point of reducing the sheet resistance, and practically also, doping is more efficient way for enhancing electrical property of graphene. One thing to be noted is that if the grain size of graphene becomes small as 1 um, expecting sheet resistance of graphene is about 2000 ohm/sq according to the ohmic scaling model. In this case, the sheet resistance of undoped graphene is high and expecting doping graphene has only 780 ohm/sq of the sheet resistance. Therefore, the best way for enhancing electrical property of graphene is that synthesize 10~50 um size of graphene (which process time is about 5 min ~ 1 hour) and conduct doping process.
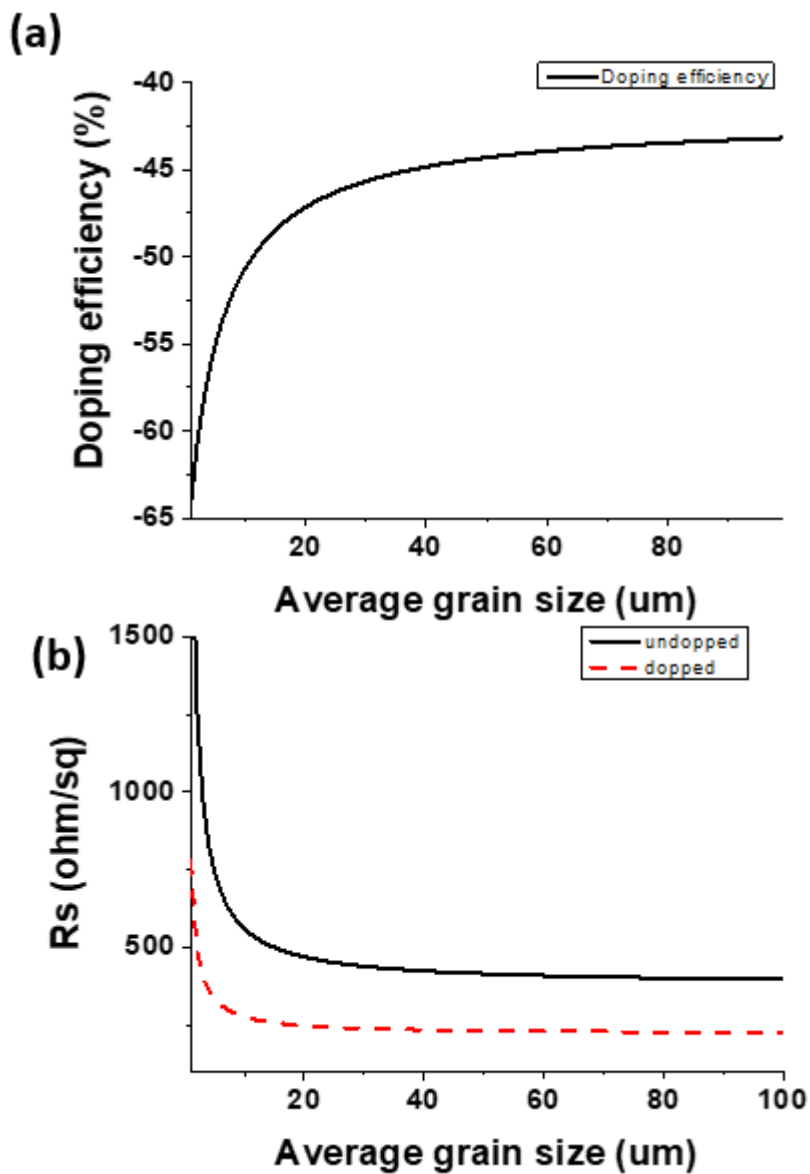
Figure 4-15. (a) the doping efficiency of the graphene with various grain size based on the

ohmic scaling model, and (b) is the expecting sheet resistance of undoped/doped graphene.
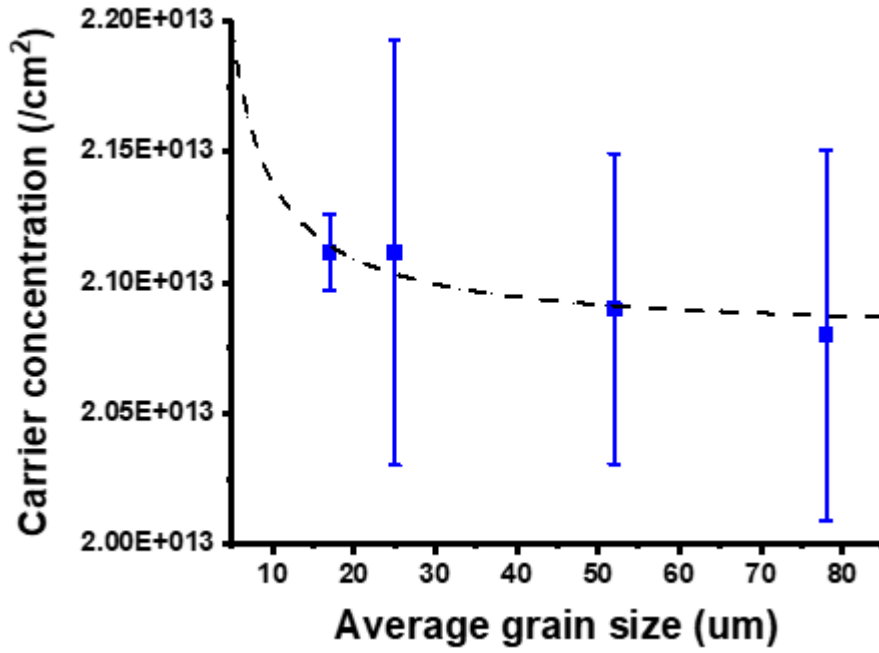
Figure 4-16. The carrier concentration fitting of graphene with various grain size, with the

assumption of $n_S^G < n_S^{GB}$.
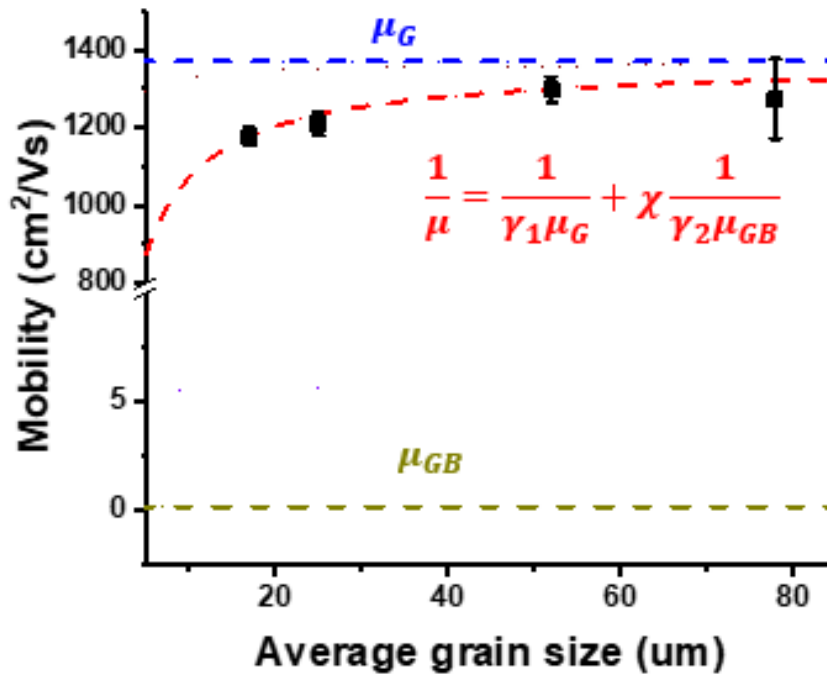
Figure 4-17. The mobility of doped graphene (square) and the calculated mobility based on the equation in the case of $n_S^G < n_S^{GB}$.

Method	Principle	Process time	Grain size	Ref.
Longtime pre-annealing	Removing nucleation site	3.5 h	1.2 mm	[30]
Low chamber pressure	Reducing C supply	9 h	2.3 mm	[29]
Oxidized Cu + H$_2$	Removing nucleation site	48 h	5 mm	[31]
NFL CVD process	Typical CVD growth	5 min	17 μm	-

Table 4-3. The summarized characterization for reported mm-sized graphene.

4.4.2. The portion of limiting factors in the sheet resistance of graphene

In section 2.2, the electrical property limiting factors of graphene can be summarized into 4 components as,

$$R_S = R_S^{bulk} + R_S^{sub} + R_S^{GB} + R_S^{etc.}$$

R_S^{bulk} and R_S^{sub} is readily calculated on section 2.2 and R_S^{GB} is calculated using ohmic scaling model R_S is the measured total sheet resistance of graphene. Therefore, $R_S^{etc.}$, also can be extracted and each portion can be expressed in **Figure 4-18** at the 17 um case. It is very interesting that, the bulk sheet resistance has only 6 % of portion and surprisingly, $R_S^{etc.}$ has 45 %. The $R_S^{etc.}$ is including impurity scattering from air environment contamination, and addition damage during transfer process (crack voids and further impurity contamination). The **Figure 4-18** postulate that devolvement of clean and stable transfer process can be one of the best ways for reducing electrical property of graphene, and prior to other limiting factors. And also, from the **Figure 4-18**, practically it is hard to change the substrate to reduce 25 % of R_S^{sub} because most of industrial standard is based on the Si and SiO$_2$, practically, removing grain boundary can play significant role to reduce the sheet resistance of graphene if $R_S^{etc.}$ is improved. The circular diagram in other grain size is in the **Figure 4-19**. It is noted that PET substrate is used in this experiment and analysis on R_S^{sub} can be different in SiO$_2$ case, however, using the same graphene growth condition, the electrical property difference between PET and SiO$_2$ substrate was minor in current CVD graphene growth and electrical property measurement system.
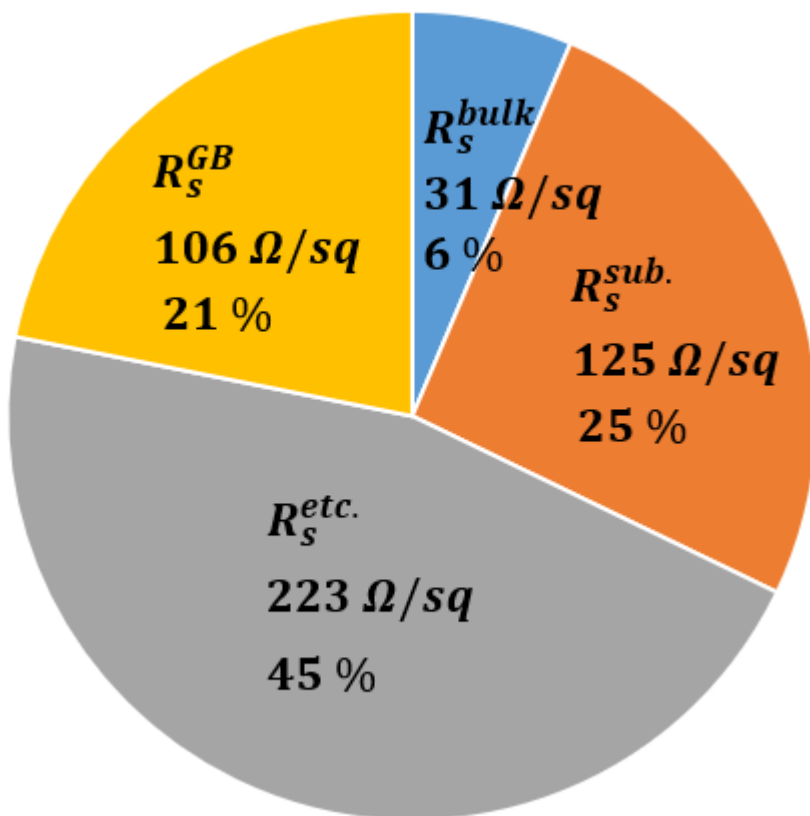
Figure 4-18. The circular diagram of electrical property limiting factors on CVD graphene at 17 um graphene grain.
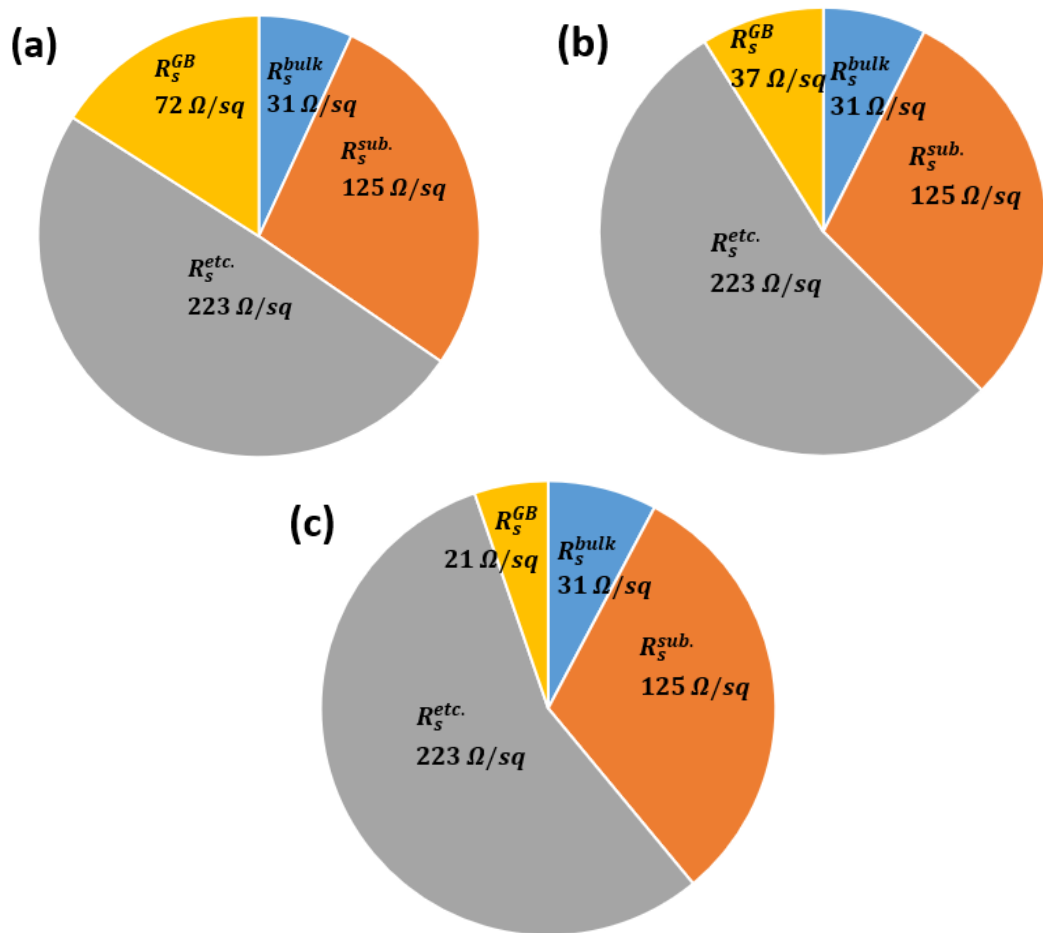
Figure 4-19. The circular diagram of electrical property limiting factors on CVD graphene at (a) 25, (b) 52, (c) 78 um graphene grain.

4.5. Summary and conclusion

The electrical property of graphene grain boundary systematically analyzed using 4 different grain sized graphene, 17, 25, 52, 78 um synthesized from chapter 3. The Hall measurement shows that the sheet resistance of graphene is reduced as the grain size increased regardless of doping because of the mobility enhancement from lowering grain boundary scattering with constant carrier concentration. In two different method, grain boundary property was analyzed, from the simple numerical calculation the ohmic scaling model and MS model which is the classical grain boundary scattering theory in thin film technology. In both ways, the graphene grain boundary is found to the strong scattering center, one of the major limiting factors on electrical property of graphene. From the doping and enlarging graphene grain size experiment which are the dominant electrical property enhancing method in graphene field, two method was compared in the point of view of the sheet resistance reducing efficiency and practical point, doping is turned out to be the effective way, however, extremely small size of graphene has significantly high sheet resistance. Therefore, the best way for enhancing electrical property of graphene is growth 10~50 um grain size of graphene and conduct doping process with high doping efficiency.

References

1. Chen, J.-H.; Jang, C.; Xiao, S.; Ishigami, M.; Fuhrer, M. S., Intrinsic and extrinsic performance limits of graphene devices on SiO2. *Nat Nano* **2008,** *3* (4), 206-209.

2. Bolotin, K. I.; Sikes, K. J.; Jiang, Z.; Klima, M.; Fudenberg, G.; Hone, J.; Kim, P.; Stormer, H. L., Ultrahigh electron mobility in suspended graphene. *Solid State Commun* **2008,** *146* (9-10), 351-355.

3. Reymond, S.; Cossy, J., Copper-Catalyzed Diels−Alder Reactions. *Chemical Reviews* **2008,** *108* (12), 5359-5406.

4. Kim, S. J.; Ryu, J.; Son, S.; Yoo, J. M.; Park, J. B.; Won, D.; Lee, E.-K.; Cho, S.-P.; Bae, S.; Cho, S.; Hong, B. H., Simultaneous Etching and Doping by Cu-Stabilizing Agent for High-Performance Graphene-Based Transparent Electrodes. *Chem Mater* **2014,** *26* (7), 2332-2336.

5. Walba, H.; Isensee, R. W., Acidity Constants of Some Arylimidazoles and Their Cations. *The Journal of Organic Chemistry* **1961,** *26* (8), 2789-2791.

6. Liu, L.; Ryu, S.; Tomasik, M. R.; Stolyarova, E.; Jung, N.; Hybertsen, M. S.; Steigerwald, M. L.; Brus, L. E.; Flynn, G. W., Graphene Oxidation: Thickness-Dependent Etching and Strong Chemical Doping. *Nano Lett* **2008,** *8* (7), 1965-1970.

7. Kang, Y.-J.; Kang, J.; Chang, K. J., Electronic structure of graphene and doping effect on ${\text{SiO}}_{2}$. *Phys Rev B* **2008,** *78* (11), 115404.

8. Isacsson, A.; Cummings, A. W.; Colombo, L.; Colombo, L.; Kinaret, J. M.; Roche, S., Scaling properties of polycrystalline graphene: a review. *2D Materials* **2016,** *4* (1), 012002.

9. Cummings, A. W.; Duong, D. L.; Nguyen, V. L.; Van Tuan, D.; Kotakoski,

J.; Barrios Vargas, J. E.; Lee, Y. H.; Roche, S., Charge Transport in Polycrystalline Graphene: Challenges and Opportunities. *Advanced Materials* **2014,** *26* (30), 5079-5094.

10. Lee, D.; Kwon, G. D.; Kim, J. H.; Moyen, E.; Lee, Y. H.; Baik, S.; Pribat, D., Significant enhancement of the electrical transport properties of graphene films by controlling the surface roughness of Cu foils before and during chemical vapor deposition. *Nanoscale* **2014,** *6* (21), 12943-12951.

11. Yu, Q.; Jauregui, L. A.; Wu, W.; Colby, R.; Tian, J.; Su, Z.; Cao, H.; Liu, Z.; Pandey, D.; Wei, D.; Chung, T. F.; Peng, P.; Guisinger, N. P.; Stach, E. A.; Bao, J.; Pei, S.-S.; Chen, Y. P., Control and characterization of individual grains and grain boundaries in graphene grown by chemical vapour deposition. *Nat Mater* **2011,** *10* (6), 443-449.

12. Huang, P. Y.; Ruiz-Vargas, C. S.; van der Zande, A. M.; Whitney, W. S.; Levendorf, M. P.; Kevek, J. W.; Garg, S.; Alden, J. S.; Hustedt, C. J.; Zhu, Y.; Park, J.; McEuen, P. L.; Muller, D. A., Grains and grain boundaries in single-layer graphene atomic patchwork quilts. *Nature* **2011,** *469* (7330), 389-+.

13. Kotakoski, J.; Meyer, J. C., Mechanical properties of polycrystalline graphene based on a realistic atomistic model. *Phys Rev B* **2012,** *85* (19), 195447.

14. Geim, A. K.; Novoselov, K. S., The rise of graphene. *Nat Mater* **2007,** *6* (3), 183-191.

15. Holzer, S., Optimization for enhanced thermal technology CAD purpose. *Dissortation in institute for microelectronics* **2010**.

16. Sondheimer, E. H., The mean free path of electrons in metals. *Adv Phys* **1952,** *1* (1), 1-42.

17.   Mayadas, A. F.; Shatzkes, M., Electrical-Resistivity Model for Polycrystalline Films: the Case of Arbitrary Reflection at External Surfaces. *Phys Rev B* **1970,** *1* (4), 1382-1389.

18.   Anderson, J. C.;   North Atlantic Treaty Organization.; Imperial College of Science and Technology., *The use of thin films in physical investigations; a NATO Advanced Study Institute held at the Imperial College of Science and Technology, University of London, 19-24 July, 1965*. Academic Press: London, New York,, 1966; p xix, 462 p.

19.   Mayadas, A. F., Intrinsic Resistivity and Electron Mean Free Path in Aluminum Films. *J Appl Phys* **1968,** *39* (9), 4241-4245.

20.   Mayadas, A. F.;   Feder, R.; Rosenberg, R., Resistivity and Structure of Evaporated Aluminum Films. *Journal of Vacuum Science and Technology* **1969,** *6* (4), 690-693.

21.   Zhu, Y. F.;   Lang, X. Y.;   Zheng, W. T.; Jiang, Q., Electron Scattering and Electrical Conductance in Polycrystalline Metallic Films and Wires: Impact of Grain Boundary Scattering Related to Melting Point. *Acs Nano* **2010,** *4* (7), 3781-3788.

22.   Smith, R. S.;   Ryan, E. T.;   Hu, C. K.;   Motoyama, K.;   Lanzillo, N.; Metzler, D.;   Jiang, L.;   Demarest, J.;   Quon, R.;   Gignac, L.;   Breslin, C.; Giannetta, A.; Wright, S., An evaluation of Fuchs-Sondheimer and Mayadas-Shatzkes models below 14nm node wide lines. *Aip Adv* **2019,** *9* (2).

23.   Gholivand, H.; Donmezer, N., Phonon Mean Free Path in Few Layer Graphene, Hexagonal Boron Nitride, and Composite Bilayer h-BN/Graphene. *IEEE Transactions on Nanotechnology* **2017,** *16* (5), 752-758.

24.   Bolotin, K. I., 9 - Electronic transport in graphene: towards high mobility. In *Graphene*, Skákalová, V.; Kaiser, A. B., Eds. Woodhead Publishing: 2014; pp 199-227.

25.   Kitaoka, Y.; Tono, T.; Yoshimoto, S.; Hirahara, T.; Hasegawa, S.; Ohba, T., Direct detection of grain boundary scattering in damascene Cu wires by nanoscale four-point probe resistance measurements. *Appl Phys Lett* **2009**, *95* (5), 052110.

26.   Avrekh, M.; Monteiro, O. R.; Brown, I. G., Electrical resistivity of vacuum-arc-deposited platinum thin films. *Appl Surf Sci* **2000**, *158* (3), 217-222.

27.   Artunç, N.; Bilge, M. D.; Utlu, G., The effects of grain boundary scattering on the electrical resistivity of single-layered silver and double-layered silver/chromium thin films. *Surface and Coatings Technology* **2007**, *201* (19), 8377-8381.

28.   Kim, M.; Kim, K.-J.; Lee, S.-J.; Kim, H.-M.; Cho, S.-Y.; Kim, M.-S.; Kim, S.-H.; Kim, K.-B., Highly Stable and Effective Doping of Graphene by Selective Atomic Layer Deposition of Ruthenium. *Acs Appl Mater Inter* **2017**, *9* (1), 701-709.

29.   Yan, Z.; Lin, J.; Peng, Z.; Sun, Z.; Zhu, Y.; Li, L.; Xiang, C.; Samuel, E. L.; Kittrell, C.; Tour, J. M., Toward the Synthesis of Wafer-Scale Single-Crystal Graphene on Copper Foils. *Acs Nano* **2012**.

30.   Wang, H.; Wang, G.; Bao, P.; Yang, S.; Zhu, W.; Xie, X.; Zhang, W.-J., Controllable Synthesis of Submillimeter Single-Crystal Monolayer Graphene Domains on Copper Foils by Suppressing Nucleation. *Journal of the American Chemical Society* **2012**, *134* (8), 3627-3630.

31.   Zhou, H.; Yu, W. J.; Liu, L.; Cheng, R.; Chen, Y.; Huang, X.; Liu, Y.; Wang, Y.; Huang, Y.; Duan, X., Chemical vapour deposition growth of large single crystals of monolayer and bilayer graphene. *Nat Commun* **2013**, *4*.

CHAPTER 5.

Enhancement of electrical property of graphene by Ru ALD

5.1. Introduction

To improve the electrical quality of CVD graphene is that doping the graphene with dozens of um size graphene according to the chapter 4, and also, the doping effect is possibly more efficient on the grain boundary, even it is still unclear. Therefore, to accomplish enhancement of electrical property of graphene and clear understanding doping effect on graphene grain boundary, the doping process was conducted based on ALD. Ideally, adsorption of precursor should be suppressed on clean surface of graphene since the surface is inert without dangling bonds and chemically active functional group. Defects (*e.g.,* grain boundaries, wrinkles, cracks, holes and residual material) should provide selective nucleation sites for ALD based on similar behavior that was observed with several metal oxides[1-3] and Pt,[4] but which was not systematically investigated with regards to transparent conducting electrode (TCE) performance and doping mechanism. Of the metals that can be deposited by ALD, Ru was selected due to it having a well-established precursor and recipe.[5] The difference in work function between graphene and Ru can also allow for work function tuning following *ex-situ* doping and carrier generation. This study therefore not only investigates the selective ALD of Ru on graphene using microanalysis tools, but also explores the electrical and optical properties of the final product. In this chapter, it was performed that the Ru ALD on graphene. Firstly, graphene was systematically investigated the selective deposition behavior using microanalysis tools. Secondly, the electrical and optical properties of Ru deposited graphene was conducted. In order to understand mechanism of graphene doping, measurement of work function was also carried out. Finally, the characteristic effect of ALD process to the electrical and

optical properties by comparing results of the Ru ALD and Ru evaporation was analyzed.

5.1.1. Experiment

52 um size of single layer graphene was synthesized based on the growth parameter on chapter 3. Graphene transfer was achieved using a typical wet chemical transfer process,[6] whereby PMMA was first spin-coated onto the as-grown graphene. The PMMA/graphene/Cu was then floated on a 0.1 M of APS solution overnight to etch away the entirety of the Cu foil. The remaining PMMA/graphene layer was then scooped onto a SiO_2(285 nm)/Si or quartz substrate for measurement of its electrical properties and optical transmittance. the residual PMMA was removed by direct heating at 380 °C in atmosphere, after which an Au/Ti (100/3 nm) electrode was deposited by e-beam evaporation using a metal shadow mask. A total of 42 such devices were prepared and subjected to Hall effect measurement under a 0.510 T magnetic field (HL 5500PC, BIO-RAD) at room temperature. A traveling wave-type ALD reactor (NCD Technology, Lucida D100) was used to deposit Ru onto graphene at a temperature of 220 °C under 1 Torr of pressure. A metalorganic precursor vapor of $C_{16}H_{22}Ru$ [(η6-1-isopropyl-4-methylbenzene) (η4-cyclohexa-1,3-diene)ruthenium, DNF Co.][5] was generated in a bubbler at 100 °C, and then carried into the process chamber by N_2 (99.999%) at a flow rate of 10 sccm. The line for precursor delivery was kept at 130 °C to prevent condensation of the precursor. The reactant used was diluted O_2 with N_2, which was introduced at a rate of 200 sccm *via* a FC-280SA Tylan mass flow controller. Each ALD cycle consisted of a 10 s Ru precursor pulse, 10 s N_2 purge, 2 s diluted O_2 pulse and a final 10 s N_2 purge. A flow rate at purge step is 200 sccm.

5.2. Characterization of Ru doped graphene

5.2.1. Microstructure analysis and Ru growth behavior

Figure 5-1 presents SEM (MERLIN compact, ZEISS) and AFM (NANO station II, Surface Image Systems) images of the as prepared graphene (**Figure 5-1(a)**), and after 20 cycles (**Figure 5-1(b)**), 50 cycles (**Figure 5-1(c)**), and 100 cycles (**Figure 5-1(d)**) of Ru ALD. The line defects evident in limited number in the SEM images are considered to be either wrinkles or grain boundaries, and it is clear that these act as nucleation sites for Ru deposition. **Figure 5-1(b)**, for example, shows that Ru is mostly deposited on top of the line defects after 20 cycles. This preferential deposition becomes even more pronounced after 50 and 100 cycles (**Figure 5-1(c-d)**), but increasing the number of cycles also causes Ru islands to start forming inside graphene grains. Considering that a continuous Ru film with a thickness of about 4 nm was formed after 50 cycles of ALD on a bare SiO_2 substrate,[5] this results clearly show that high selectivity of the ALD of Ru due to the chemical stability of the basal plane of graphene.

TEM analysis (JEM-300F, high-resolution transmission microscope, JEOL) was used to gather more detailed structural information regarding the growth behavior of Ru on graphene. **Figure 5-2(a)** shows a bright-field TEM image of graphene after 20 cycles of Ru ALD, in which lines defining the triple boundary of a graphene grain can be clearly seen. Three regions (named A, B and C) were as different grains based on the dark field images (**Figure 5-2(b)** and **Figure 5-3**) and diffraction patterns. In addition, the diffraction pattern of each graphene grain in **Figure 5-2(c-f)** show that Region B and C were mismatched to Region A by 16.0° and 20.5°. The bright-field TEM images in **Figure 5-**

4(a-f) clearly show the evolution of Ru growth on the triple boundary of a graphene grain with an increasing number of Ru ALD cycles. The diffraction pattern for each cycle is shown in **Figure 5-5(a-f)**. As shown in **Figure 5-4(a)** and **Figure 5-6**, Ru nanoparticles measuring only a few nm in size were formed on the triple junction of graphene after 5 cycles of Ru ALD. As the number of Ru ALD cycles was increased, however, the Ru nanoparticles became larger and more widely deposited on the graphene grain boundaries. This clearly shows the selective deposition behavior of Ru ALD, in that Ru nucleation preferentially occurs on the grain boundaries of graphene. With and increasing number of ALD cycles additional nucleation sites are limited, and so the growth of existing Ru particles tends to dominate. In this way, Ru nanoparticles are selectively deposited on graphene grain boundaries and enlarged according to the number of ALD cycles.

Nucleation of Ru nanoparticles occurs not only at the graphene grain boundary lines but also around the grain boundary area. It may be related to the status of graphene grain boundary. For instance, grain boundaries of graphene can be overlapped during the growth process[7, 8] generating more nucleation sites for the ALD process. On the other hands, graphene grain boundaries did not stitch together during the growth process or could be damaged during the transfer process forming empty areas that also act as nucleation sites for the ALD process. It is believed that under those grain boundary status, the Ru deposition could occur around the grain boundary area as shown in **Figure 5-4(b)** and **Figure 5-4(c)**.
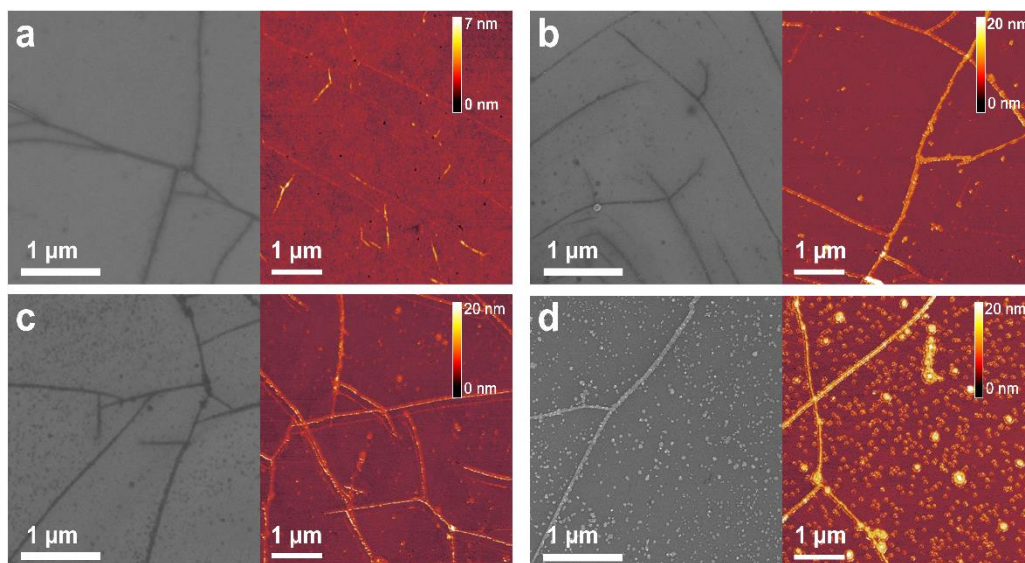
Figure 5-1. Selective deposition of Ru on graphene. SEM and AFM images of graphene
(a) as prepared, and after (b) 20, (c) 50, and (d) 100 cycles of Ru ALD.
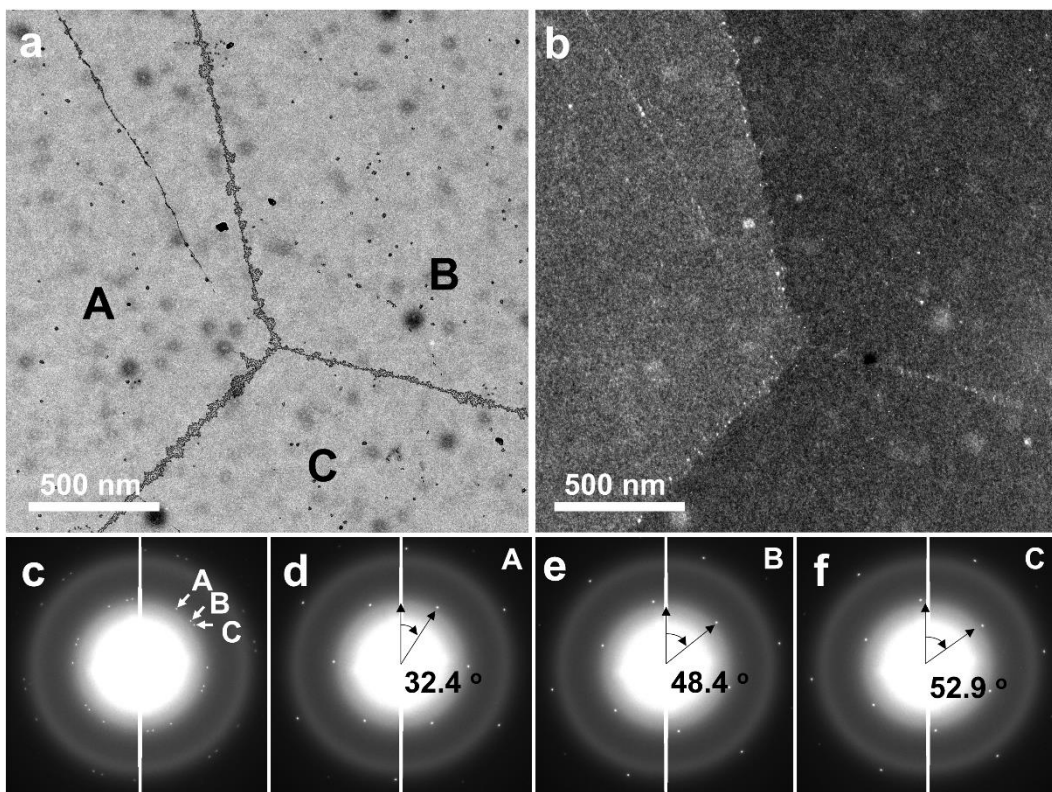
Figure 5-2. TEM images of graphene after 20 cycles of Ru ALD. (a) Bright-field and (b) dark-field TEM images of the same region. Diffraction patterns for (c) the total region, (d) Region A, (e) Region B, and (f) Region C.
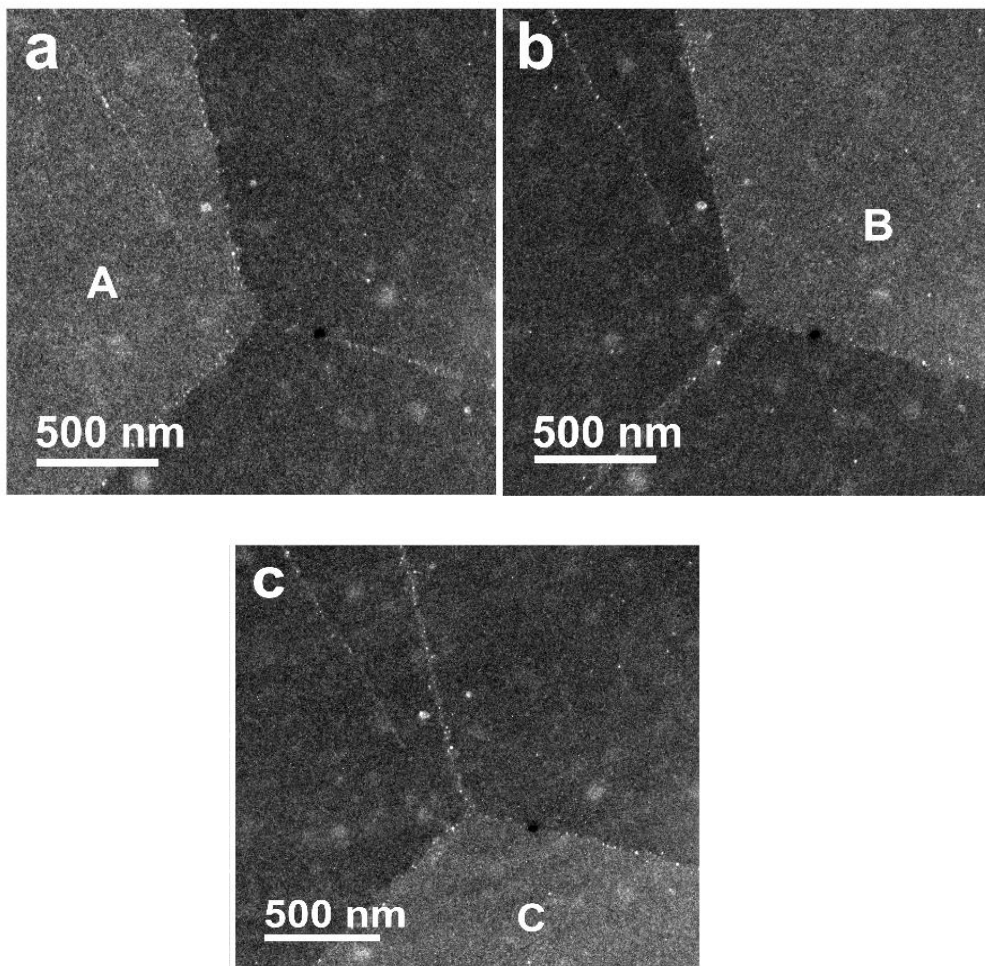
Figure 5-3. Dark-field TEM images obtained with different diffraction beams from (a) Region A, (b) Region B, and (c) Region C in **Figure 5-2(a)**.
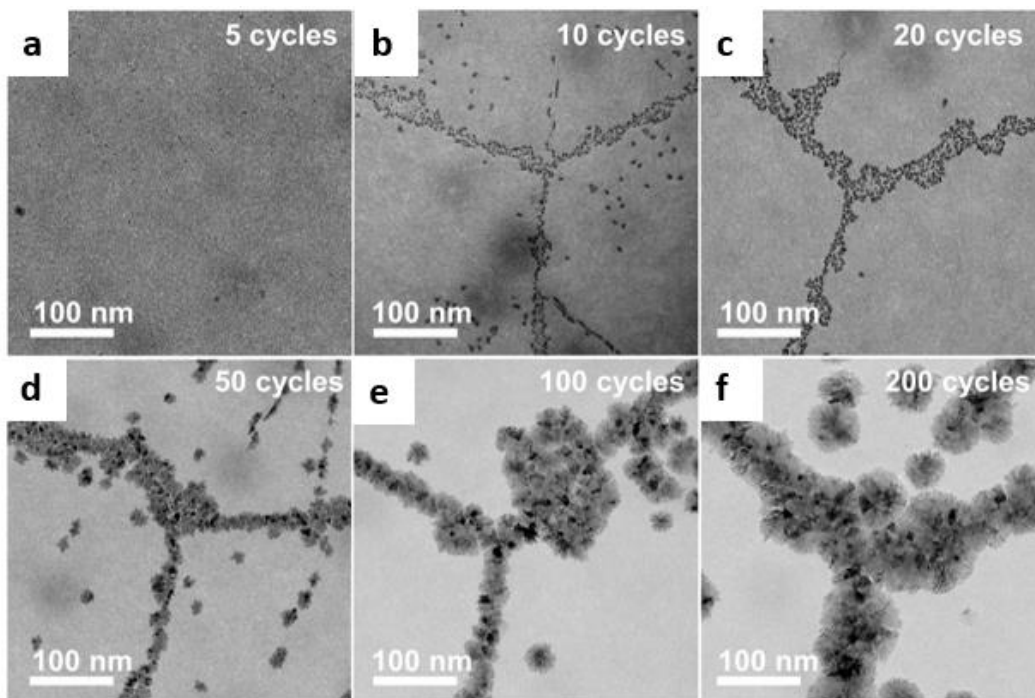
Figure 5-4. (a-f) Evolution of Ru growth on graphene triple grain boundaries shown through magnified bright-field TEM images taken after 5, 10, 20, 50, 100 and 200 ALD cycles, respectively.
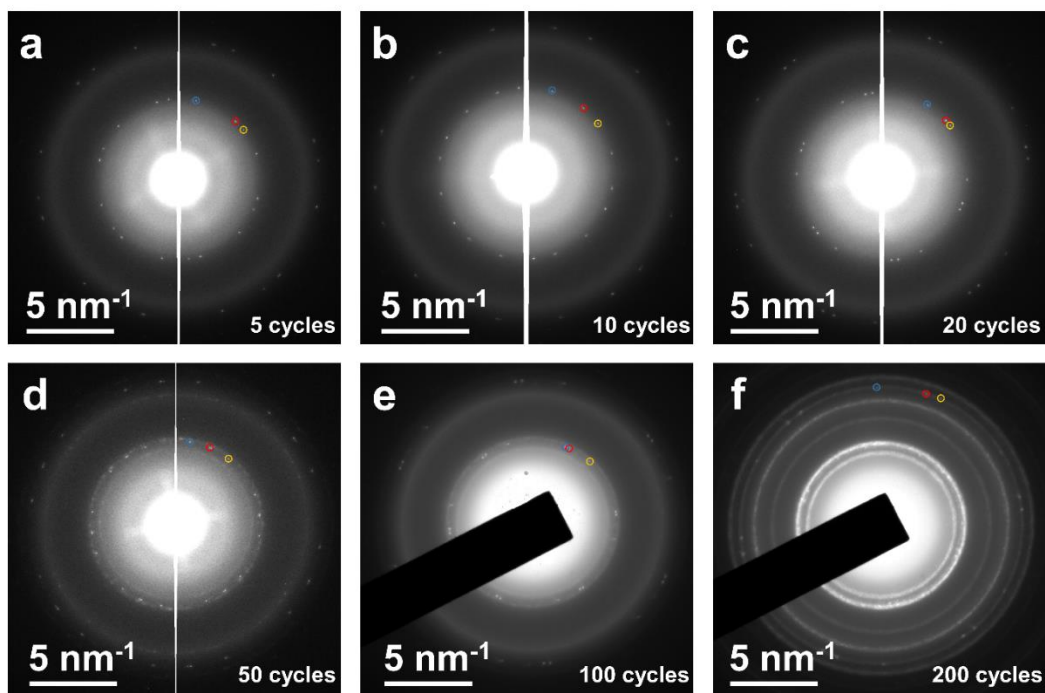
Figure 5-5. (a-f) Diffraction patterns for triple grain boundary of graphene with various Ru ALD cycles corresponding to **Figure 5-4(a)** to **Figure 5-4(f)**. Three different diffraction peaks for each graphene grain are indicate by circles.
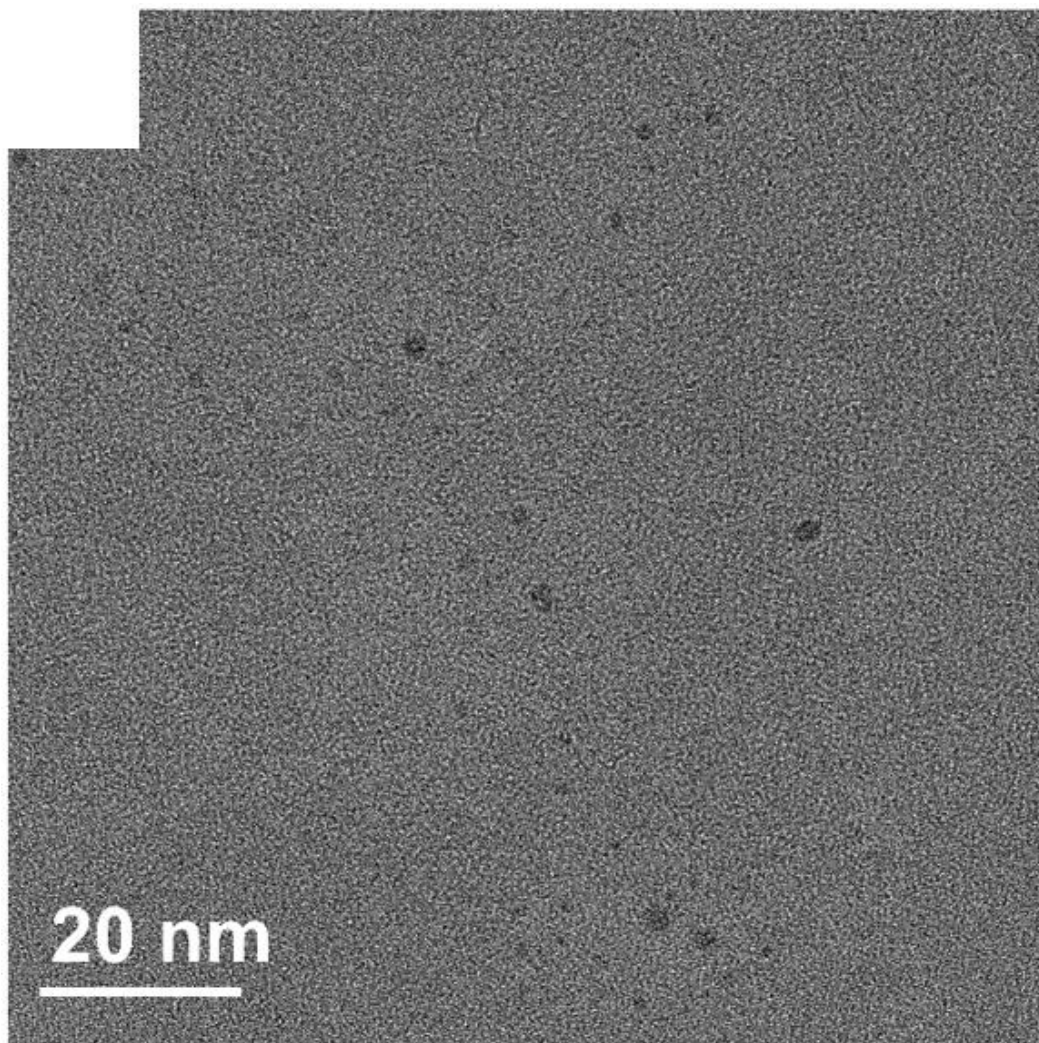
Figure 5-6. Magnified bright-field TEM image of **Figure 5-4(a)**.

5.2.2. The electrical property of Ru doped graphene

The electrical properties of the graphene were characterized by Hall measurement. **Figure 5-7(a)** shows that the sheet resistance of the graphene drastically decreased from 519 Ω/sq to 125 Ω/sq after 50 cycles of Ru ALD, and to below 100 Ω/sq after 100 cycles. The carrier density and mobility presented in **Figure 5-7(b)** clearly show the doping effect of Ru ALD, with the carrier density of graphene increasing from 1.9×10^{13} cm^{-2} to 2.2×10^{15} cm^{-2} as the number of ALD cycles is increased up to 200. Surprisingly, the carrier density was found to increase to more than 5.7×10^{13} cm^{-2} after just 20 cycles. The overall trend of mobility, on the other hand, was a decrease with an increasing number of ALD cycles. This decrease in carrier mobility may be due to charged impurities scattering with an increasing concentration of dopant, which has been previously reported in both theoretical and experimental research. [9-11] Additionally, one thing to be aware is that Ru on graphene also can work as current path. The electron microscope images (**Figure 5-1** and **Figure 5-4**) show Ru islands on graphene are connected with increasing of the number of ALD cycles. High carrier density such as 2.2×10^{15} cm^{-2} which means 0.6 carrier (hole) generation per one carbon atom in graphene can be controversial. To clarify how much Ru itself can account for the reduction in sheet resistance of graphene, Ru ALD on SiO$_2$/Si substrate without graphene was conducted. The sheet resistances of Ru thin films are in **Figure 5-7(a)** (circles). If it is assumed that the Ru thin film is electrically connected with graphene in parallel and there is no doping effect, the sheet resistance of the graphene-Ru composite can be calculated. Here, the sheet resistance will depend on the coverage of Ru thin film, and the Ru thin film coverage required to meet the Ru ALD deposited graphene can be estimated. Considering 20 and 50 cycles of Ru ALD where drastic reduction of sheet

resistance starts to occur, the sheet resistance could not be measured at 20 cycles because a continuous Ru layer was not formed. At 50 cycles, the Ru thin film without graphene has sheet resistance of about 850 Ω/sq, compared to 519 Ω/sq for as-prepared graphene. Even with 100 % Ru thin film coverage, the Ru graphene composite gives sheet resistance of 322 Ω/sq, which is more than 2 times higher than that of Ru ALD on graphene. In addition, 50 % and 35 % Ru thin film coverage meet the sheet resistance of Ru ALD on graphene at 100 cycles and 200 cycles. According to **Figure 5-1**, the deposited Ru coverage seems lower than the calculated Ru thin film coverage. The effect of Ru itself as a conduction path is considered to increase as the Ru ALD cycles increased. However, Ru ALD graphene has only a few percent of Ru coverage by selective deposition and the overall Hall coefficient for the Ru ALD on graphene was positive. Therefore, drastic decrease of sheet resistance of graphene after Ru ALD dominantly occurs by doping of graphene. Consequently, it is evident that low resistance graphene film can be achieved by the Ru ALD doping. Doping stability is also an important issue in terms of practical application. **Figure 5-7(c)** shows the sheet resistance over 8 weeks, which demonstrates the stability of graphene doping by Ru ALD that is considered one of the major advantages of this process.

  Figure 5-7(d) shows the optical transmittance at 550 nm of Ru deposited on graphene (circles) and on a bare substrate (squares) as a function of the number of ALD cycles. This confirms that Ru is selectively deposited on graphene, as the transmittance of Ru on graphene is clearly higher than that of Ru on a bare substrate; *i.e.,* the adsorption of Ru precursor was suppressed by the basal plane of graphene, while the low transmittance of the bare substrate clearly indicates that there is no selectivity on non-graphene regions. This difference in selectivity is further demonstrated by the picture taken after 100 cycles

of Ru ALD shown in the inset of **Figure 5-7(d)**, in which the high optical transmittance of the region in which graphene was transferred (as marked in red) can by clearly seen by the naked eye. Encouragingly, the transmittance only decreased from 97.7 to 92.1 % after 50 cycles, yet this was accompanied by a relatively low sheet resistance of 125 Ω/sq owing to the high selectivity of Ru deposition. With an increase in the number of ALD cycles, however, there was a strong decrease in transmittance due to the nucleation and growth of Ru islands inside graphene grains shown in **Figure 5-1(d)**.

  Figure 5-8 shows the work function of graphene, as measured by UPS as a function of the number of ALD cycles. **Figure 5-9** presents the raw data from this UPS measurement. The first thing to note here is that the increase in work function from 4.6 to 5.1 eV provides clear proof for the p-type doping of graphene, in that this difference in work function creates charge transfer between graphene and Ru. More specifically, electrons near the Fermi energy level (E_F) in graphene move to Ru due to its greater work function (4.71–5.14 eV),[12, 13] as well as the fact that the E_F of graphene is located at a lower energy level than before this charge transfer. This mechanism is roughly described in the inset of **Figure 5-7(d)**, and has been widely accepted both experimentally [14-16] and theoretically[12, 17] as a basic principle of graphene doping through graphene-metal contact. One thing to note here, however, is that the work function becomes saturated when the number of ALD cycles is more than 50, yet the carrier density continues to increase. This implies that simple charge transfer cannot be the only mechanism of graphene doping, as otherwise the work function would constantly increase with the number of ALD cycles. Previous theoretical research has already suggested other doping mechanisms, with it well known that Ru is chemically adsorbed on graphene and strongly interacts with it.[12, 18] During this chemisorption, an

electronic interaction in the form of a hybridization between the π-electrons of graphene and d-electrons of Ru significantly disrupts the intrinsic linear π-band dispersion of graphene.[12] The result of this has been theoretically demonstrated with various transition metals adsorbed on graphene to be a change in the density-of-state independent work function,[19, 20] and so it stands to reason that the same mechanism would apply in the case of Ru-graphene contact created through ALD. This would provide a valid explanation for the saturated work function with increasing charge carrier density.
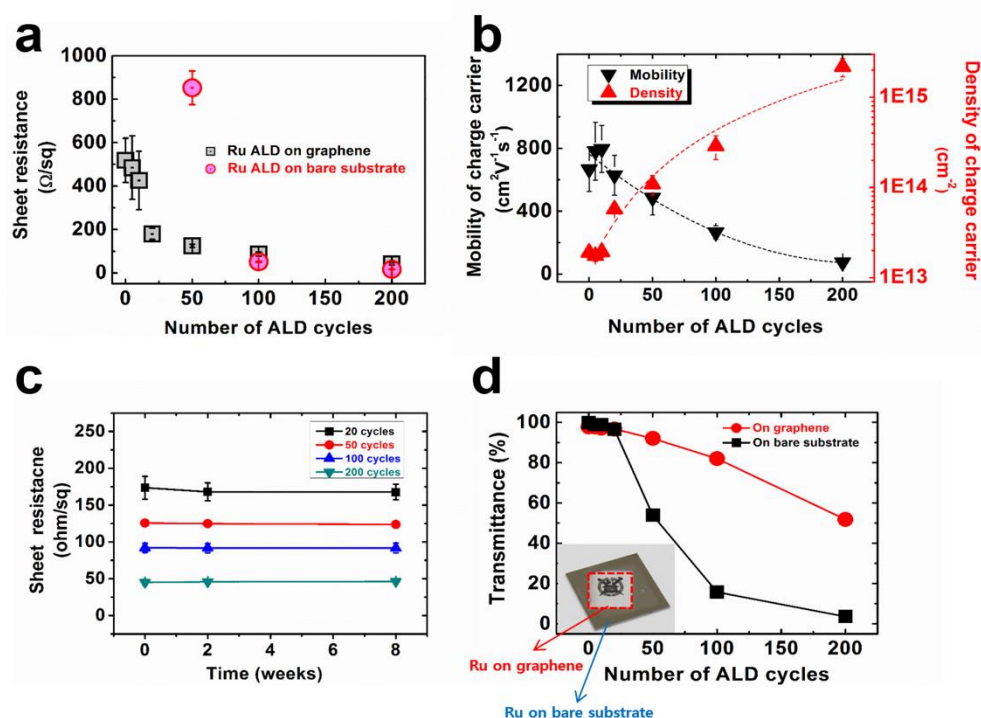
Figure 5-7. Electrical and optical properties of graphene. (a) Sheet resistance of graphene after Ru ALD (gray square) and Ru ALD without graphene (red circle), (b) density and mobility of charge carriers, (c) sheet resistance as a function of time, (d) optical transmittance at 550 nm as a function of the number of ALD cycles.
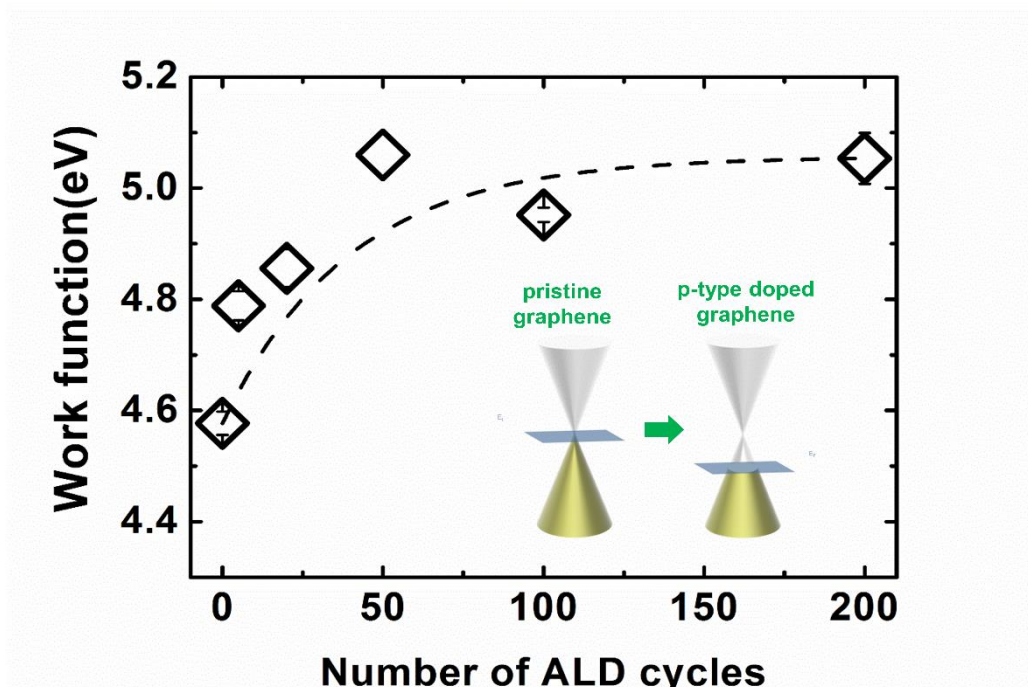
Figure 5-8. Work functions of graphene as a function of the number of ALD cycles.
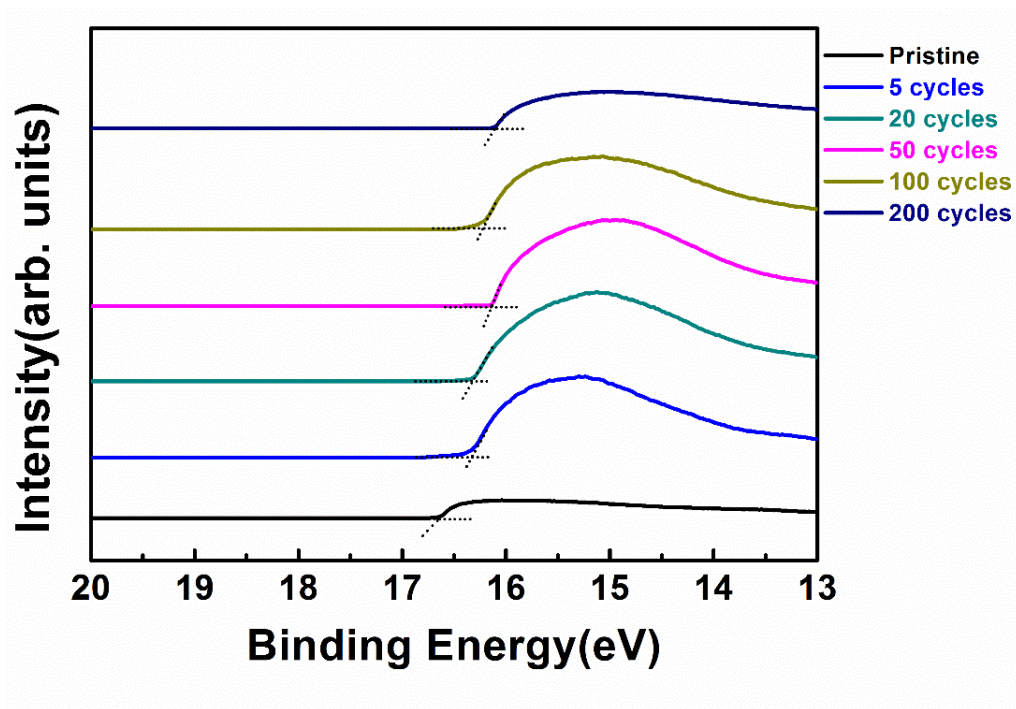
Figure 5-9. UPS spectra of graphene.

5.3. Comparative study of graphene doped by Ru ALD and Ru evaporation

To clarify the effect of the selective nature of Ru ALD on the electrical properties of graphene, Ru was non-selectively deposited onto graphene *via* evaporation. **Figure 5-10(a)** shows the sheet resistance of graphene after this deposition of Ru by evaporation, while **Figure 5-10(b)** shows its mobility and carrier density. The sheet resistance constantly increased with Ru deposition thickness up to 1 nm, but decreased with any further increase in thickness beyond this. The carrier density data shows that doping of graphene is also achieved by evaporation, but the reduction in sheet resistance is weaker than was seen with Ru ALD due to the drastic degradation of mobility. **Figure 5-10(c)** shows the optical transmittance at 550 nm as a function of evaporated Ru deposition thickness, which unlike the data for Ru ALD, was always less than 2.6 ± 0.9 % that of the bare substrate. Given that a single layer of graphene absorbs 2.3 % of light at this wavelength, it would seem that Ru deposited by evaporation grows non-selectively on both graphene and a bare substrate.

To compare how the two different growth methods, generate carrier density, the carrier densities produced with each are shown in **Figure 5-10(d)** as a function of optical transmittance. This reveals that graphene with a 0.5 nm-thick Ru deposited by evaporation has an optical transmittance of 88 %, a carrier density of 3.8×10^{13} cm^{-2} and a mobility of 355 cm^{2}V^{-1}s^{-1}. Graphene after 50 cycles of Ru ALD has a similar optical transmittance of 92 %, but a much higher carrier density (1.1×10^{14} cm^{-2}) and mobility (485 cm^{2}V^{-1}s^{-1}). In

other words, the Ru ALD data exhibits a carrier density increase that is one order of magnitude higher than as prepared graphene, but with Ru evaporation it is only doubled. To reach the same level of carrier density with evaporation would require a 3 nm-layer thick layer of Ru, whereas after 50 cycles of ALD, the Ru formed on line defects can reach heights of 4 nm based on a deposition rate of 0.086 nm/cycle.[30] Thus, although it has a much larger graphene-Ru contact area, 3 nm of Ru deposited by evaporation would have a similar carrier density to graphene after 50 cycles of Ru ALD. This data clearly indicates that charge carrier increase predominantly occurs in defect regions, and not in the basal plane of graphene.

  In addition to carrier density, selective deposition also affects carrier mobility. The mobility decreases by about 66 % with a 0.5 nm-thick Ru deposited by evaporation, but only by 27 % after 50 Ru ALD cycles and with around 90 % optical transmittance. As Ru has a much lower mobility than graphene and functions as a scattering center, it is selectively deposited on line defects where mobility is intrinsically lower. With evaporation, however, the enhanced scattering on the basal plane of graphene leads to a more drastic reduction in mobility. In summary, although p-type doping was confirmed with evaporation, this method was not able to achieve an efficient reduction in sheet resistance or a high optical transmittance when compared to ALD. The valuable outcomes of Ru ALD in terms of improving the electrical and optical properties of graphene must therefore originate from the selective deposition it creates. This not only effectively dopes graphene and generates a high carrier density, but also minimizes the loss of mobility and transmittance by restricting the adsorption of Ru onto the basal plane of graphene. The use of Ru ALD therefore presents a very efficient doping process for TCE applications.
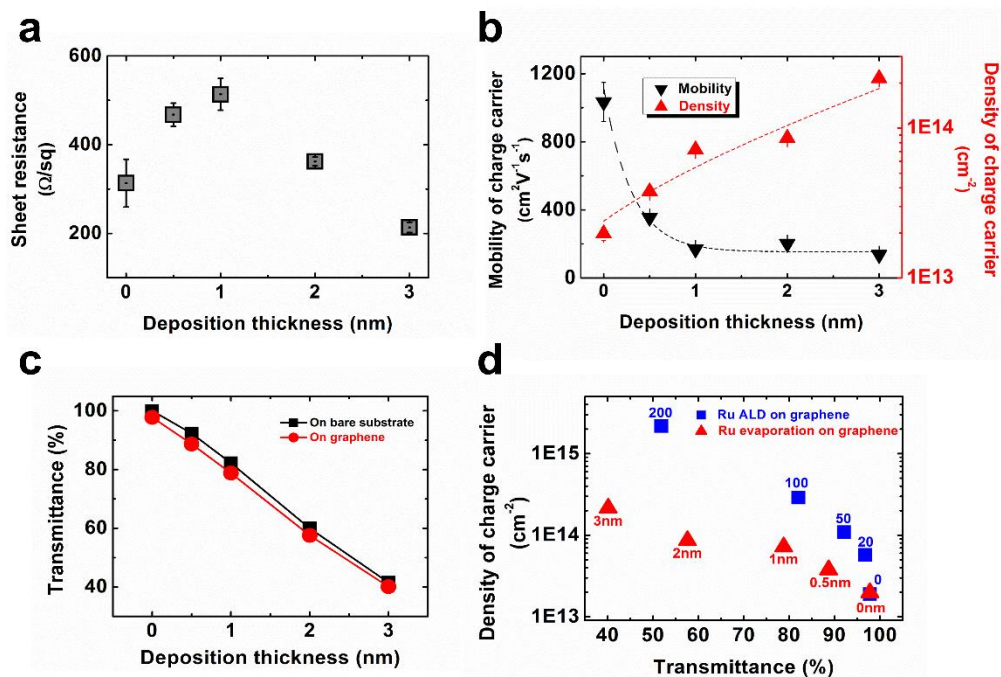
Figure 5-10. Electrical and optical properties of Ru deposited on graphene by evaporation as a function of deposition thickness. (a) Sheet resistance, (b) density and mobility of charge carrier, (c) transmittance at 550 nm, and (d) density of charge carrier as a function of transmittance (numbers represent evaporated layer thickness and number of ALD cycles).

5.4. Summary and conclusions

Highly doped p-type graphene with a high optical transmittance has been successfully achieved through atomic layer deposition of Ru on graphene. The sheet resistance of graphene was reduced to 180 and 125 Ω/sq after 20 and 50 cycles of ALD, respectively, with an accompanying increase in carrier density to 5.7×10^{13} and 1.1×10^{14} cm^{-2}. This novel *ex-situ* doping process produces very stable results, even over an extended period of several months. The optical transmittance of graphene is also maintained, decreasing to just 96.7 and 92.1 % after 20 and 50 cycles, respectively. The increase in the work function of graphene from 4.6 to 5.1 eV with Ru ALD provided clear evidence of hole carrier generation as a result of an electronic interaction between graphene and Ru. Finally, it has also been confirmed that the selective nature of Ru ALD provides a more efficient way of doping graphene than Ru evaporation, as it helps to minimize the loss of mobility and optical transmittance. This demonstration of strong and stable doping of graphene with a high optical transmittance is therefore expected to contribute to the use of graphene as a TCE, and in other fields.

References

1.　　　Wang, X.;　Tabakman, S. M.; Dai, H., Atomic Layer Deposition of Metal Oxides on Pristine and Functionalized Graphene. *Journal of the American Chemical Society* **2008,** *130* (26), 8152-8153.

2.　　　Park, K. S.;　Kim, S.;　Kim, H.;　Kwon, D.;　Koo Lee, Y.-E.;　Min, S.-W.; Im, S.;　Choi, H. J.;　Lim, S.;　Shin, H.;　Koo, S. M.; Sung, M. M., Wafer-scale single-domain-like graphene by defect-selective atomic layer deposition of hexagonal ZnO. *Nanoscale* **2015,** *7* (42), 17702-17709.

3.　　　Van Lam, D.;　Kim, S.-M.;　Cho, Y.;　Kim, J.-H.;　Lee, H.-J.;　Yang, J.-M.; Lee, S.-M., Healing defective CVD-graphene through vapor phase treatment. *Nanoscale* **2014,** *6* (11), 5639-5644.

4.　　　Kim, K.;　Lee, H.-B.-R.;　Johnson, R. W.;　Tanskanen, J. T.;　Liu, N.;　Kim, M.-G.;　Pang, C.;　Ahn, C.;　Bent, S. F.; Bao, Z., Selective metal deposition at graphene line defects by atomic layer deposition. *Nat Commun* **2014,** *5* (1), 4781.

5.　　　Eom, T.-K.;　Sari, W.;　Choi, K.-J.;　Shin, W.-C.;　Kim, J. H.;　Lee, D.-J.; Kim, K.-B.;　Sohn, H.; Kim, S.-H., Low Temperature Atomic Layer Deposition of Ruthenium Thin Films Using Isopropylmethylbenzene-Cyclohexadiene-Ruthenium and O[sub 2]. *Electrochemical and Solid-State Letters* **2009,** *12* (11), D85.

6.　　　Kim, K. S.;　Zhao, Y.;　Jang, H.;　Lee, S. Y.;　Kim, J. M.;　Kim, K. S.;　Ahn, J.-H.;　Kim, P.;　Choi, J.-Y.; Hong, B. H., Large-scale pattern growth of graphene films for stretchable transparent electrodes. *Nature* **2009,** *457* (7230), 706-710.

7.　　　Dong, J.;　Wang, H.;　Peng, H.;　Liu, Z.;　Zhang, K.; Ding, F., Formation mechanism of overlapping grain boundaries in graphene chemical vapor deposition growth.

Chemical Science **2017,** *8* (3), 2209-2214.

8.   Lee, G.-H.;   Cooper, R. C.;   An, S. J.;   Lee, S.;   van der Zande, A.;   Petrone, N.;   Hammerberg, A. G.;   Lee, C.;   Crawford, B.;   Oliver, W.;   Kysar, J. W.; Hone, J., High-Strength Chemical-Vapor–Deposited Graphene and Grain Boundaries. *Science* **2013,** *340* (6136), 1073-1076.

9.   Bult, J. B.;   Crisp, R.;   Perkins, C. L.; Blackburn, J. L., Role of Dopants in Long-Range Charge Carrier Transport for p-Type and n-Type Graphene Transparent Conducting Thin Films. *Acs Nano* **2013,** *7* (8), 7251-7261.

10.   Chen, J. H.;   Jang, C.;   Adam, S.;   Fuhrer, M. S.;   Williams, E. D.; Ishigami, M., Charged-impurity scattering in graphene. *Nature Physics* **2008,** *4* (5), 377-381.

11.   Perebeinos, V.; Avouris, P., Inelastic scattering and current saturation in graphene. *Phys Rev B* **2010,** *81* (19), 195442.

12.   Gong, C.;   Lee, G.;   Shan, B.;   Vogel, E. M.;   Wallace, R. M.; Cho, K., First-principles study of metal–graphene interfaces. *J Appl Phys* **2010,** *108* (12), 123711.

13.   Halas, S.; Durakiewicz, T., Work functions of elements expressed in terms of the Fermi energy and the density of free electrons. *Journal of Physics: Condensed Matter* **1998,** *10* (48), 10815-10826.

14.   Kwon, K. C.;   Choi, K. S.; Kim, S. Y., Increased Work Function in Few-Layer Graphene Sheets via Metal Chloride Doping. *Advanced Functional Materials* **2012,** *22* (22), 4724-4731.

15.   Shin, H.-J.;   Choi, W. M.;   Choi, D.;   Han, G. H.;   Yoon, S.-M.;   Park, H.-K.;   Kim, S.-W.;   Jin, Y. W.;   Lee, S. Y.;   Kim, J. M.;   Choi, J.-Y.; Lee, Y. H., Control of Electronic Structure of Graphene by Various Dopants and Their Effects on a

Nanogenerator. *Journal of the American Chemical Society* **2010,** *132* (44), 15603-15609.

16.   Khan, M. F.;   Iqbal, M. Z.;   Iqbal, M. W.; Eom, J., Improving the electrical properties of graphene layers by chemical doping. *Science and Technology of Advanced Materials* **2014,** *15* (5), 055004.

17.   Giovannetti, G.;   Khomyakov, P. A.;   Brocks, G.;   Karpan, V. M.;   van den Brink, J.; Kelly, P. J., Doping Graphene with Metal Contacts. *Phys Rev Lett* **2008,** *101* (2), 026803.

18.   Ishii, A.;   Yamamoto, M.;   Asano, H.; Fujiwara, K., DFT calculation for adatom adsorption on graphene sheet as a prototype of carbon nanotube functionalization. *Journal of Physics: Conference Series* **2008,** *100* (5), 052087.

19.   Hu, L.;   Hu, X.;   Wu, X.;   Du, C.;   Dai, Y.; Deng, J., Density functional calculation of transition metal adatom adsorption on graphene. *Physica B: Condensed Matter* **2010,** *405* (16), 3337-3341.

20.   Chan, K. T.;   Neaton, J. B.; Cohen, M. L., First-principles study of metal adatom adsorption on graphene. *Phys Rev B* **2008,** *77* (23), 235430.

CHAPTER 6.

Summary and conclusions

The remarkable electrical property of single crystal graphene is limited in application because of the synthesis method of single crystal graphene by mechanical cleavage method, which only produce dozens of um size. The one of the most promising large scaling with high quality synthesis method is CVD, however, as described in chapter 2, electrical property limiting factors such as substrate scattering, grain boundary scattering, impurity scattering and additional damage from transfer process down grade the sheet resistance of graphene from 30 ohm/sq to 500 ohm/sq. To overcome those limiting factors, numerous studies were conducted and the doping and increasing grain size are the major research trends. For clear understanding and accomplish electrical property enhanced CVD graphene, first, various size of graphene was synthesized from basic study of graphene growth. 4 different sizes of graphene with 17 ~78 um were synthesized, enlarging its grain size from decreasing carbon source supply, minimizing heterogeneous nucleation site from electropolishing process, applying two-step growth method to solve the unfilled gap between graphene grains which caused by JMAK growth behavior. The various size of graphene was evaluated by Hall measurement, before and after doping, the resultant shows that the sheet resistance of graphene is reduced as the average grain size is increased regardless of doping. The carrier concentration is almost constant over experimental range, however, the carrier mobility was increased as the average grain size increased, implying that grain boundary scattering effect is reduced when the grain size increased as previously reported articles. The experimental data is further analyzed by two different model, ohmic scaling model which is extracting grain boundary portion by simple numerical calculation and MS model which is considering grain boundary as a scattering center. It was revealed that the grain boundary has about 20 % of the sheet resistance portion, and the reflection

coefficient of graphene is fitted as 0.97 in undoped graphene, tells that in both model analysis, graphene grain boundary acts as strong scattering center, one of the major degrading factors on electrical property of CVD graphene. Also, from the conjugated experiment of doping and enlarging grain size, most effective way for enhancing electrical property of graphene is that growing dozens of size of graphene and conducting doping process. Another noticeable presumptive fact from doping and enlarging grain size conjugated experiment is that the doping process seem to be more efficient on the graphene grain boundary. In chapter 5, by selective Ru ALD on graphene grain boundary, this presumptive theory was studied. The Ru p-type dopant was well deposited on graphene grain boundaries and other defects such as wrinkles and cracks which is confirmed by SEM, AFM, and TEM analysis. The resultant electrical property of Ru doped graphene by ALD process is that 180 ohm/sq at 20 cycle, and 125 ohm/sq at 50 cycle, showing more enhanced electrical property from doped by dipping process in BZ solution in chapter 4. The doping effectiveness on graphene grain boundary studied further by employing Ru evaporation which deposit Ru homogeneously all over the graphene plane. The experimental result shows that Ru evaporation is also act as dopant, however, it turns out that quantitatively, grain boundary-oriented doping by ALD is more effective in carrier concentration generation and mobility degrading point of view.

  In summary, research on enhancing electrical property of graphene is conducted via characterizing grain boundary effect and doping. Furthermore, it is found out that the doping is more effective and doping in grain boundary is even more effective on graphene. Therefore, this study can contribute to the basic of graphene grain boundary in electrical property and the doping graphene processes.

Abstract (in Korean)

그래핀은 뛰어난 전기적, 기계적 광학적 특성을 보여주는 2차원 재료로, 2D 재료 연구 분야를 여는데 있어 크게 이바지한 물질이다. 그러나, 대부분의 유망한 특성은 단결정 그래핀으로부터 나오는데, 이때 단결정 그래핀은 수십 마이크로 미터 단위밖에 제작이 불가능하다. 웨이퍼 스케일로 그래핀을 합성하기 위하여, 화학적 방법으로 합성하는 방법 (chemical exfoliation), SiC 기판에서 Si을 선택적으로 승화하는 방법 및 CVD (Chemical vapor deposition) 방법이 있는데, CVD는 거의 무한한 크기로의 합성이 가능하며 품질이 좋아 가장 각광받는 방법 중 하나이다. 하지만 CVD로 합성한 그래핀은 몇 가지의 이유로 단결정 그래핀의 좋은 특성을 보여주지 않기 때문에 CVD 그래핀의 전기적 특성을 높이기 위한 대규모 노력과 연구가 수행되었다.

1장과 2장은 서론으로, 1 장에서는 그래핀의 기본 물성과 합성하는 방법에 대하여 소개하였다. 2 장에서는 그래핀의 전기적 특성을 제한하는, 기판 산란, 결정립 산란 및 기타 산란 인자의 대하여 고찰해 보았으며, 이러한 한계를 극복하고 그래핀의 전기적 특성을 향상시키기 위하여 현재 어떠한 연구가 이루어지고 있는지에 대하여 요약하였다. 그 중에서도 도핑하는 방법과 그래핀의 도메인 크기를 키우는 방법이 현재 주된 연구의 흐름이다.

3장은 4장의 준비 부분으로, 그래핀의 결정립이 미치는 영향을 살펴보기 위하여 다양한 크기의 그래핀을 합성하였다. 그래핀의 CVD 성장에 대한 기본 이론을 통하여, 메탄가스의 양을 감소시킴으로써 도메인 크기 성장을 꾀할 수 있었으며 실험 상태의 최적화를 위하여 heterogeneous 핵생성을 막기 위한 전기연마 공정과, 낮은 메탄가스 공급에 의하여 그래핀의 성장이 저해되는 현상을 막기 위하여 2 단계 성장 과정이 제안되었다.

4장은 이 연구의 두 본문 중 하나로, 그래핀의 결정립이 전기적 특성에 미치는 영향에 대하여 고찰하였다. 그 결과 도핑 유무에 관계없이 도메인 크기가 증가함에 따라 면저항의 감소를 관찰할 수 있었으며, 이는 캐리어 이동도의 증가에 기인한다는 현상을 발견하였다. Ohmic scaling 모델을 통하여 추가로 분석한 결과 17 um의 도메인을 가지는 그래핀의 경우 20% 만큼의 면저항의 비중을 결정립이 차지하고 있다는 것을 알 수 있었다. 또한 Mayadas-Shatzkes 모델에 적용한 결과 R 값이 0.97로 굉장히 높은 값을 띄고 있다는 것을 확인할 수 있었으며, 결국 두 모델을 이용한 연구를 통하여 그래핀의 결정립이 강산 캐리어 산란 효과를 가지고 있음을 밝힐 수 있었다. 도핑 공정은 또한 다양한 크기의 그래핀에 적용을 하여, 그래핀의 결정립이 도핑하지 않았을 때와 유사하게 강한 산란효과를 가짐을 확인할 수 있었고, 추가적으로 관찰된 사실 중 하나는 그래핀의 도핑 효율이 결정립에서 더 높다는 것이었다. 도핑 방법과 그래핀의 도메인 크기를 키우는 두 가지 방법을 종합한 결과, 10 um 이상의 그래핀을 증착한 후 도핑을 수행하는 것이 가장 효과적으로 그래핀의 전기적 특성을 향상시킬 수 있다는 사실을 발견하였다.

5장에서는 Ru을 단원자증착법을 (ALD) 통하여 결정립에만 선택적으로 도펀트를 증착하였으며, 그래핀의 결정립이 도핑에 미치는 영향에 대하여 고찰하였다. 그 결과 ALD 20 사이클에서 180 ohm/sq, 50 사이클에서 125 ohm/sq 로 전기적 특성이 뛰어난 그래핀을 증착할 수 있었다. 또한 Ru evaporation을 그래핀에 수행하여 그래핀 표면에 homogeneous하게 Ru을 증착함으로써, ALD 를 통하여 도핑하였을 때와 비교하였으며, 그 결과 그래핀의 결정립에서 도핑의 효율이 더 높다는 것을 밝혀내게 되었다. 위 연구를 통하여 그래핀의 결정립이 전기적 특성에 미치는 영향에 대하여 잘 파악할 수 있었으며, 추후 그래핀의 결정립을 포함하는 전기적 특성, 도핑 효과에 대한

연구에 기초로 활용할 수 있을 것으로 기대한다.

주요어: 그래핀, 결정립, 도핑, 단원자층 증착법, 도핑, 면저항, 전기적 특성 향상

학번: 2011-20622